MATHEMATICAL MODELS OF FIBRINOLYSIS

by

Brittany E. Bannish

A dissertation submitted to the faculty of
The University of Utah
in partial fulfillment of the requirements for the degree of

Doctor of Philosophy

Department of Mathematics

The University of Utah

August 2012

The University of Utah Graduate School

STATEMENT OF DISSERTATION APPROVAL

The dissertation of **Brittany E. Bannish**

has been approved by the following supervisory committee members:

Aaron L. Fogelson	, Chair	**6/19/2012** Date Approved
James P. Keener	, Member	**6/19/2012** Date Approved
Frederick R. Adler	, Member	**7/3/2012** Date Approved
Yekaterina Epshteyn	, Member	**6/19/2012** Date Approved
John W. Weisel	, Member	**6/19/2012** Date Approved

and by **Peter E. Trapa**, Chair of the Department of **Mathematics**

and by Charles A. Wight, Dean of The Graduate School.

ABSTRACT

Fibrinolysis, the proteolytic degradation of the fibrin fibers that stabilize blood clots, is initiated when tissue-type plasminogen activator (tPA) activates plasminogen to plasmin, the main fibrinolytic enzyme. Many experiments have shown that coarse clots made of thick fibers lyse more quickly than fine clots made of thin fibers, despite the fact that individual thick fibers lyse more slowly than individual thin fibers. Other experiments show the opposite result. Reaction-diffusion models have been the standard tool for investigating fibrinolysis, and have been successful in capturing the wave-like behavior of lysis seen in experiments. These previous models treat the distribution of fibrin within a clot as homogeneous, and therefore cannot be used directly to study lysis of fine and coarse clots. We create a model that includes a spatially heterogeneous fibrin concentration, as well as a more accurate description of the role of fibrin as a cofactor in the activation of plasmin. Our model predicts spatiotemporal protein distributions in reasonable quantitative agreement with experimental data. The model also predicts observed behavior such as a front of lysis moving through the clot with an accumulation of lytic proteins at the front.

In spite of the model improvements, however, we find that one-dimensional (1-D) continuum models are unable to accurately describe the observed differences in lysis behavior between fine and coarse clots. Hence, we develop a three-dimensional (3-D) stochastic multiscale model of fibrinolysis. A microscale model representing a fiber cross section and containing detailed biochemical reactions provides information about single fiber lysis times and the length of time tPA stays bound to a given fiber cross section. Data from the microscale model is used in a macroscale model of the full fibrin clot, from which we obtain lysis front velocities and tPA distributions. We find that the number of fibers in a clot impacts lysis rate, but so does the number of tPA molecules relative to the surface area of the clot exposed to those molecules. Depending on the values of these two quantities (tPA number and surface area), for given kinetic parameters, the model predicts coarse clots lyse faster or slower than fine clots, thus providing a possible explanation for the divergent experimental observations. We also use the model to predict values of unmeasured reaction rates and to suggest desirable characteristics of fibinolytic drugs. We find that a tPA

variant that binds less strongly to fibrin causes faster degradation rates than normal tPA. We conclude by studying the effect of the inhibitors α_2-antiplasmin (α_2-AP), plasminogen activator inhibitor-1 (PAI-1), and thrombin activatable fibrinolysis inhibitor (TAFI) on lysis. We find that α_2-AP is the stongest inhibitor, but lysis is most delayed when α_2-AP and TAFI work together.

To my family, for their endless love and support.

CONTENTS

LIST OF FIGURES

LIST OF TABLES

ACKNOWLEDGEMENTS

Thank you to my family for your constant support, confidence, and love. Thanks for asking questions about what I do and at least feigning interest in my answers. I am sure I would not have made it to, and then through, graduate school without you all.

To Dr. Aaron Fogelson, for guiding me through these past six years. I cannot imagine a better adviser. I am so appreciative of the time you gave me, every week, to talk about my work and my life (and the Celtics). Thank you also for your ability to detect when I needed a pep talk or a kind word; you'll never know how well-timed and meaningful those words were!

To Dr. James Keener, for being such a caring, fearless leader. I am so proud to be a part of the University of Utah mathematical biology community that you work(ed) so hard to create. Thank you for always being willing to talk about a research problem (or a funding problem, or a homework problem, or ...), regardless of how busy you are. I know my graduate career would have been much less enjoyable without cabin parties, so thanks for hosting all those parties, too!

To Dr. John Weisel, for taking the time to Skype with a young math graduate student who thought she might be interested in fibrinolysis, and then for humoring all my questions about biology once the project got rolling. I truly appreciate your willingness to collaborate with mathematicians, and I always enjoy our meetings.

To Drs. Frederick Adler and Yekaterina Epshtyen, for being so willing to sit on my committee and providing a fresh perspective on my work.

To Dr. Nelson Beebe, for sharing your vast wealth of knowledge and for helping me debug and improve lots of code. Also to Nelson, Pieter Bowman, and Victor Gabrenas for your wonderful job keeping the computer system running smoothly and coming to my rescue whenever I had problems.

To every office member who helped my graduate experience proceed smoothly. Thanks especially to Paula Tooman, Sandy Hiskey, and April Taylor, for always being ready with a smile and caring ear to lend.

To Erica Graham for so much laughter, support, and commiseration over the past six years. As far as roommates, officemates, friends, and singing partners go, you're pretty awesome. Thank you and congratulations – can you believe we made it?!

To Sean Laverty, for too much to list here. Thank you for leading the way, and for giving me confidence and reassurance at every step. Thanks for being such a great editor of my talks and papers, and for putting up with me while I pouted and complained about your suggestions; it took a day or two, but I usually admitted your revisions were helpful. Thank you for your advice, support, and love.

Finally, thanks to my wonderful friends who managed to make graduate school fun. I would have gone crazy without you all.

Thank you.

CHAPTER 1

INTRODUCTION

Intravascular blood clots (thrombi) are composed of platelets, red blood cells, and a stabilizing mesh of fibrin fibers. Fibrinolysis is the proteolytic degradation of fibrin fibers. Occlusive thrombi can form if fibrinolysis happens too slowly, causing heart attack or stroke. Rapid fibrinolysis impedes formation of blood clots, leading to excessive bleeding. Understanding the tightly regulated fibrinolytic process is important from both physiological and clinical standpoints. Safely and effectively increasing lysis rates therapeutically is a goal of much ongoing research. We develop mathematical models of the fibrinolytic system to explore the underlying mechanisms of fibrinolysis and to propose potential targets for new fibrinolytic therapies.

1.1 Biological background

Plasmin, the main fibrinolytic enzyme, is activated from its inactive precursor plasminogen (PLG) by tissue-type plasminogen activator (tPA). tPA is fibrin-selective and preferentially activates fibrin-bound PLG, creating a source of plasmin on the surface of fibrin fibers. Plasmin exists in the blood plasma at extremely low concentration due to strong plasmin inhibitors (the most important being α_2-antiplasmin), so the local creation of plasmin on fibrin fibers is a critical step of fibrinolysis. Once plasmin is formed, it degrades the fibrin by cleaving peptide bonds formed by the carboxyl group of lysine. The cleavage exposes initially cryptic C-terminal lysines to which more tPA and PLG may bind, potentially creating a positive feedback for plasmin activation and fibrin degradation (Figure 1.1).

It has been shown that a therapeutic bolus of tPA administered near a clot increases the rate of fibrinolysis in patients [?, ?, ?]. In several experiments mimicking therapeutic lysis, a bolus of tPA is added to the edge of a fibrin clot in the absence of fluid flow [?, ?, ?]. These studies show that lysis moves across the clot as a front, with a high accumulation of lytic enzymes bound to fibers at the lysis front.

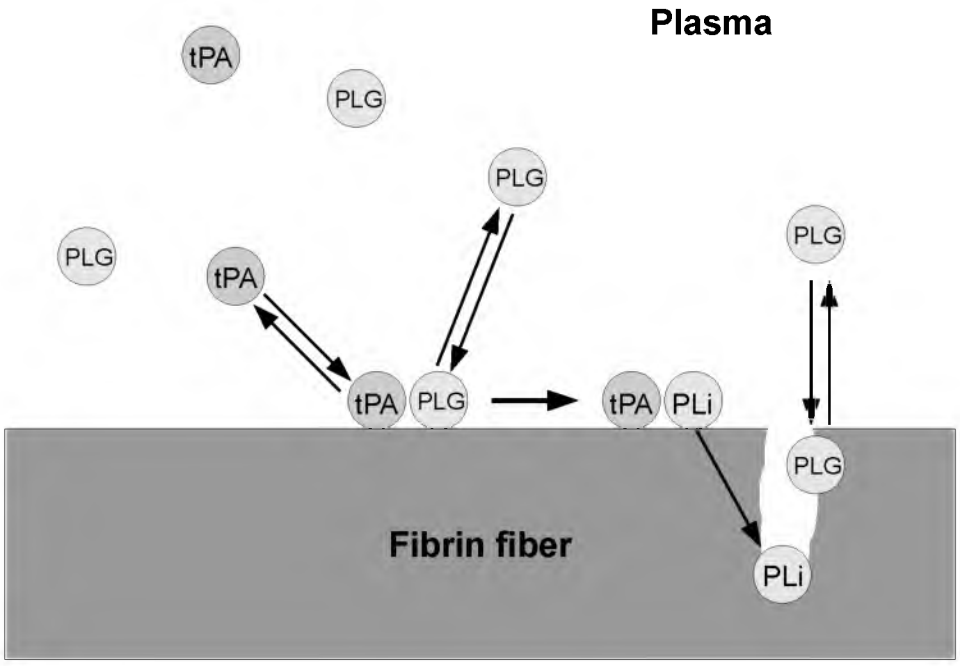

Figure 1.1. Cartoon of fibrinolysis (not to scale). Plasminogen (PLG) and tPA diffuse in the plasma and can bind to fibrin. If tPA and PLG bind in close proximity to one another, the tPA can convert the PLG to plasmin (PLi). PLi then degrades the fibrin by cutting across the fiber. New binding sites for tPA and PLG are exposed as plasmin cleaves fibrin. Plasma concentration of PLG ≈ 2 μM, and plasma concentration of tPA ≈ 70 pM.

Plasmin-mediated degradation of fibrin fibers seems to occur by transverse cutting across fibers, rather than by uniform degradation around fiber diameters [?, ?, ?]. This is likely due to the fiber configuration, which has binding sites located 6 nm apart transversely, and 22.5 nm apart lengthwise. A single fiber is a lateral aggregation of many two-stranded protofibrils (long chains composed of half-staggered 45-nm-long fibrin monomers). The protofibrils in a fiber are in register and clear striations across the fiber are seen in electron micrographs [?]. This half-staggering distributes binding sites in 22.5 nm intervals along a fiber, while lateral aggregation spaces protofibrils about 5-6 nm apart transversely. It is hypothesized that plasmin can "crawl" to the transverse binding sites, but is unable to reach farther away binding sites, which directs degradation across a fiber [?].

Despite the seemingly tight packing of protofibrils into fibers, fibrin fibers are about 20% protein and 80% water [?, ?]. Hence, on the scale of a single fiber, it is believed there are pores through which small molecules can diffuse [?]. A calculation of protofibril spacing in a fibrin fiber suggests that the edge-to-edge distance between protofibrils is approximately

5 nm, on average (Appendix A). There is some debate about the size of a PLG molecule, which has been estimated to have a diameter of 9-11 nm [?], and a radius of gyration between 3.05-3.9 nm [?, ?]. All of these estimates are large enough to imply that PLG *cannot* diffuse through the pores of a single fibrin fiber. However, since PLG is present in the plasma during fibrin formation, it is reasonable to assume that PLG can be bound to any protofibril in a fiber.

On the clot scale, there are much larger pores *between* fibers. The structure of a fibrin clot depends on the environment in which it forms. Conditions of high salinity or thrombin concentration yield fine clots with thin, tightly packed fibers (small pores), while conditions of low salinity or thrombin concentration produce coarser clots with thicker fibers and larger pores. Despite the fact that individual thick fibers lyse more slowly than individual thin fibers [?, ?], some experiments have shown that coarse clots made of thick fibers lyse more quickly than fine clots made of thin fibers [?, ?]. However, other experiments show fine clots lyse faster than coarse clots, or show no significant difference in lysis rates [?, ?, ?]. We create mathematical models to elucidate the factors that influence lysis speeds in clots of varying structure, in an effort to suggest targets for the design of new fibrinolysis therapeutics.

1.2 Literature review

The use of continuum models to explore fibrinolysis is the prevailing trend in the mathematical modeling literature, with many models consisting of one-dimensional (1-D) advection-reaction-diffusion equations [?, ?, ?, ?]. All of these models assume that initially fibrin is distributed homogeneously throughout the domain. We discuss a few of these models to put our own models in context.

Zidanšek and Blinc [?] study the spatial distribution of plasmin inside clots exposed to pressure-driven permeation of urokinase-type plasminogen activator (uPA). Like tPA, uPA converts plasminogen to plasmin, but unlike tPA it does so in plasma. uPA has no fibrin specificity, and therefore the possible positive feedback provided by plasmin exposure of new binding sites is absent in situations of uPA-induced lysis. uPA activation of plasmin and plasmin inactivation by α_2-antiplasmin are modeled as Michaelis-Menten reactions. The model does not distinguish between plasma-phase and fibrin-bound species. Degradation of fibrin is represented by a decrease in the concentration of peptide bonds in the fibrin network that can be cleaved by plasmin. When the proportion of plasmin-susceptible peptide bonds falls to 2/3, the clot has dissolved. The clot is a three-dimensional (3-D) uniformly-shaped

semi-infinite circular cylinder which is reduced to 1-D by symmetry. The clot is assumed to be homogeneous, composed of uniform concentrations of fibrin and plasminogen, with no uPA present initially. The relative concentrations of uPA and plasmin are calculated in a clot experiencing steady-state lysis. The lysis front is found to move with a constant velocity. Incorporating advection to model plasma flow results in the front moving with the same velocity as the flow. In the absence of flow, the diffusion constants of uPA and plasmin limit the speed of lysis, leading to the conclusion that permeation enhances fibrinolysis.

A higher-dimensional model of fibrinolysis was proposed by Zidanšek et al. [?]. Magnetic resonance imaging shows that pressure-driven uPA can generate finger-like patterns of degradation within a clot [?, ?]. In developing a two-dimensional (2-D) random walk model to predict these types of lysing patterns, the authors start with the same Michaelis-Menten kinetics and advection-reaction-diffusion equations as in Zidanšek and Blinc [?], but approximate the effect of the reactions by a single "reaction time", t_R. t_R represents the time lag between the arrival of uPA and the actual clot dissolution at a given point, and depends on reaction rate constants, the steady-state concentration of uPA in the blood, and the plasmin concentration. The clot is described as a rectangle separated by a sharp boundary from the blood. Using t_R, the system of reactions is reduced to a problem of moving boundaries. The blood–thrombus interface and the boundary created by the uPA front are tracked. The variation in clot porosity is accounted for by solving the Laplace equation for pressure with lattice Green's functions. The Green's functions are calculated with a random walk simulation, which results in pressure at a point r being proportional to the probability that r was visited by a random walker. The magnitude of t_R affects solutions of the random walk model, with high t_R values resulting in finger-like patterns of lysis. Model solutions show "remarkable similarities to experimental and clinical observations" of lysis velocity and of the dependence of lysis patterns on the enzyme transport parameters, however no quantitative comparison between the model and experiments is provided. The authors conclude that accounting for the random character of clot porosity results in the model equations displaying the ability to produce the finger-like, drug-induced clot degradation patterns observed experimentally.

To date, the most influential modeling paper of fibrinolysis is by Diamond and Anand [?]. The authors extend the model of Zidanšek and Blinc [?] by accounting for the evolution of fiber diameter, considering reactions under nonequilibrium conditions, and including kinetics of individual reactions. The impact of diffusion and permeation on the fibrinolytic

system is studied. 1-D advection-reaction-diffusion equations model lysis and concentration profiles of lytic species in a 1 cm long clot. The clot contains fibers with time-evolving diameters. Lysis of a fiber is modeled as plasmin-induced degradation from the outside in, resulting in a fiber diameter that decreases with time. (Since the publication of Diamond and Anand's paper, it has been shown that lysis proceeds by transverse cutting across the fiber, rather than by uniform digestion around the fiber [?, ?].) The percentage of lysis at a particular location is calculated as the number of cuts made by plasmin at that location divided by the number of cuts needed to degrade one subunit of fibrin. Concentrations of free uPA and free and fibrin-bound tPA, PLG, and plasmin are included in the model. Proteins are allowed to bind only to sterically accessible sites located on the surface of the fiber. This is a simplification, because tPA molecules are small enough to diffuse through pores in the fibrin fibers and are not confined to the fiber surface. However, most tPA is likely located near the surface of the fiber due to the strong binding affinity of tPA to fibrin.

Results under different flow conditions (i.e., different pressure drops across the clot) all show a sharp front of lysis moving across the clot. The faster permeation velocities generate increased lysis front velocities. Concentration profiles for bound and free phase enzymes are obtained 15 minutes after tPA is introduced, but the time evolution of these concentrations is not presented. The bound plasmin concentration peaks dramatically at the lysis front due to rapid local conversion of PLG to plasmin, while the bound tPA concentration is modestly increased at the front. An increase in free phase PLG and tPA is observed near the lysis front, due to the release of bound species from the fully lysed front of the clot.

By changing the fiber radius (from 25-500 nm) while keeping the bulk fibrin concentration the same, the effects of fiber radius on transport and kinetics can be examined. To keep bulk fibrin concentration fixed while increasing fiber radius it is necessary to decrease the concentration of available binding sites on the fiber surface; a lower fraction of the fibrin monomers are exposed on the surface of a thick fiber than on the surface of a thin fiber. Because of this, when the Peclet number is held constant (and the pressure drop adjusted to enforce this), fine fibers are lysed faster than coarse fibers. A constant Peclet number corrects for the fact that clots with thin fibers have a lower specific permeability than clots with thick fibers. If the pressure drop is held constant, coarse fibers, which have enhanced permeation, lyse faster than fine fibers, which have reduced permeation. The authors conclude that permeation is the dominant mode of transport for lytic species. Additionally, by varying kinetic parameters they conclude that: strong binding of tPA to

fibrin slows its penetration into the clot; adjusting the tPA dissociation constant does not cause an increase in lysis rates (the wildtype tPA dissociation constant is nearly optimal); and the concentration of PLG already on/in the clot has a strong impact on lysis rates.

While Diamond and Anand's model [?] is more detailed than previous fibrinolysis models, it omits some essential features of lysis. For instance, we now know that lysis occurs by transverse cutting across fibers, not uniform degradation around the diameter. Diamond and Anand's definition of lysis, as well as their calculation for the sterically accessible lytic protein binding sites, relies on degradation occurring uniformly around the fiber diameter. Also, their model does not account for effects of the plasmin inhibitor α_2-antiplasmin, competition for binding sites between tPA and PLG, or exposure of new binding sites in partially degraded fibrin. Failing to account for exposure of new binding sites eliminates the possibility of positive feedback.

Wootton et al. [?] modify Diamond and Anand's model to account for the effect of partial fibrin degradation. They develop a 2-D advection-reaction-diffusion model with porous viscous flow, which after scaling is reduced to a 1-D reaction-diffusion model. The model tracks the plasma-phase and fibrin-bound concentrations of tPA, PLG, and plasmin, the plasma-phase concentration of α_2-antiplasmin, and the fibrin solid volume fraction. It is assumed that all binding sites are accessible and uniformly distributed throughout the domain, and that PLG and plasmin compete for binding sites on fibrin. The authors assume that partial degradation increases the affinity and binding site density for PLG, but not for tPA. Unlike Diamond and Anand, Wootton et al. do not model fiber radius, but rather fibrin volume fraction. Consequently, Wootton et al. are better able to investigate clot lysis than Diamond and Anand, whose "clot" is one long fiber. The trade off, however, is that Wootton et al. are unable to investigate individual fiber lysis.

To achieve lysis, Wootton et al. require higher tPA, PLG, and plasmin binding rates than those presented in Diamond and Anand [?]. With the higher binding rates, they find that lysis occurs more slowly than predicted by Diamond and Anand's model and with a much larger accumulation of plasma-phase tPA, PLG, and plasmin at the lysis front (five times or more higher than the bulk concentration). Additionally, the lysis front is sharper. The lysis front is a zone about 15-30 μm thick, in agreement with experiments [?]. Lysis proceeds at a relatively constant rate after an initial delay while plasmin is created. Wootton et al. do not present any model results pertaining to distributions or concentrations of bound lytic proteins, nor do they discuss the time evolution of lytic protein concentrations. The

authors primarily use the model to complement their experimental observations of the effect of shear stress on fibrinolysis. The experiments show that at low to arterial shear stress (4 dyn/cm^2 to 18 dyn/cm^2), outer flow slightly accelerates lysis; the average lysis front velocities are 1.4×10^{-5} and 1.5×10^{-5} cm/s, respectively. In contrast, at high shear stresses (41 dyn/cm^2), lysis is greatly accelerated to 3.1×10^{-5} cm/s. The model results for increasing shear stress show accelerated lysis, but the quantitative results are far smaller than the experimentally measured values. This suggests that increased outer convection alone cannot account for the lysis rates observed experimentally at shear stresses between 18-40 dyn/cm^2. In fact, the authors suggest that outer convection modulates lysis only at shear stresses below 10 dyn/cm^2. They offer no explanation for other mechanisms that may be responsible for the increased lysis front velocities obtained at increased shear stresses.

More recent models use reaction-diffusion equations to simulate simultaneous fibrinolysis and coagulation [?, ?]. The models include activated and resting platelets, many coagulation factors, fibrin, fibrinogen, thrombin, prothrombin, tPA, PLG, plasmin, and α_2-antiplasmin. The models also include blood flow, platelet activation, reactions leading to clot formation and growth, viscoelastic properties of the clot, and fibrinolysis. In a model with so many components, it is difficult to identify subtle influences on the predicted outcomes. The main results of these models are predicted time courses of fibrin concentration; specific questions about fibrinolysis are not addressed.

We have made significant progress in understanding fibrinolysis by creating and analyzing mathematical models. In Chapter 2, we discuss our 1-D reaction-diffusion model that extends the preceding models by considering more detailed reaction chemistry and the spatial heterogeneity of fibrin. Our multiscale model, introduced in Chapter 3 and extended in Chapters 4 and 5, is the first model of fibrinolysis to simultaneously include multiple dimensions, unbound and bound chemical species, spatial heterogeneity of fibrin, stochastic treatment of tPA and plasmin, tPA and PLG competition for binding sites, and the effect of partially degraded fibrin on PLG binding rates. The impact of our mathematical models of fibrinolysis and future work are discussed in Chapter 6.

CHAPTER 2

ONE-DIMENSIONAL CONTINUUM MODEL OF FIBRINOLYSIS

As discussed in Chapter 1, experiments have shown that coarse clots made of thick fibers sometimes lyse more quickly than fine clots made of thin fibers, despite the fact that individual thick fibers lyse more slowly than individual thin fibers. Proposed mechanisms for this apparent paradox include enhanced movement of tPA through coarse clots (and therefore earlier activation of PLG), and lateral transection of fibers by plasmin [?, ?]. If degradation occurs by transverse cutting across fibers (rather than by uniform digestion around fibers) [?, ?, ?], presumably a coarse clot with fewer fibers to transect might be degraded faster than a fine clot with a higher fiber density. While this explanation seems to be widely accepted, it is difficult to confirm experimentally. In this chapter, we aim to use a one-dimensional (1-D) model of fibrinolysis to elucidate the mechanism by which coarse clots lyse more quickly than fine clots.

The use of continuum models to explore fibrinolysis is the prevailing trend in the literature, with many models consisting of 1-D advection-reaction-diffusion equations (Chapter 1.2) [?, ?, ?, ?]. All of these models assume that initially fibrin is distributed homogeneously throughout the domain. We create a 1-D continuum model of the fibrinolytic system that extends the preceding models in several ways: we allow for tPA and PLG to compete for newly exposed binding sites; we allow only PLG that is bound to fibrin in close proximity to bound tPA to be converted to plasmin; and perhaps most importantly, we account for the spatially heterogeneous concentration of fibrin within clots. By treating fibrin concentration heterogeneously, we are able to explore for the first time the effects of lysis on single fibrin fibers, as well as on fibrin clots of varying structure.

Patients with blood clots are often treated with a therapeutic bolus of tPA, which has been shown under certain conditions to increase the rate of fibrinolysis when administered near the clot. We model the experiment by Collet et al., which mimics this clinical situation [?]. In the experiment, a bolus of tPA is added to the edge of a native plasma fibrin

clot in the absence of fluid flow. First, we test the model with a homogeneous fibrin concentration to verify that it produces results similar to those from previous models [?, ?]. Then spatial inhomogeneity is added to the model (so we can distinguish between fine and coarse clots), and the resulting predictions are compared to published experimental data. We conclude that 1-D continuum models are capable of quantitatively predicting the spatial distribution of lytic enzymes, but cannot capture the observed behavior of lysis in clots of varying structure. 1-D continuum models can therefore be used to answer questions about spatiotemporal variation in lytic enzyme concentrations, but more sophisticated models are necessary to answer quantitative questions about structural aspects of lysis.

2.1 The model

We develop a 1-D reaction-diffusion model to study the spatiotemporal dynamics of lytic protein concentrations. In our model, tPA and PLG can each be in one of two states: free in solution (where they diffuse), or bound to fibrin. Because tPA and PLG must be bound to fibrin in proximity to one another for tPA to convert PLG to plasmin, fibrin is represented by binding doublets. Each binding doublet has two sites to which tPA and/or plasmin(ogen) may bind and from which they may unbind. If tPA occupies one site and PLG occupies the other, then PLG may be converted to plasmin. Such a doubly occupied doublet is analogous to the enzyme-substrate complex in standard enzyme kinetic models. We include binding doublets in an attempt to incorporate small scale spatial effects in the model. Doublets provide us with more information about *where* proteins are located on fibrin; if tPA and PLG are bound to the same doublet, the proteins are close enough together to create plasmin. If we model the concentrations of bound enzymes without the use of doublets, then we know only that tPA and PLG are bound somewhere on fibrin, but not how closely located they are to each other.

There are two types of binding doublets: specific and nonspecific. On a specific binding doublet, tPA may bind only to the first site, and PLG/plasmin may bind only to the second (Figure 2.1). For nonspecific doublets, tPA and PLG can each bind to either site. Only specific binding doublets are available initially, but as lysis proceeds, nonspecific binding doublets are exposed by plasmin. Multiple doublets may exist at the same location.

Next, we describe the terms in the model equations before presenting the full model. Two variations of this model are considered, one with a homogeneous concentration of fibrin and the other with a heterogeneous concentration of fibrin.

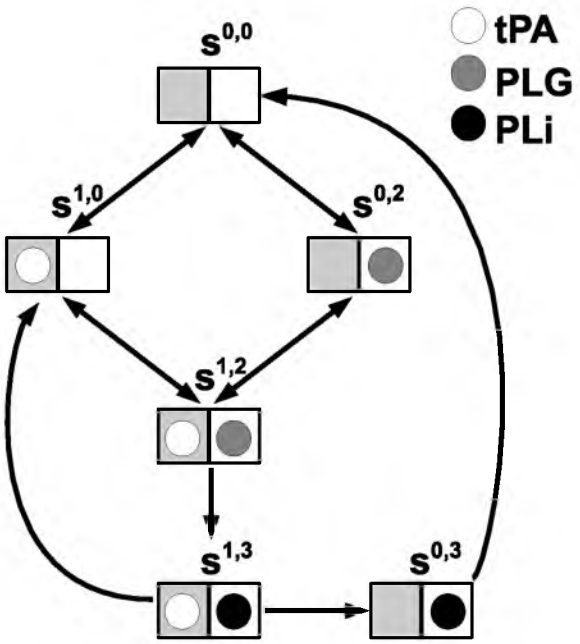

Figure 2.1. Reaction diagram for specific binding doublets. tPA may only bind to the gray sites and PLG and plasmin (PLi) may only bind to the white sites.

2.1.1 Model variables

We track the concentrations of free tPA and PLG (denoted a and p, respectively), as well as the concentrations of all possible configurations of binding doublets (e.g., a specific doublet with tPA bound but no PLG). $s^{i,j}$ represents a specific binding doublet with index i describing tPA ($i = 0$ if tPA is not bound, $i = 1$ if tPA is bound), and with index j describing plasmin(ogen) ($j = 0$ if neither PLG nor plasmin are bound, $j = 2$ if PLG is bound, and $j = 3$ if plasmin is bound) (Table 2.1 and Figure 2.1). $n^{i,j}$ is the concentration of a nonspecific binding doublet with indices $i, j = 0, 1, 2$, or 3. For example, $n^{2,3}$ refers to nonspecific doublets with PLG bound to the first site and plasmin bound to the second. Due to high concentrations of plasmin inhibitors, the plasma concentration of plasmin is effectively zero. Consequently, we neglect free plasmin. If plasmin unbinds from fibrin, it is assumed to be instantaneously inhibited and is removed from the model. The final variable is n, the concentration of the pool of initially unexposed binding sites that can be exposed by plasmin.

Table 2.1. Continuum model notation.

Notation	Description
$s^{i,j}$	specific binding doublet concentration
$n^{i,j}$	nonspecific binding doublet concentration
n	unexposed binding doublet concentration
i or $j = 0$	nothing bound
i or $j = 1$	tPA bound
i or $j = 2$	PLG bound
i or $j = 3$	PLi bound

2.1.2 Binding and unbinding

Free tPA and PLG can diffuse and interact with fibrin, but once bound to a doublet, the proteins no longer move. Doublet concentrations are changed by protein binding and unbinding. For example,

$$\frac{ds^{1,3}}{dt} = \underbrace{k_{\text{on}}^{\text{a},0,3} u s^{0,3}}_{\substack{\text{tPA binds to doublet} \\ \text{with PLi already bound}}} - \underbrace{k_{\text{off}}^{\text{a},1,3} s^{1,3} - k_{\text{off}}^{\text{i},1,3} s^{1,3}}_{\substack{\text{tPA (1st term) or PLi} \\ \text{(2nd term) unbind}}} + \cdots .$$

These are basic terms obtained from reaction diagrams like Figure 2.1. $k_{\text{on}}^{q,u,v}$ is the forward rate for species q binding to doublet $s^{u,v}$ or $n^{u,v}$, and $k_{\text{off}}^{q,u,v}$ is the reverse rate for species q unbinding from doublet $s^{u,v}$ or $n^{u,v}$, for $q = a, p$, or i (plasmin), and $u, v = 0, 1, 2$, or 3.

2.1.3 Degradation

The terms for plasmin-mediated degradation of fibrin are derived using a quasi-steady state analysis for two substrates competing for one enzyme. Unexposed nonspecific sites, n, and exposed sites, *doublets*, compete for plasmin. The concentration of plasmin is $\sigma = s^{0,3} + s^{1,3} + n^{0,3} + n^{1,3} + n^{2,3} + 2n^{3,3}$. Quasi-steady state analysis gives differential equations for degradation products created from *doublets* (p_d), and for degradation products created from n (p_n):

$$\frac{dp_d}{dt} = \frac{k_{\text{cat}} \sigma \, doublets}{K_{\text{M}} + doublets + \frac{K_{\text{M}}}{K_{\text{M}}^{\text{n}}} n}$$
$$\frac{dp_n}{dt} = \frac{k_{\text{cat}}^{\text{n}} \sigma n}{K_{\text{M}}^{\text{n}} + n + \frac{K_{\text{M}}^{\text{n}}}{K_{\text{M}}} doublets},$$

where the total concentration of doublets is

$$doublets = s^{0,0} + s^{0,2} + s^{0,3} + s^{1,0} + s^{1,2} + s^{1,3} + n^{0,0} + n^{1,0} + n^{0,2} + n^{1,1} + n^{1,2} + n^{2,2} + n^{1,3} + n^{2,3} + n^{0,3} + n^{3,3}.$$

The catalytic rates and Michaelis-Menten constants are k_{cat}, K_{M} for plasmin degradation of exposed sites, and $k^{\mathbf{n}}_{\mathrm{cat}}$, $K^{\mathbf{n}}_{\mathrm{M}}$ for plasmin "degradation" (i.e., exposure) of unexposed sites. Assuming that each fibrin species (e.g., $s^{1,3}$) is degraded in proportion to its fraction of the total amount of exposed binding sites, and that plasmin can degrade any doublet at the same location (not just the doublet to which it is bound), the degradation terms take the form:

$$\frac{ds^{1,3}}{dt} = \left(\frac{s^{1,3}}{doublets}\right)\left(\frac{-k_{cat}\sigma\, doublets}{K_M + doublets + \frac{K_M}{K^n_M}n}\right) + \cdots = -\frac{k_{\mathrm{cat}}\sigma s^{1,3}}{K_{\mathrm{M}} + doublets + \frac{K_{\mathrm{M}}}{K^{\mathrm{n}}_{\mathrm{M}}}n} + \cdots.$$

The other degradation term, obtained similarly, describes the conversion of unexposed sites, n, to exposed sites, $n^{0,0}$:

$$\frac{dn}{dt} = -\frac{k^{\mathbf{n}}_{\mathrm{cat}}\sigma n}{K^{\mathbf{n}}_{\mathrm{M}} + n + \frac{K^{\mathrm{n}}_{\mathrm{M}}}{K_{\mathrm{M}}} doublets}.$$

When fibrin is degraded by plasmin, the binding doublets (and any bound plasmin) disappear, and the bound tPA and PLG are released into the solution.

2.1.4 Moving plasmin

Based on the observation that plasmin inhibitors have high concentration in plasma, plasmin in solution is ignored. Plasmin, however, can move between binding sites at the same spatial location. With the parameter values used in this model (Table 2.2), plasmin does not unbind from doublets – it is only released by degradation of the doublet to which it is bound. Consequently, the tPA molecule that created the plasmin is inhibited from producing more plasmin until it unbinds and rebinds elsewhere; it cannot encounter PLG while bound to a doublet occupied by plasmin. Allowing plasmin to move locally (where it is protected from plasmin inhibitors), frees up the binding site for PLG, which can then be converted to plasmin.

Of all the doublets that contain plasmin, $s^{1,3}$ and $n^{1,3}$ are most abundant. For simplicity, we assume that only plasmin from these doublets can move, and that plasmin may move

Table 2.2. 1-D model parameter values. References for parameter values are as follows: *[?, ?], †[?], ‡[?], ⋆[?], §[?].

Description (units)	Notation	Value
tPA diffusion coefficient ($\mathrm{cm^2 s^{-1}}$)	D_{tPA}	5×10^{-7}
PLG diffusion coefficient ($\mathrm{cm^2 s^{-1}}$)	D_{PLG}	5×10^{-7}
tPA dissociation constant in absence of PLG/PLi (μM)	k_{D}^{a}	0.36 *
tPA dissociation constant in presence of PLG/PLi (μM)	k_{D}^{a}	0.02 †
tPA binding rate ($\mu\mathrm{M}^{-1}\mathrm{s}^{-1}$)	k_{on}^{a}	1.0
tPA unbinding rate (s^{-1})	k_{off}^{a}	$k_{\mathrm{D}}^{a} k_{\mathrm{on}}^{a}$
PLG dissociation constant (μM)	k_{D}^{p}	38.0 ‡
PLG binding rate ($\mu\mathrm{M}^{-1}\mathrm{s}^{-1}$)	k_{on}^{p}	0.1 ⋆
PLG unbinding rate (s^{-1})	k_{off}^{p}	$k_{\mathrm{D}}^{p} k_{\mathrm{on}}^{p}$
PLi unbinding rate (s^{-1})	k_{off}^{i}	0.0
rate constant for conversion of PLG to PLi by tPA (s^{-1})	k_{cat}^{ap}	50
rate constant for PLi digestion of activated doublets (s^{-1})	k_{cat}	10 §
constant for enzymatic digestion of activated doublets (μM)	k_M	0.1
rate constant for activation of un-activated doublets (s^{-1})	k_{cat}^{n}	50
constant for enzymatic digestion of un-activated doublets (μM)	k_M^n	0.1

only to the most common doublets, $s^{0,0}$ and $n^{0,0}$. Movement is modeled as a reaction. For example, the reactions

$$s^{1,3} + s^{0,0} \xrightarrow{k_{\mathrm{move}}} s^{1,0} + s^{0,3},$$

$$s^{1,3} + n^{0,0} \xrightarrow{k_{\mathrm{move}}} s^{1,0} + n^{0,3}$$

give terms

$$\frac{ds^{1,3}}{dt} = \; - \; k_{\mathrm{move}}(s^{1,3}s^{0,0} \; + \; 2s^{1,3}n^{0,0}) + \cdots .$$

The factor of 2 arises because plasmin can move to either of the two available binding sites on nonspecific doublet $n^{0,0}$.

2.1.5 Creation of plasmin

Finally, we model the conversion of PLG to plasmin. When tPA and PLG are bound to the same doublet, tPA converts PLG to plasmin at rate $k_{\mathrm{cat}}^{\mathrm{ap}}$. Therefore, tPA-mediated

conversion is modeled by $k_{\text{cat}}^{\text{ap}} s^{1,2}$ (for specific doublets) and $k_{\text{cat}}^{\text{ap}} n^{1,2}$ (for nonspecific doublets).

2.1.6 Sample equation

We now write out one model equation in its entirety. For the full model, see Appendix B. Combining the pieces described above gives the equation:

$$\frac{ds^{1,3}}{dt} = \underbrace{k_{\text{cat}}^{\text{ap}} s^{1,2}}_{\substack{\text{tPA converts}\\ \text{PLG to PLi}}} + \underbrace{k_{\text{on}}^{\text{a},0,3} a s^{0,3}}_{\substack{\text{tPA binds to doublet}\\ \text{with PLi already bound}}} - \underbrace{k_{\text{off}}^{\text{a},1,3} s^{1,3} - k_{\text{off}}^{\text{i},1,3} s^{1,3}}_{\substack{\text{tPA (1st term) or PLi}\\ \text{(2nd term) unbind}}}$$

$$- \underbrace{k_{\text{move}}(s^{1,3} s^{0,0} + 2 s^{1,3} n^{0,0})}_{\substack{\text{PLi from } s^{1,3} \text{ moves onto } s^{0,0}\\ \text{or } n^{0,0} \text{ at same spatial location}}} - \underbrace{\frac{k_{\text{cat}} \sigma s^{1,3}}{K_{\text{M}} + \textit{doublets} + \frac{K_{\text{M}}}{\kappa_{\text{M}}^{\text{n}}} n}}_{\text{PLi degrades fibrin}}.$$

The other model equations are similar.

2.1.7 Initial and boundary conditions

An indicator function $\chi(x)$ is used to specify where fibrin is found at $t = 0$. For the homogeneous model, the domain is $0 \le x \le 300$ μm ($0 \le x \le 1$ nondimensionally) and $\chi = 1 - 0.5(1 + \tanh(\frac{0.1-x}{0.01}))$, which corresponds to fibrin being nearly uniformly distributed over the interval 30 μm $< x <$ 300 μm. For the heterogeneous model, the fibrin concentration varies as indicated in Equation (2.3). The fibrin concentration is high at locations occupied by a fiber, and zero between fibers, with transitions smoothed for numerical simulation. The nonzero fibrin concentration is chosen so that the fibrin concentration averaged over the whole domain is 6 μM. The domain is 100 μm long, with the first 10 μm free of fibrin (Figure 2.2). Using an average fiber diameter from experiments [?] and an average pore size (gap between fibers), we calculate the number of fibers in the clot. For example, in a fine clot (pore size 1 μm) made of thin fibers (diameter 299 nm), there are $\frac{100\ \mu\text{m} - 10\ \mu\text{m}}{1.299\ \mu\text{m}} \approx 69$ fibers in the clot domain. Constraints on computational time motivate the use of a variable space step that ranges in nondimensional size from 2^{-10} to 2^{-14} (Figure 2.2).

We assume that bound plasminogen is initially in equilibrium with the plasma plasminogen at concentration $p_0 = 0.5$ μM, and that only specific doublets are exposed. A quasi-steady state analysis for $s^{0,0}$ and $s^{0,2}$ in the presence of this free plasminogen gives initial conditions

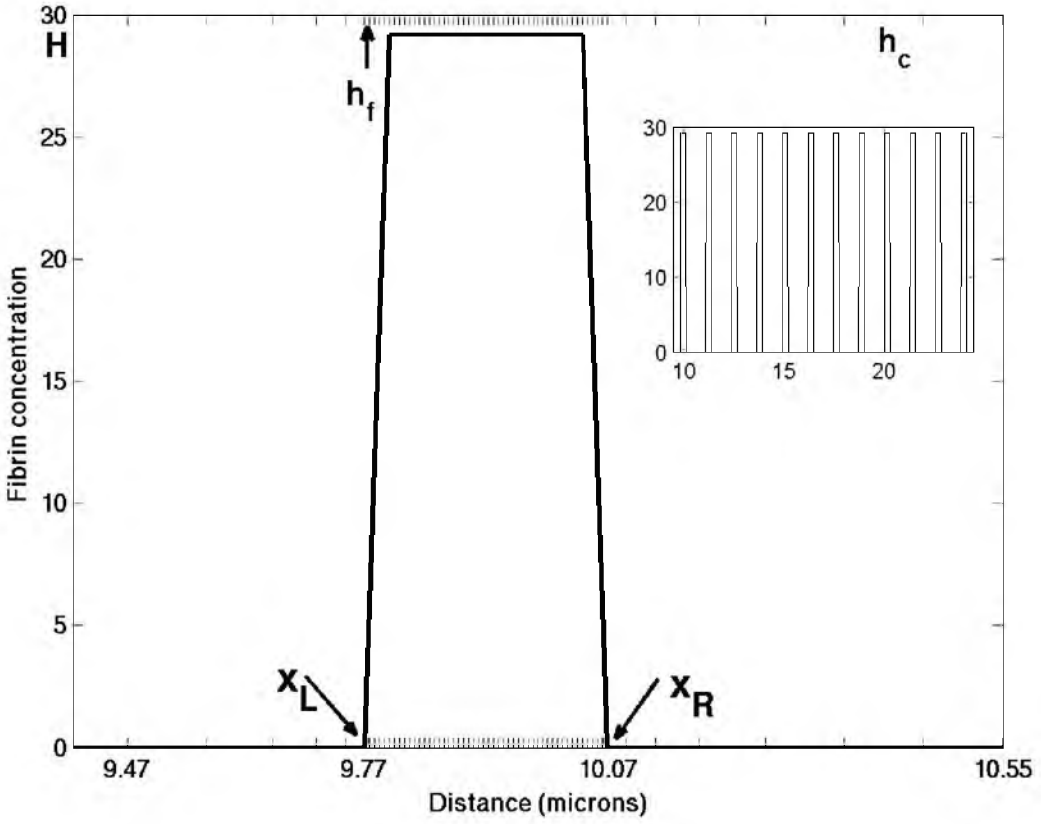

Figure 2.2. Fibrin concentration in a region of the heterogeneous model containing one fiber. Position along the clot, measured in microns, is indicated on the horizontal axis. The total clot length is 100 μm. Fiber width is indicated by the nonzero region of the black curve. x_L denotes the left edge of the fiber, x_R denotes the right edge, and H denotes the fibrin concentration within the fiber. Tick marks on the horizontal axis correspond to the numerical grid spacing used in solving the equations. A coarse step, h_c, is used in fiber-free regions of the domain. A fine step, h_f, is used in regions of the domain containing fibers. Four progressively smaller steps are used to transition from h_c to h_f, and those same steps are used in ascending order to transition from h_f to h_c. Inset: A portion of the clot domain before lysis begins. Axes are the same as in main figure. The first fiber is the same one shown in the large figure, and is the first fiber in the clot – there is no fibrin to the left of this fiber. The pattern of fibers continues in this manner to fill the rest of the domain.

$$s^{0,0}(x,0) = \frac{k_{\text{off}}^{\text{p},0,2} s_{tot}}{(k_{\text{on}}^{\text{p},0,0} p_0 + k_{\text{off}}^{\text{p},0,2})} \cdot \chi, \quad \text{and} \tag{2.1}$$

$$s^{0,2}(x,0) = (s_{tot} - s^{0,0}(x,0)) \cdot \chi, \tag{2.2}$$

where s_{tot} is the total specific binding site density, taken to be 1 μM. Because fibrin is concentrated in fibers, the initial conditions involve χ, the initial clot indicator function:

$$\chi = \begin{cases} \frac{H}{5h_f}(x - x_L(i)) & \text{if } x_L(i) \le x \le x_L(i) + 5h_f \\ \frac{H}{5h_f}(x - x_R(i)) & \text{if } x_R(i) - 5h_f \le x \le x_R(i) \\ H & \text{if } x_L(i) + 5h_f < x < x_R(i) - 5h_f \\ 0 & \text{otherwise,} \end{cases} \tag{2.3}$$

for $i = 1, 2, \ldots, N_f$ (total fiber number), where H is the height of the trapezoid, h_f is the finest numerical space step, and $x_L(i)$, $x_R(i)$ are the left-most and right-most points in fiber i, respectively (Figure 2.2). All other specific and nonspecific doublets are initially zero. Fibers are aggregates of protofibrils, 2-stranded fibrin polymers in which each strand is composed of 3 chains: α, β, and γ [?]. We assume that degradation of a single protofibril requires six cuts (one for each chain), and we take the total fibrin concentration to be 6 μM. This means the concentration of potential, unexposed binding doublets is 5 times the concentration of specific doublets, $n(x,0) = 5 \cdot s_{tot} \cdot \chi$. At the start of each experiment, a 5×10^{-3} μM bolus of tPA is added in the fibrin free region to the left of the clot (smoothed using a hyperbolic tangent function). The boundary conditions for tPA and PLG at $x = 0$ and $x = 1$ (nondimensional end of the domain) are:

$$\begin{aligned} \frac{\partial a(0,t)}{\partial x} &= 0, \\ p(0,t) &= p_0, \\ \frac{\partial a(1,t)}{\partial x} &= \frac{\partial p(1,t)}{\partial x} = 0. \end{aligned} \tag{2.4}$$

The initial and boundary conditions described above (Equations (2.1), (2.2) and (2.4)), along with Equations (B.1) - (B.19) (Appendix B), comprise the entire model. These equations hold regardless of clot heterogeneity, which requires only a different definition of the clot function, χ.

2.2 Results

The model equations are nondimensionalized and solved numerically using a fractional step method with a Crank-Nicholson scheme for the diffusion and a second-order Runge-Kutta method for the reactions. For the parameter values in Table 2.2, the homogeneous model predicts that lysis proceeds as a front (Figure 2.3). Free PLG concentrations remain roughly constant and bound concentrations of tPA, PLG, and plasmin are all elevated at the lysis front, in qualitative agreement with experiments [?, ?]. Bound PLG concentrations are predicted to be five times higher at the lysis front compared to the initial bound concentration, with elevated concentrations over an average distance of 34.2 μm, about one-tenth of the domain length.

The homogeneous fibrin model displays important features of lysis, but is unable to

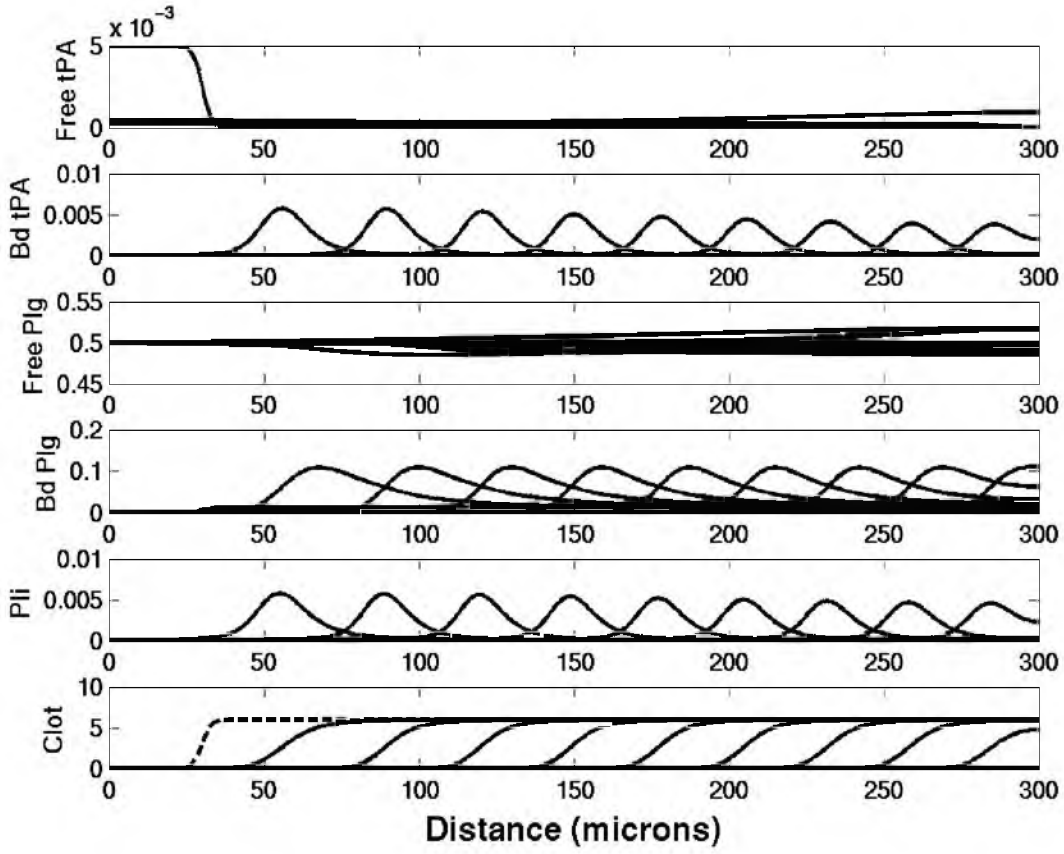

Figure 2.3. Dynamics of the homogeneous fibrin model. Total run time is 30 minutes, with successive traces moving right each separated by 3 minutes. In the bottom panel, the dotted line indicates the initial clot function. The vertical axes are concentrations measured in μM. "Bd" means "bound".

predict the degradation of different types of clots. Based on the observation that blood clots contain highly concentrated fibrin *fibers* (and not uniform concentrations of fibrin throughout the clot volume), we study a heterogeneous fibrin model. We investigate differences in the lysis speeds of coarse and fine clots by using the same total fibrin concentration, with several different fiber configurations: a fine clot made of 69 299-nm-wide fibers spaced 0.976 μm apart; a coarse clot made of 42 476-nm-wide fibers spaced 1.66 μm apart; and as an extreme case, a very coarse clot made of ten 1886-nm-wide fibers spaced 7.03 μm apart. In each of these cases, the initial fibrin concentration per fiber (i.e., H, the value of the nonzero part of the piecewise clot indicator function) is 29.16 μM.

Since the model is one-dimensional, we must choose fiber widths in a way that reflects the two-dimensional geometry of the fibrin fibers. The amount of fibrin in a cross section of a thin fiber is the product of fiber cross sectional area, $\pi(r_{\text{thin}})^2$, and the concentration of fibrin in a thin fiber, c_{thin}. Likewise, the amount of fibrin in a cross section of a thick fiber is $c_{\text{thick}}\pi(r_{\text{thick}})^2$. If we assume the concentration of fibrin in a single fiber is the same regardless of fiber thickness, then $c_{\text{thin}} = c_{\text{thick}}$ and the amount of fibrin in a thick fiber is related to the amount of fibrin in a thin fiber by the factor $(\frac{r_{\text{thick}}}{r_{\text{thin}}})^2$. Taking W^{1D}_{thin} (the width of a 1-D thin fiber) to be equal to r_{thin} gives the following equation for the 1-D width of a thick fiber:

$$W^{1D}_{\text{thick}} = \left(\frac{r_{\text{thick}}}{r_{\text{thin}}}\right)^2 W^{1D}_{\text{thin}} = \frac{(r_{\text{thick}})^2}{r_{\text{thin}}}. \tag{2.5}$$

The amount of fibrin in a fiber cross section does not scale linearly with radius, so rather than simply use the 2-D radius as our 1-D fiber thickness, we compute the 1-D thickness using Equation (2.5). Using experimentally measured radii [?], Equation (2.5) gives a 1-D thick fiber width of 476 nm.

We explore the effect of fibrin concentration per fiber on lysis speed using two simulated clot structures: a coarse clot with 42 376-nm-wide fibers spaced 1.86 μm apart and fibrin concentration per fiber 37.32 μM (henceforth referred to as a "thick, tall" clot because a higher fibrin concentration results in a taller trapezoid); and a very coarse clot with ten 751-nm-wide fibers spaced 8.2 μm apart and fibrin concentration per fiber 75.06 μM (henceforth referred to as a "very thick, tall" clot). These concentrations are calculated by keeping the total number of fibers constant and adjusting the fiber widths and pores sizes. For the coarse clot, the fiber diameter is taken from experiments [?], and for the very coarse clot, the fiber diameter is back-calculated using Equation (2.5). Once we know the number

Table 2.3. Heterogeneous model results. Unless otherwise noted, parameters from Table 2.2 were used. Each simulation was run for one diffusion time (200 seconds). After 200 seconds, the total remaining amount of fibrin was calculated to obtain the percent of clot remaining. "Published k_D" means $k_D^a = 0.36$ μM, $k_D^p = 38$ μM; "small k_D" means $k_D^a = 0.0036$ μM, $k_D^p = 0.38$ μM.

Type of fibers	**Fiber width (nm)**	**Pore size (μm)**	**Concentration of fibrin per fiber (μM)**	**Percent remaining (published k_D)**	**Percent remaining (small k_D)**
thin	299	0.976	29.16	61.3%	39.3%
thick	476	1.66	29.16	61.8%	36.7%
very thick	1886	7.03	29.16	60.8%	26.2%
thick,"tall"	376	1.86	37.32	62.2%	33.8%
very thick ,"tall"	751	8.2	75.06	60.6%	7.1%

of fibers and fiber diameter, we calculate the pore size and choose the fibrin concentration per fiber such that the total fibrin concentration in the clot is 6 μM.

Contrary to experimental evidence [?], this model predicts no appreciable difference in the lysis rates for the different clot types (columns 1-5 of Table 2.3). With dissociation constants from the literature, the lysis front moves at the same speed regardless of clot structure (Figure 2.4, gray lines). The model does, however, exhibit a wave-like motion of lysis and higher concentrations of bound enzymes at the lysis front compared to bound enzymes elsewhere in the clot (Figure 2.5).

To test if the model can produce different lysis rates for different clot structures, we increase the binding rates of tPA and PLG by two orders of magnitude while keeping the unbinding rates fixed. This gives dissociation constants that are 100 times smaller than those presented in the literature, and also reflects a stronger binding of proteins to fibrin. Stronger binding reduces the effective diffusion of molecules into the clot, and as a result, bound enzymes localize near the lysis front (Figures 2.6 and 2.7), and lysis rates vary for different clot structures (Table 2.3, column 6 and Figure 2.4, black lines). Concentrations of free enzymes also peak near the clot front (Figure 2.8). The representation of 2-D fiber geometry in the 1-D model affects lysis speed; the thick, tall fibers (which have a higher fibrin concentration per fiber than the thin fibers), result in coarse clots lysing approximately 1.2-times faster than fine. In the very coarse, tall clot, with thicker fibers and wider pores, lysis speeds increase even more (up to 1.6-times the fine speed).

With the smaller dissociation constants ($k_D^a = 0.0036$ μM and $k_D^p = 0.38$ μM), the fibrin-bound concentration of PLG is roughly an order of magnitude higher than the initial

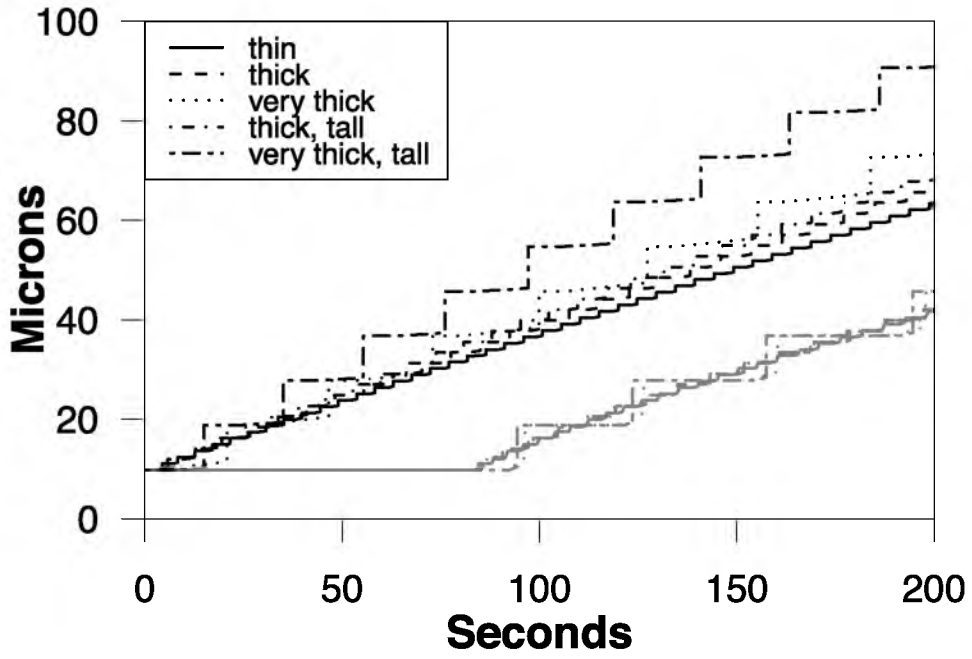

Figure 2.4. Comparison of lysis front velocities in different clot geometries, for published ($k_{\mathrm{D}}^{a} = 0.36$ μM, $k_{\mathrm{D}}^{p} = 38.0$ μM, gray lines) and small ($k_{\mathrm{D}}^{a} = 0.0036$ μM and $k_{\mathrm{D}}^{p} = 0.38$ μM, black lines) dissociation constants. The first location in the clot where the fibrin concentration remains at least 50% of the maximum concentration is plotted versus time. The lysis front velocities are the slopes of the lines fitted to the above data. The step-like appearance is due to the gaps between fibers. The lysis front must move across the fibrin-free space between the fibers before degradation begins on the next fiber, hence the step-like regions where the location of the front is not moving in time. The clots with thicker fibers have wider pores, so the steps are longer in these cases.

bound concentration in a small region at the front of the lysing clot (about 8.35 μm for fine clots and 11.4 μm for coarse clots, on average). The lysis front is much sharper than when dissociation constants from the literature are used, with almost an entire fiber being degraded before any lysis begins on the next fiber (Figure 2.6).

To measure the lysis rate of individual fibers we focus on the first fiber in the domain. Recording the time at which the average fibrin concentration in this fiber first reaches 10% of its initial concentration gives a measure of lysis time. Because the first fiber in the different clot types begins at the same position in the domain and we initialize tPA the same way regardless of clot type, we can compare the times it takes the first fiber to lyse for each case. With dissociation constants from the literature, a single thin fiber lyses slightly faster than a thick fiber, which lyses slightly faster than a very thick fiber: 72.5, 74.0, and 78.85 seconds, respectively (Table 2.4). With small dissociation constants there is more of an increase in lysis time with increasing diameter, but the predicted times are not physical (6.065, 7.415, and 20.415 seconds for thin, thick, and very thick fibers, respectively).

2.3 Discussion

The existence of a front of lysis moving through a clot when plasminogen activator is introduced at the clot edge is well supported in the experimental literature [?, ?, ?, ?]. With both spatially homogeneous and heterogeneous fibrin concentrations, our model predicts that lysis moves as a front with peaks in the concentrations of lytic proteins at the front. This confirms results from earlier modeling efforts [?, ?], although consistent with Wootton et al. [?], we find that attaining realistic lysis profiles necessitates using larger binding rates than those proposed by Diamond and Anand [?]. Even with adjusted binding rates, however, neither our homogeneous nor heterogeneous fibrin models, with dissociation constants taken from the literature, can quantitatively reproduce the protein concentration and

Table 2.4. Heterogeneous model single fiber results. Unless otherwise noted, parameters from Table 2.2 were used. The lysis time is defined as the time at which the average fibrin concentration in the fiber first reaches 10% of its initial concentration. "Published k_{D}" means $k_{\mathrm{D}}^a = 0.36$ μM, $k_{\mathrm{D}}^p = 38$ μM; "small k_{D}" means $k_{\mathrm{D}}^a = 0.0036$ μM, $k_{\mathrm{D}}^p = 0.38$ μM.

Type of fibers	**Fiber width**	**Lysis time (s) (published k_{D})**	**Lysis time (s) (small k_{D})**
thin	299 nm	72.5	6.065
thick	476 nm	74.0	7.415
very thick	1886 nm	78.85	20.415

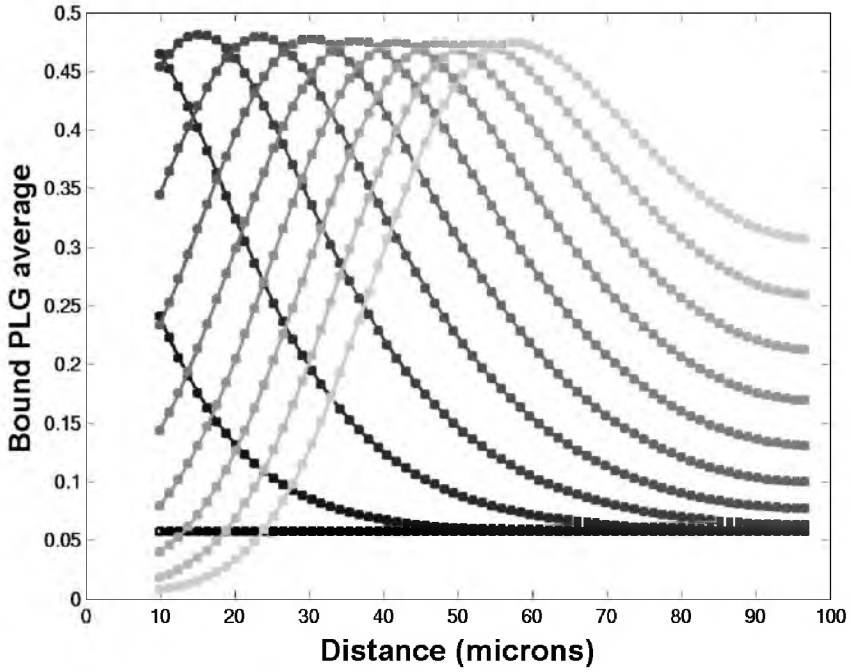

(a) Average concentration of bound PLG per fiber

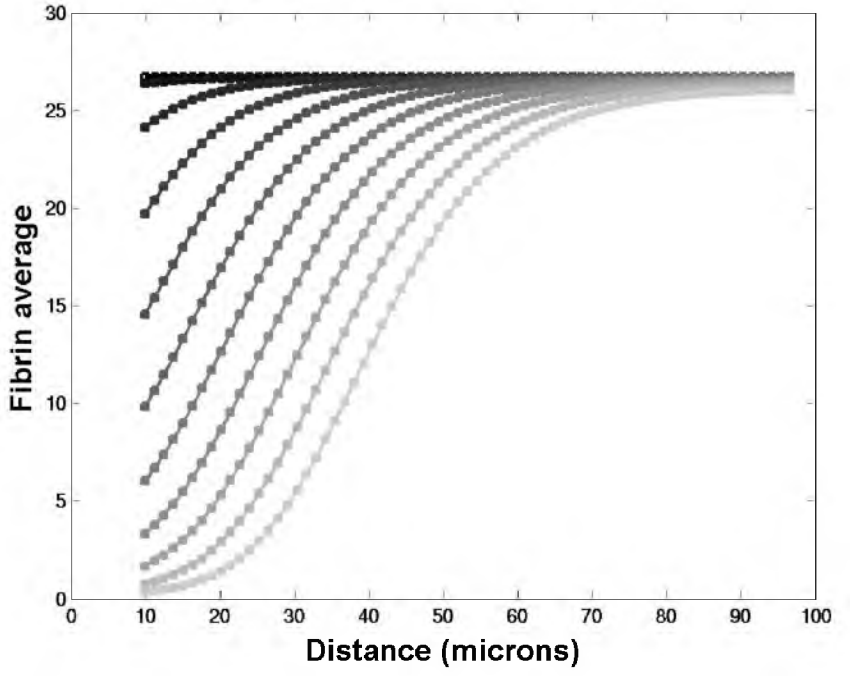

(b) Average concentration of fibrin per fiber

Figure 2.5. Average bound PLG and fibrin concentrations (μM) for the heterogeneous model in a fine clot with thin fibers and dissociation constants from the literature ($k_{\mathrm{D}}^{a} = 0.36$ μM, $k_{\mathrm{D}}^{p} = 38.0$ μM). Averages are plotted at the fiber midpoints. The open symbols denote the initial average concentration, and each successively lighter gray line is 20 seconds later than the one before it. (a) Bound PLG. (b) Fibrin.

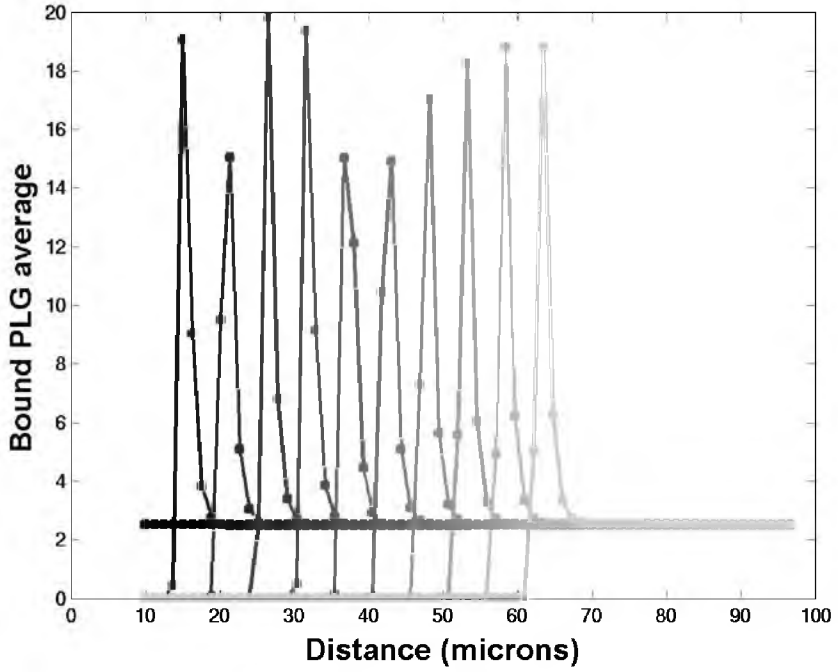

(a) Average concentration of bound PLG per fiber

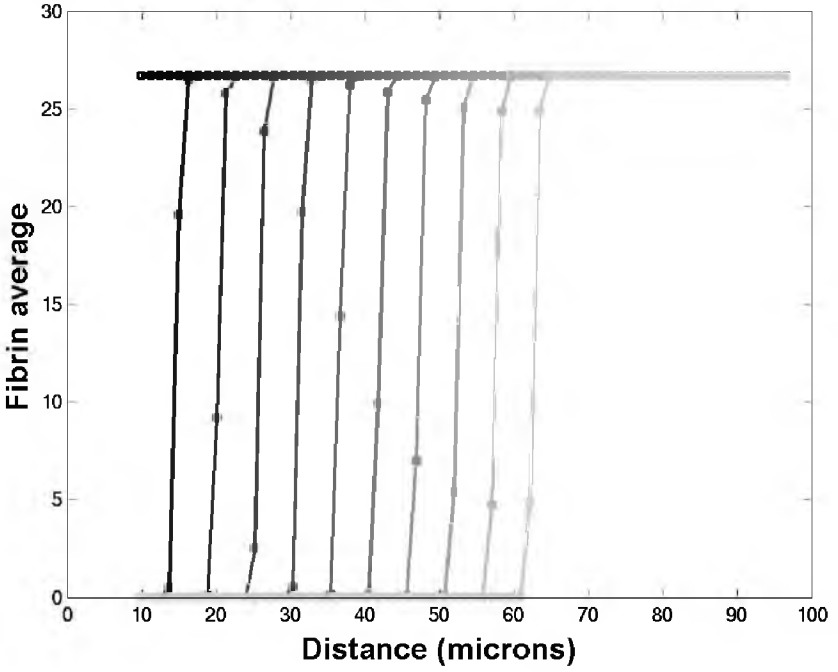

(b) Average concentration of fibrin per fiber

Figure 2.6. Average bound PLG and fibrin concentrations (μM) for the heterogeneous model in a fine clot with thin fibers and small dissociation constants ($k_{\mathrm{D}}^{a} = 0.0036$ μM, $k_{\mathrm{D}}^{p} = 0.38$ μM). Averages are plotted at the fiber midpoints. The open symbols denote the initial average concentration, and each successively lighter gray line is 20 seconds later than the one before it. (a) Bound PLG. (b) Fibrin.

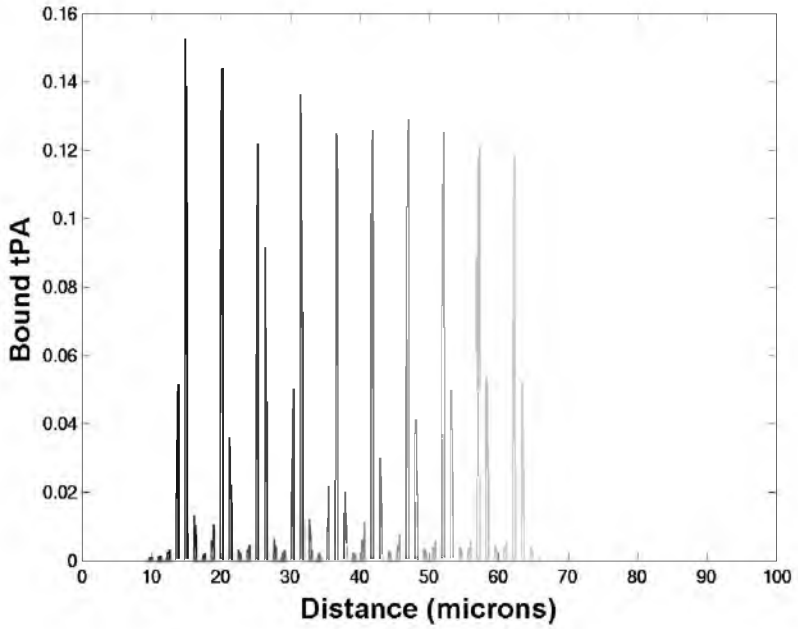

(a)

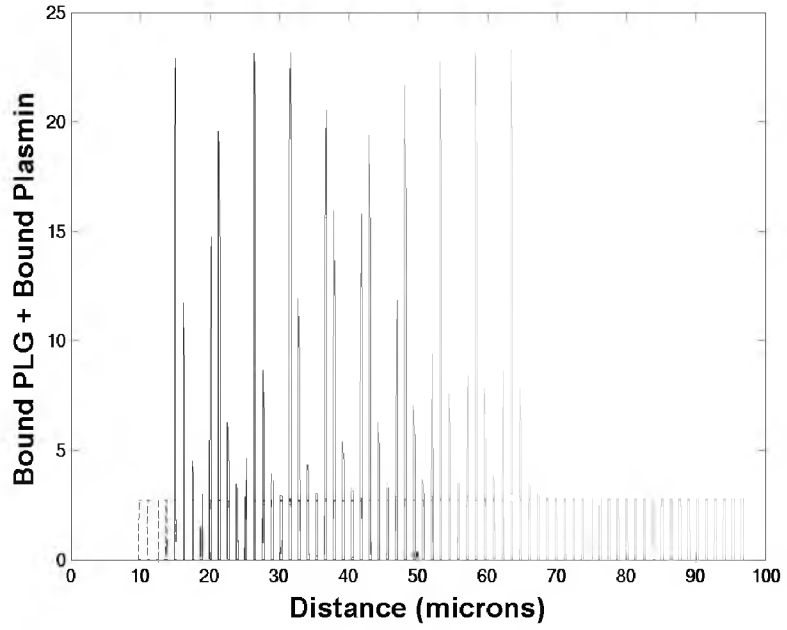

(b)

Figure 2.7. Bound lytic protein concentrations for the heterogeneous model of a fine clot with thin fibers and small dissociation constants ($k_{\mathrm{D}}^{a} = 0.0036$ μM and $k_{\mathrm{D}}^{p} = 0.38$ μM). (a) Bound tPA concentration. (b) Bound PLG plus plasmin concentration. In each plot, the dashed line denotes the initial condition, and each successively lighter shade of gray describes the given spatial distribution 20 seconds after the previous plot, for a total of 200 seconds. The peaks are different heights because the times that are plotted do not necessarily correspond to the lysis front speed. All concentrations are in μM.

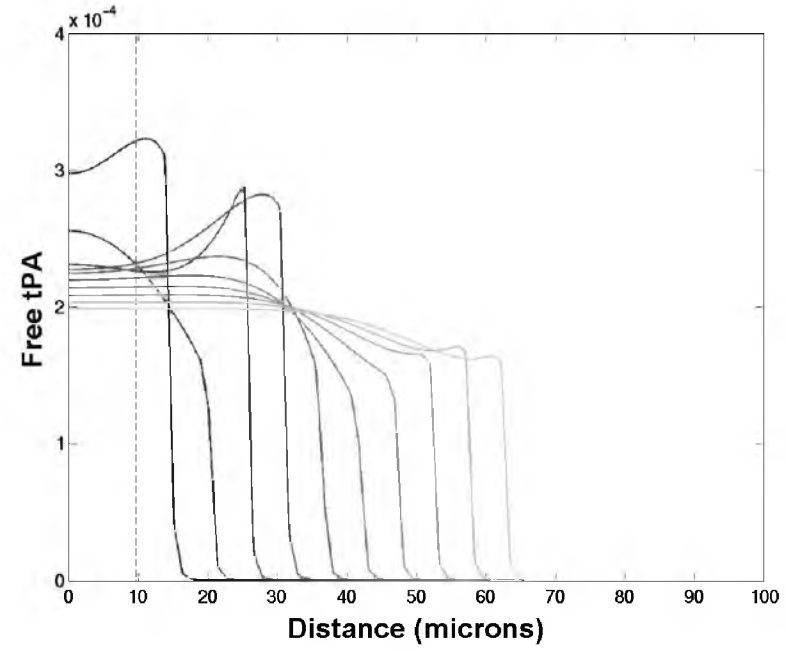

(a)

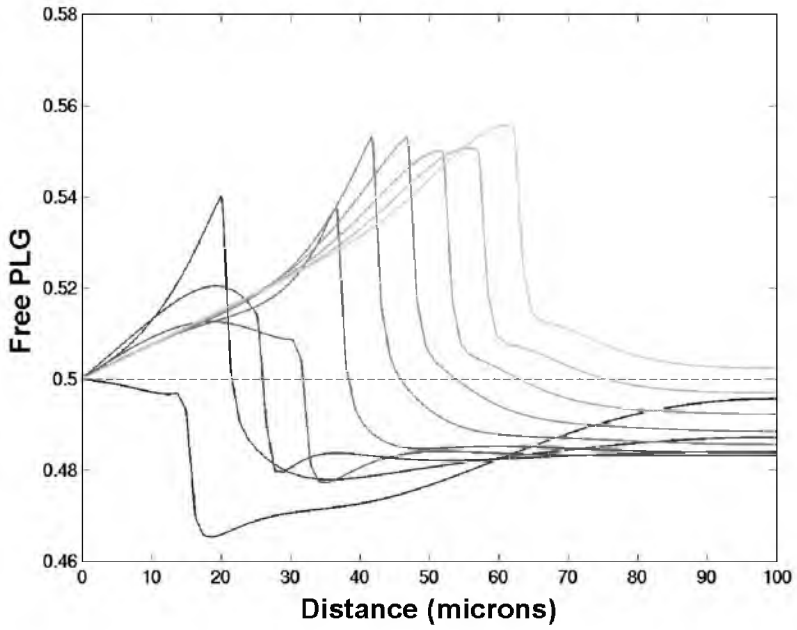

(b)

Figure 2.8. Free lytic protein concentrations for the heterogeneous model of a fine clot with thin fibers and small dissociation constants ($k_{\mathrm{D}}^{a} = 0.0036$ μM and $k_{\mathrm{D}}^{p} = 0.38$ μM). (a) Free tPA concentration. (b) Free PLG concentration. In each plot, the dashed line denotes the initial condition, and each successively lighter shade of gray describes the given spatial distribution 20 seconds after the previous plot, for a total of 200 seconds. The peaks are different heights because the times that are plotted do not necessarily correspond to the lysis front speed. All concentrations are in μM.

distribution results from Sakharov et al. [?]. There the authors report PLG concentrations in fibrin agglomerates on the lysis front to be 30 times higher than the concentration in the surrounding plasma, PLG concentrations in the 3-μm region comprising the lysis front to be 9 times higher than the plasma concentration, and PLG concentrations in a 20-μm-wide region adjacent to the front to be at least 2 times higher than the plasma concentration. The "peaks" of PLG in Figures 2.3 and 2.5 are wider (about 34.2 μm and 51 μm, respectively), and are barely higher than the free concentration (0.5 μM), but nonetheless are qualitatively similar to the Sakharov et al. results [?]. In reasonable quantitative agreement with Sakharov et al., the heterogeneous model with small dissociation constants results in peaks of PLG occurring in an 8-12 μm region at the lysis front, with a concentration almost 50 times higher than the plasma-phase concentration (Figures 2.7 and 2.8). These results are more consistent with Sakharov et al.'s data than any previous models. Wootton et al. show increases in plasma-phase enzyme concentrations at the lysis front, across distances of about 25-50 μm, but give no results for bound concentrations [?]. Diamond and Anand, in a model with permeation of proteins, find a high concentration of bound plasmin at the lysis front over a distance of about 2000 μm, with an increased concentration that is lower than the plasma-phase PLG concentration [?]. Our heterogeneous model accurately predicts the width of the region of accumulating proteins (8-12 μm), and is within a factor of 2 of the largest measured PLG increase (50 times higher than surrounding plasma concentration in our model vs. 30 times higher in the experiments by Sakharov et al. [?]).

In addition to using our model to investigate concentration profiles, we aim to explain why coarse clots lyse more quickly than fine clots, even when the total fibrin concentration is constant. When spatial heterogeneity of the clot structure is taken into account and parameter values from the literature are used, fine clots degrade at the same speed as coarse clots (Figure 2.4, Table 2.3). By lowering the tPA and PLG dissociation constants from the literature by two orders of magnitude, we observe localization of lytic enzymes at the front and variation in lysis rates for different clot structures (Figures 2.4, 2.6, 2.7, and 2.8). Stronger binding results in a decrease in the effective diffusion constant; molecules bind to fibrin and thus are prevented from diffusing farther into the clot. The tPA molecules remain bound until the fiber degrades, and it is only then that they can diffuse to the next fiber and initiate lysis. This localization of tPA results in sequential degradation of fibers, with one fiber degrading before degradation of the next fiber begins. Taking into account the fact that after tPA binds there is a delay before plasmin is produced and lysis begins

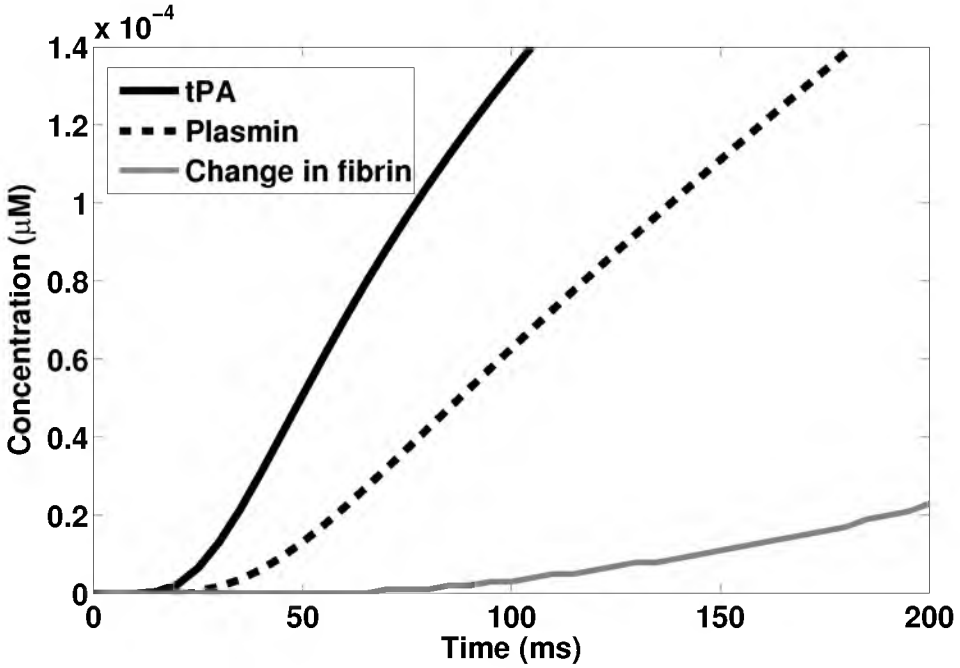

Figure 2.9. Delay in lysis after tPA binds. Average concentrations of tPA (solid black) and plasmin (dashed) bound to a single thin fiber in a fine clot are shown as functions of time. The change in fibrin concentration in the fiber (concentration at time 0 minus concentration at time t) is plotted in gray. There is a delay after tPA binds before plasmin is produced, and another delay after plasmin production before lysis begins, i.e., before the change in fibrin concentration is nonzero. These results were obtained using small dissociation constants ($k_{\mathrm{D}}^{a} = 0.0036$ μM and $k_{\mathrm{D}}^{p} = 0.38$ μM).

(Figure 2.9), we see how coarse clots can lyse faster than fine. When lysis is sequential (as when the smaller dissociation constants are used), the number of fibers in the clot is important; with fewer fibers, lysis needs to be started fewer times, and therefore there are fewer delays while plasmin is created. In this situation, a coarse clot with fewer fibers can lyse more quickly than a fine clot.

The large accumulation of lytic proteins appears to be the cause of the variation in lysis rates. Using dissociation constants from the literature, the increase in enzyme concentrations, and therefore lysis, occur over a larger region which contains multiple fibers. With smaller dissociation constants, almost complete lysis of one fiber occurs before degradation of any other fiber begins. This suggests that the number of fibers in a clot (and not their thickness) is the main determinant of lysis rate; with fewer fibers, the lytic process must be started fewer times, which outweighs the longer time required to degrade individual thick fibers. Lysis is slower in the thick and very thick clots compared to their "tall"

clot counterparts, because the number of fibers are the same, but fibers are thinner in the "tall" clots, allowing them to lyse more quickly. We cannot explain why it is necessary to have dissociation constants that are 100 times smaller than measured values in order for the model to predict that coarse and fine clots lyse at different rates. Either the meaning of the dissociation constant is different in the 1-D model compared to the experimental quantity, or a 1-D model is simply incapable of distinguishing between lysis of fine clots and lysis of coarse clots without significant assumptions (like rate constants that are orders of magnitude different than measured values). The challenge of determining whether either of these options explains our results remains to be resolved.

The heterogeneous fibrin model poorly predicts single fiber lysis – not only are the lysis times too fast, but the relative lysis times between fibers of varying diameter are too small. Experiments show that, on average, a thin fiber takes 3.1 minutes to degrade, while a thick fiber degrades in 5.4 minutes [?]. Therefore, a thin fiber lyses about 1.74 times faster than a thick fiber. With dissociation constants from the literature ($k_{\mathrm{D}}^{a} = 0.36$ μM and $k_{\mathrm{D}}^{p} = 38$ μM), our model predicts thin fibers lyse 1.021 times faster than thick fibers (74 s/72.5 s) and only 1.086 times faster than very thick fibers (78.75 s/72.5 s); essentially all fibers lyse in the same amount of time. With smaller dissociation constants ($k_{\mathrm{D}}^{a} = 0.0036$ μM and $k_{\mathrm{D}}^{p} = 0.38$ μM) the relative speeds increase, but the individual lysis times are unrealistically fast: thin fibers lyse 1.22 times faster than thick fibers (7.415 s/6.065 s) and 3.37 times faster than very thick fibers (20.415 s/6.065 s).

While model results for single fibers are qualitatively correct and show that thin fibers lyse faster than thick fibers, the results are not quantitatively accurate, perhaps for several reasons. First, our single fiber fibrin concentration may be too small. The fibrin concentration per fiber has been estimated to be about 824 μM [?, ?], significantly higher than the 29 μM we use. Second, the definition of lysis is likely different experimentally than it is in the model. We consider a fiber to be lysed when 90% of its initial fibrin concentration has degraded. Experimentally, lysis of a fiber is simply the time at which the fiber is no longer visible through the microscope. It is unclear how this relates to relative fibrin concentration. Finally, a 1-D model cannot account for transverse cutting. Real lysis seems to proceed by transverse cutting across fibers, but with only one dimension there is no way to model plasmin crawling across a fiber. We believe a higher dimensional model is required to study lysis of individual fibers.

An important feature of blood clots is the *mesh* of fibers. Fine clots contain more

fibers and have a higher density of branch points than coarse clots [?], which could affect the number of times lytic enzymes must initiate lysis. A 1-D model cannot capture the complicated geometry of a blood clot. This limitation of a 1-D model is demonstrated by the inability of the model to produce different fine and coarse front velocities upon inclusion of a more realistic, spatially varying fibrin concentration. Because clot structure plays an important role in the effectiveness of lysis, higher dimensional models are likely to be required in order to answer questions about the patterns and rates of lysis of different clot configurations.

Using a continuum model to investigate the fibrinolytic system may also be problematic because of the extremely low concentration of tPA. Even in experiments that inject a bolus of tPA at concentration 5 nM (much higher than the plasma concentration of 70 pM), there are only 3 tPA molecules per cubic micron in the clot. Assuming a pore size of 1 μm in a fine clot, the volume enclosed by nearest-neighbor fibers is on the order of 1 μm^3. This observation may partially explain why fibers are cut laterally, rather than uniformly degraded [?]. With 3 tPA molecules per cubic micron, there is a distinct possibility that a particular fiber will encounter only a single tPA molecule. That tPA molecule will facilitate the local creation of plasmin, but will not contribute to plasmin production outside of this local region. Thus, plasmin activity on the fibrin fiber will be concentrated to a narrow segment of the fiber length.

If there are only 3 tPA molecules in a characteristic volume of clot, it is not valid to treat tPA as a continuum. This observation, coupled with the conclusion that higher dimensional models are necessary to study lysis of individual fibers and of varying clot structures, motivates the development of a 3-D stochastic model described in Chapter 3.

CHAPTER 3

THREE-DIMENSIONAL STOCHASTIC MULTISCALE MODEL OF FIBRINOLYSIS

We want to elucidate the factors that influence lysis speeds in clots of varying structure, in an effort to suggest targets for the design of new therapeutics aimed at breaking up blood clots. If plasmin cuts across fibers, a coarse clot with fewer fibers to transect will presumably be degraded faster than a fine clot with a higher fiber density because fewer "cuts" have to be made. This explanation seems intuitive, however it is difficult to confirm both experimentally and with one-dimensional mathematical models (see Chapter 2). In the current chapter we use a multiscale mathematical model of fibrinolysis to show that fiber number impacts lysis speed, but so does the number of tPA molecules relative to the surface area of the clot exposed to those molecules. Depending on the values of these two quantities (tPA number and surface area), coarse clots lyse faster or slower than fine clots.

Our microscale model of single fiber lysis is described in detail in Section 3.1.1, and our macroscale model of full clot lysis is described in Section 3.1.2. Results from both models are presented in Section 3.2, and implications of these results are discussed in Section 3.3.

3.1 The model

In Chapter 2, we included spatial heterogeneity in a deterministic 1-D reaction diffusion model in an attempt study lysis of fine and coarse clots. We concluded that these types of models are insufficient, both qualitatively and quantitatively, to explore lysis speeds for varying clot structures. Here we develop a three-dimensional (3-D), stochastic, multiscale model of fibrinolysis of a fibrin clot formed in plasma. Because tPA appears in such low concentration (70 pM in plasma [?], but even the 5 nM concentration used in some experiments is only 3 molecules/μm^3 [?]), a deterministic model (based on reaction diffusion PDEs) is not appropriate; our stochastic model tracks individual tPA molecules rather than tPA concentrations. In contrast, the plasma concentration of PLG is 2 μM [?]. How the

model tracks PLG, as well as plasmin and fibrin, is described in detail below. The microscale model represents an individual fiber cross section, while the macroscale model represents the full, 3-D fibrin clot. Data collected from the microscale model is used in the macroscale model.

Experimental evidence suggests fibers are cut transversely [?, ?, ?], so we assume that lysis of a fiber can be approximated by the degradation of fibrin within a single cross section. Furthermore, we assume the cross section is an arrangement of protofibril cross sections. Each strand of a two-stranded protofibril has three chains, α, β, and γ (Figure 3.1), which must be cleaved by plasmin, for a total of six chains requiring cutting [?].

Terminology used from this point forward is as follows. A "binding site" is a structure on fibrin to which one of the proteins tPA, PLG, or plasmin can bind. A "binding doublet" is a pair of adjacent binding sites. A "binding location" is a physical region on a fiber where binding doublets are located. "Exposed binding doublets" are doublets to which proteins can bind. "Cryptic (or unexposed) binding doublets" are doublets that must be exposed by plasmin-mediated degradation before they are able to bind proteins. "Available binding sites" refers to all the binding sites on the surface of a fiber, which we assume are the binding sites accessible to tPA.

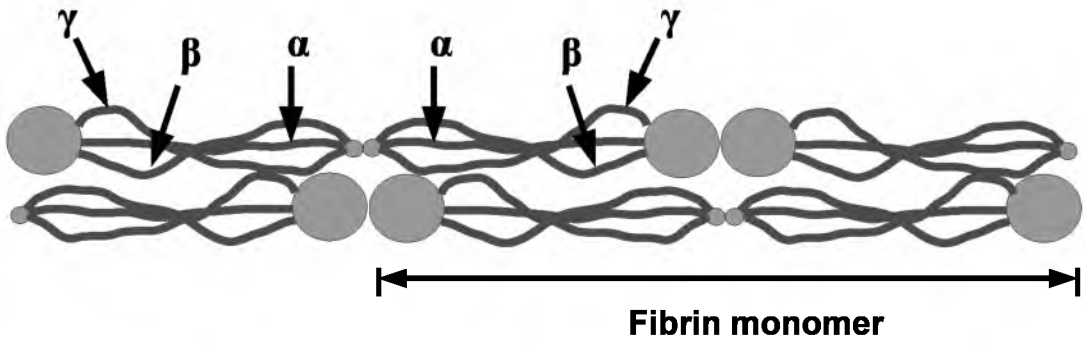

Figure 3.1. Schematic of a two-stranded protofibril. A protofibril is a linear aggregation of fibrin monomers. Each fibrin monomer has two pairs of three chains, α, β, and γ. Since a protofibril consists of two strands of half-staggered fibrin monomers, there are a total of 6 chains (two each of α, β, and γ) that must be cut by plasmin to degrade the protofibril.

3.1.1 Microscale model

Biochemical reactions that occur in a fiber cross section are considered in the microscale model. To simplify the numerics, the domain is a square of equal area to a circular fiber cross section. A thin cylindrical fiber with diameter 100 nm has cross sectional area $A = \pi(50\,\text{nm})^2 \approx (90\,\text{nm})^2$, so we use a square domain with side 90 nm. Plasminogen and tPA binding sites are located 6 nm apart across a fiber [?], yielding 15 binding locations along a distance of 90 nm. This gives a total of 15^2 equally-spaced binding locations within the square domain (Figure 3.2(c)). A thick fiber (200 nm diameter) has 30^2 binding locations. Each binding location is a physical region containing a specified number of binding doublets (Figure 3.2(d)), which are pairs of binding sites to which tPA, PLG, or plasmin can bind. Initially each binding location contains one exposed doublet, with five other cryptic doublets that can be exposed by plasmin-mediated cleavage. We think of a binding location as a cross section of a protofibril, and that the 6 binding doublets represent the 6 protofibril chains.

Several different reactions are included in the microscale model (Figure 3.3). The enzymes tPA, PLG, and plasmin bind to, and unbind from, binding doublets distributed throughout the domain. When tPA and PLG are bound to the same doublet, tPA can activate PLG to plasmin. It is believed that PLG molecules are small enough to diffuse freely through pores in the fiber [?], so we assume that PLG from the plasma phase can bind anywhere within a fiber cross section. Our calculation in Appendix A seems to contradict the idea that PLG can diffuse through a fiber; however, since PLG is present while fibrin fibers form, it is still reasonable to assume that PLG can be bound anywhere in a fiber cross section. We assume that the binding affinity of tPA to fibrin is so strong that tPA only binds to doublets on the fiber surface, even though it is capable of diffusing through the fiber ($k_D^{\text{tPA}} = 0.36\ \mu\text{M}$ [?]). When plasminogen and tPA unbind from doublets, they return to the plasma phase. When plasmin unbinds, we imagine it is preparing to crawl to a neighboring binding site or binding location (i.e., within a protofibril or to a neighboring protofibril), as proposed in Weisel et al. [?], rather than entering the plasma phase. This protects the plasmin from strong plasma-phase inhibitors, and consequently prevents the loss of plasmin molecules from the system. Plasmin crawling will be discussed in more detail in the following paragraph.

A binding doublet, which represents a portion of a fibrin monomer, can be degraded by a bound plasmin molecule. When a doublet is degraded, all proteins bound to it are

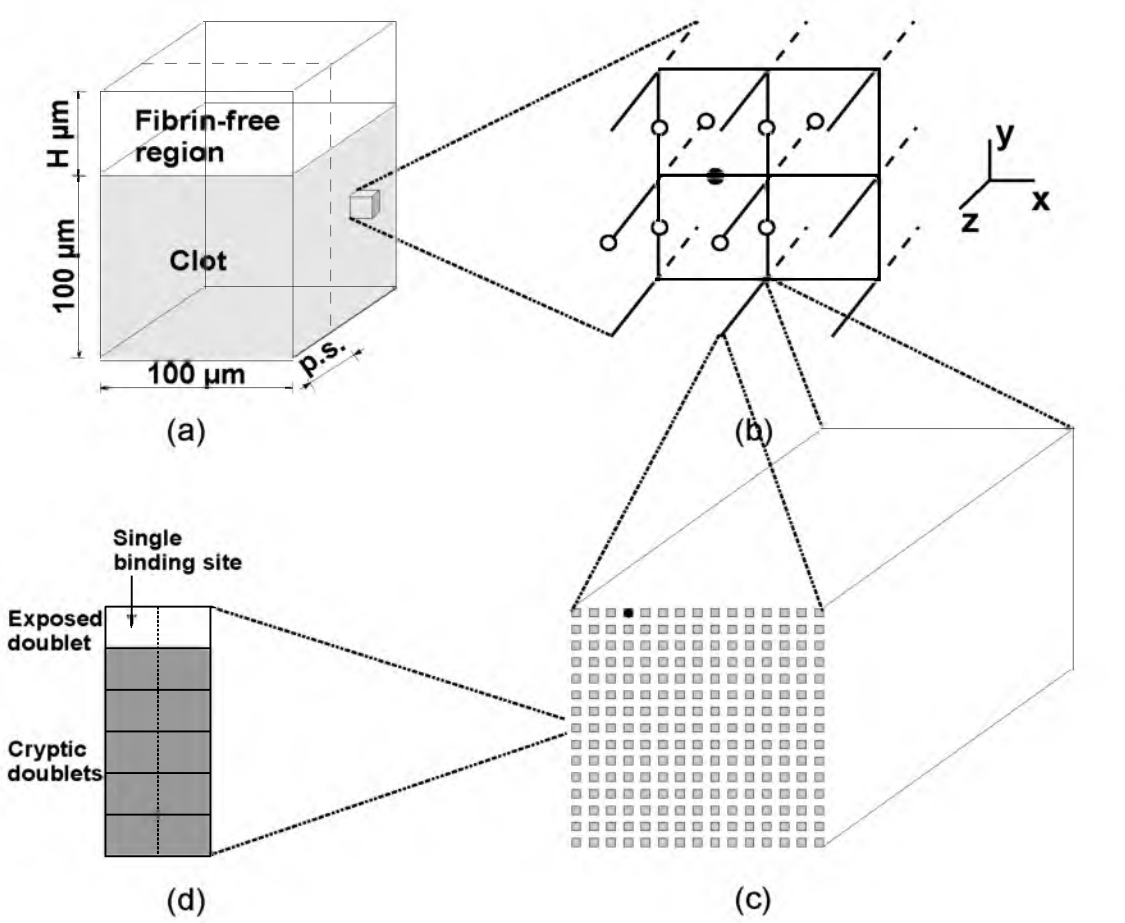

Figure 3.2. Schematic of multiscale model. (a) Diagram of macroscale clot. The clot is formed in a chamber with a fibrin-free region in which tPA is added. When we simulate the model, we only consider a 100-μm $\times$ 100-μm $\times$ $p.s.$ (pore size) periodic slab of the clot, denoted by the dashed line. We consider fibrin-free regions of different sizes, so H (height of fibrin-free region) varies. (b) Macroscale diffusion of tPA on a lattice. White circles indicate the fibers that the tPA molecule (black circle) can reach in one time step. The tPA molecule can diffuse to the four neighboring edges in the plane of the page, diffuse out of the page to the two neighboring solid edges (which each represent half of a fiber extending out of the plane), or diffuse into the page to the two neighboring dotted edges (which represent half of the fibers extending into the plane). Boundary conditions are periodic in the z-direction, and reflecting in the other two dimensions. (c) Microscale domain for thin fiber. This is a 90 nm $\times$ 90 nm square domain with 225 binding locations (gray squares) spaced 6 nm apart (not drawn to scale). One tPA molecule (black dot) is randomly placed on a doublet in the first row of the domain, which represents the fiber surface. (d) One binding location. Each binding location initially contains one exposed doublet (white boxes) and five unexposed doublets (gray boxes). A binding doublet is composed of two binding sites.

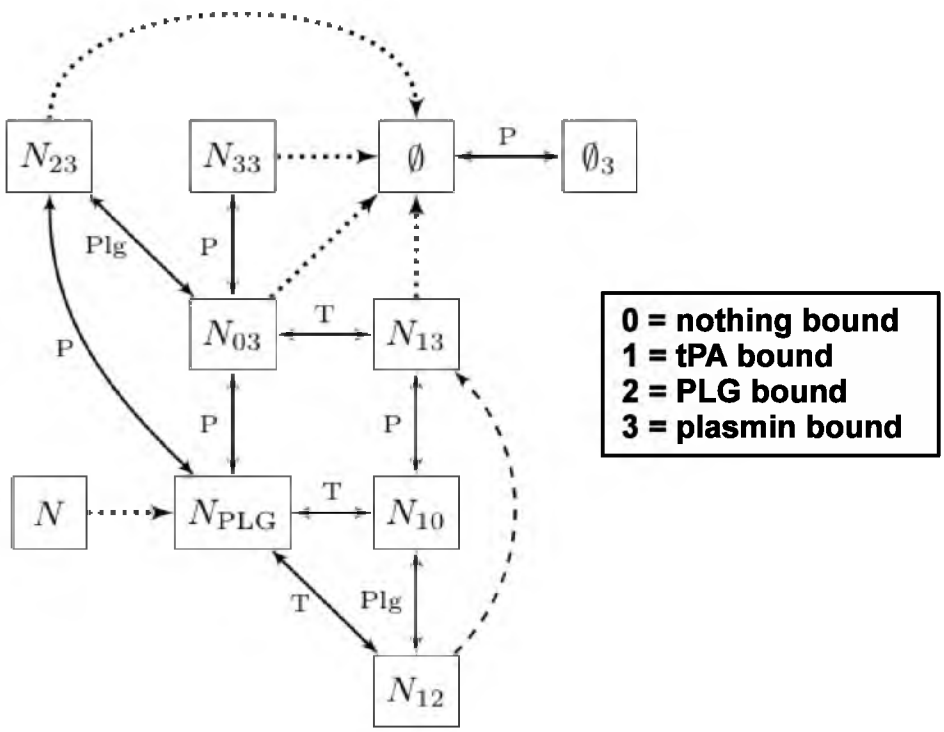

Figure 3.3. Microscale model reaction diagram. The arrows show the possible reactions for each time step. Solid arrows indicate binding and unbinding of enzymes, with letters identifying which enzyme is involved (T is tPA, P is plasmin, and Plg is plasminogen). Dashed arrow indicates activation of plasminogen to plasmin, and dotted arrows indicate plasmin-mediated degradation of doublets or exposure of cryptic binding sites. A note on notation: N_{ij} is a doublet with species i and j bound, for i, j=0 (nothing), 1 (tPA), 2 (PLG), or 3 (plasmin). N is a cryptic doublet, and N_{PLG} is a doublet with only plasminogen or nothing bound (N_{22}, N_{02}, or N_{00}). $\emptyset$ is a degraded doublet, and $\emptyset_3$ is a degraded doublet with a bound plasmin molecule.

immediately released and treated as if they had unbound. We assume that PLG and tPA are no longer able to bind to this degraded doublet. However, because we assume that plasmin is never entirely unbound, but rather crawls to neighboring doublets in the cross section, we allow plasmin to move anywhere in the domain, regardless of whether or not the doublets are degraded. We imagine plasmin cuts a "groove" in the fiber, with frayed ends of protofibrils on either end of the groove. By assuming that there are always frayed ends of fiber to which plasmin can crawl, we allow plasmin to occupy a doublet that has been degraded, but do not allow it to degrade that doublet any further. However, bound

plasmin can expose initially cryptic doublets at whatever binding location it occupies, even if it is bound to a degraded doublet. We assume that only one plasmin molecule can be bound to a particular degraded doublet.

Our simulation of the lytic process begins with one tPA molecule placed randomly on the surface of the fiber (the first row of the computational domain, Figure 3.2(c)). Because tPA is found at low concentrations, we consider only cross sections with a single tPA molecule. We apply the Gillespie algorithm [?, ?] to find the event times for the various microscale reactions depicted in Figure 3.3. The Gillespie algorithm gives a statistically exact realization of the process described by the master equation,

$$\frac{\partial P}{\partial t}(\underline{x}, t|\underline{x}_0, t_0) = \sum_{j=1}^{22}[a_j(\underline{x} - \underline{v}_j)P(\underline{x} - \underline{v}_j, t|\underline{x}_0, t_0) - a_j(\underline{x})P(\underline{x}, t|\underline{x}_0, t_0)].$$

Here $P(\underline{x}, t|\underline{x}_0, t_0)$ is the probability that the system is in state $\underline{x}$ at time t having been in state $\underline{x}_0$ at time t_0. Given the current state $\underline{x}$ at time t, and the set of possible reactions and reaction rates as described by the stoichiometric vectors $\underline{v}_j$ and propensity function $\underline{a}$, the Gillespie algorithm makes provisional choices of the length of time after t that each possible reaction will happen. (See Appendix C for details about the Gillespie algorithm, $\underline{x}$, $\underline{v}_j$, $\underline{a}$.) The next time step (and associated event) is chosen to be the minimum of the Gillespie provisional reaction times.

We explicitly model only the doublets that contain tPA or plasmin. Empty doublets and doublets with only PLG bound are grouped into one state called N_{PLG} (see Figure 3.3 caption for explanation of notation). Assuming that PLG binding is in quasi-steady state gives us probabilities of PLG being on doublets. We do not model individual PLG molecules. The dissociation constant for PLG binding to fibrin changes depending on whether fibrin is intact or "nicked" (partially degraded): $k_D^{\mathrm{intact}} = 38\ \mu\mathrm{M}$, $k_D^{\mathrm{nicked}} = 2.2\ \mu\mathrm{M}$ [?, ?]. In the model, any doublet that was cryptic initially and became exposed is considered to be on nicked fibrin. The probability of a nicked or intact N_{PLG} being in state N_{00}, N_{02}, or N_{22} is calculated using the quasi-steady state assumption for PLG (Appendix D).

When a reaction releases the tPA molecule (either by unbinding or degradation of the doublet to which it was bound), we calculate the probability of the molecule rebinding to the same cross section, rather than diffusing away. If the tPA rebinds, we assume it binds to an available binding site on a doublet at most two binding locations away from where

it unbound. If the molecule does not rebind, we assume it has diffused away from the cross section, and is removed from the system, and that no more plasmin can be produced. We calculated the rebinding probability by solving a 3-D escape problem as described in Appendix E, and found that for the situation and parameters of relevance here, tPA essentially never rebinds.

We define lysis to be complete (i.e., the fiber to be cleaved) when a specific fraction (typically 2/3) of the total number of binding doublets (exposed plus unexposed) have been degraded by plasmin. We assume fibers are under tension [?], hence fibers snap after a percentage of binding doublets are degraded. Our assumption that both thin and thick fibers lyse when 2/3 of the doublets are degraded is reasonable if we assume that thick fibers are under four times as much tension as thin fibers. We present an intuitive justification for this assumption. Imagine we pull on a fine and on a coarse clot (described in the following section) with a fixed force in a fixed direction. The cross sectional areas of the two clots are the same, but there are different numbers of fibers in each area. In fact, there are about four times as many thin fibers in a given area as there are thick. So, if the same load is distributed among the given fibers, a single thick fiber must bear four times the load of a single thin fiber.

In summary, the microscale model is written algorithmically as follows:

1. Initialize the system, set t_{final}[1] (a prescribed final time), and randomly place one tPA molecule on the first row of binding locations.

2. Determine whether the tPA-containing doublet is N_{10} or N_{12} using the quasi-steady state approximation for PLG.

3. While $t < t_{\text{final}}$:

  a. apply Gillespie algorithm to each doublet containing a tPA or plasmin molecule to determine the next reaction event and associated time.

  b. assign the smallest time from step **a** as the next time step. Update t and use the corresponding event to update the system.

    i. If the event results in the unbinding of tPA, calculate the rebinding probability to determine whether tPA rebinds or is removed. For our parameters, tPA is always removed.

[1] t_{final} is sufficiently large so that it does not interrupt degradation of a fiber undergoing lysis

ii. If the event results in the unbinding (i.e., crawling) of plasmin, randomly assign plasmin to an available binding site on a neighboring binding location (it is allowed to stay on its current binding location), and update the state of the new doublet.

d. calculate the percentage of degraded doublets.

i. If degradation $< 2/3$, return to step **a**.

ii. If degradation $\geq 2/3$, stop the algorithm because lysis is complete.

4. If $t \geq t_{\text{final}}$, algorithm terminates and lysis fails.

From the microscale model we save the time tPA unbound from the cross section (the tPA leaving time), the number of plasmin molecules that were created, and the time at which lysis completed (the lysis time). We use this information from hundreds of microscale model simulations to create distributions that we use in the macroscale model.

3.1.2 Macroscale model

Data generated from the microscale model are used in a macroscale model of clot lysis. We make the simplifying assumption that the clot is a 3-D square lattice (rather than a tangled mesh of fibers), with each lattice edge representing one fiber. Pore size, defined as the distance between fibers, is the length of one fiber. To mimic experiments, the clot is assumed to be contained in a small chamber with volume V = depth $\times$ width $\times$ height (Figure 3.2(a)). We assume the width and height of the chamber are equal, and that the depth of the chamber is of the same order of magnitude. Rather than model the full 3-dimensional system, we consider a periodic slice of clot, with depth equal to a single pore size. We think of this slice as running between edge midpoints, so the 1-fiber-depth is actually composed of two halves of two separate fibers. To obtain the lattice dimensions we fix the fibrin concentration per fiber at 824 μM [?, ?], the fibrin concentration in the clot at 8.8 μM [?], and the height and width of the chamber at 100 μm (to assure the system is big enough to avoid boundary effects). Then using the radii of the fibers, we calculate the pore size and the number of fibers required to keep the concentrations at their fixed values. This results in a fine clot with 13,333 fibers and pore size 1.42 μm, and a coarse clot with 3,400 fibers and pore size 2.84 μm. N, the number of nodes in one row of the lattice, is thus equal to 67 for a fine clot and 34 for a coarse clot.

A fibrin-free space of height H extends above the clot chamber (Figure 3.2(a)). We fill this fibrin-free volume with a tPA solution to mimic a therapeutic bolus of tPA administered at the edge of a clot (this also mimics many *in vitro* experiments). We prescribe the initial tPA concentration in the fibrin-free space and we can vary the bolus size by changing H. The tPA molecules are uniformly distributed on ghost lattice edges in this fibrin-free volume. These edges are arranged in the same square lattice formation as the clot, but they do not contain fibrin and hence cannot be degraded.

Since our aim is to compare macroscale lysis velocities between two different clots, it is necessary to use the same total fibrin concentration in both fine and coarse clots, and to use the same relative amount of tPA to initiate lysis. We imagine the coarse and fine clots are formed in the same size chamber, so their volumes are equal. Since we only model a periodic slab of each clot, of depth equal to pore size, and because the pore size is twice as big in the coarse clot, the volume of clot (as well as the volume of the fibrin-free region) is also twice as big. Therefore, we put twice as many tPA molecules in the fibrin-free region abutting the coarse clot as we do in the fine clot. This assures that the total tPA concentration averaged over the fibrin-free volume is conserved.

Detailed biochemistry was considered in the microscale model, so the macroscale model includes only tPA binding, unbinding, and diffusion, as well as degradation of fibers. When a tPA molecule binds to a fiber it initiates the lytic cascade on the microscale. The molecule is assigned a leaving time using the microscale model leaving-time distribution. When the current time is greater than or equal to the leaving time, the tPA molecule unbinds. Using microscale data, the tPA leaving time determines the number of plasmin molecules that will be created in that particular cross section. The number of plasmin molecules determines the time it will take the fiber to be cut (see Section 3.2.1.3 for more details). In this way, every edge to which tPA binds has an associated degradation time. When the current time is greater than or equal to an edge's degradation time, the edge is degraded and any tPA still bound to it is released.

During each fixed time step, we allow tPA to bind or unbind and any unbound tPA to move by diffusion to a neighboring fiber. tPA in the fibrin-free region can only diffuse, as there is no fibrin to which it may bind. Reflecting boundary conditions are imposed on the four sides of the clot adjacent to the walls of the microchamber, and periodic boundary conditions are imposed in the small third dimension since we consider a periodic slab of clot.

The size of the fixed time step used in the macroscale model is the typical time needed for one molecule to diffuse to one of the eight neighboring edges. In the simulations, we associate every tPA molecule with a particular edge so that all the macroscale events happen on the lattice edges. By associating each tPA molecule with one edge, we approximate the 3-D diffusion problem by having tPA hop on the lattice (Figure 3.2(b)). In this approximation, we think of an unbound molecule associated with an edge as being anywhere within a small distance of that edge, not necessarily directly on the fiber. A bound tPA molecule is bound directly to the edge on which it resides, but we do not model the exact location of tPA on a fiber, only which fiber tPA occupies. For simplicity in deriving the macroscale diffusion rules, we assume that molecules associated with a particular edge are located at the fiber midpoint (white circles in Figure 3.2(b)). When multiple tPA molecules are bound to the same fiber, we assume they are bound to different binding sites along the length of the entire fiber (and therefore capable of starting lysis in different cross sections), but for the purpose of diffusion we still consider them to be at fiber midpoints. The degradation time for an edge with multiple bound tPA molecules is the minimum of the times obtained for each molecule. Since tPA can still diffuse in the whole domain regardless of degradation status of edges, tPA molecules may be associated with degraded edges, but cannot bind to them.

To derive the time it takes a molecule to diffuse to a neighboring fiber, consider a tPA molecule on one of the horizontal edges (Figure 3.2(b)). A neighboring edge is defined as one of the eight closest edges, as measured diagonally from the edge midpoint. So the neighboring edges of a fiber oriented in the x-direction will be oriented in the y- and z-directions, since these are closer, diagonally, than any other x-direction edges. Let $P^n_{i,j,k}$ be the probability of a tPA molecule being at edge i, j, k at time n. Let q be the probability of its moving to a neighboring edge. Then

$$\begin{aligned} P^{n+1}_{i,j,k} &= (1-q)P^n_{i,j,k} + \frac{q}{8}\big\{P^n_{i-1,j+1,k} + P^n_{i+1,j+1,k} + P^n_{i+1,j-1,k} + P^n_{i-1,j-1,k} \\ &\quad + P^n_{i-1,j,k+1} + P^n_{i+1,j,k+1} + P^n_{i+1,j,k-1} + P^n_{i-1,j,k-1}\big\} \\ \Longrightarrow \Delta t\frac{\partial P}{\partial t} &\approx \frac{q}{8}\big\{P(x-\Delta x, y+\Delta y, z) + P(x+\Delta x, y+\Delta y, z) + P(x+\Delta x, y-\Delta y, z) \\ &\quad + P(x-\Delta x, y-\Delta y, z) + P(x-\Delta x, y, z+\Delta z) + P(x+\Delta x, y, z+\Delta z) \\ &\quad + P(x+\Delta x, y, z-\Delta z) + P(x-\Delta x, y, z-\Delta z) - 8P(x,y,z)\big\}. \end{aligned}$$

Expanding the right hand side gives

$$\Delta t \frac{\partial P}{\partial t} = \frac{q}{8}\left(4\Delta x^2 \frac{\partial^2 P}{\partial x^2} + 2\Delta y^2 \frac{\partial^2 P}{\partial y^2} + 2\Delta z^2 \frac{\partial^2 P}{\partial z^2}\right), \tag{3.1}$$

where $\Delta x = \Delta y = \Delta z = \frac{1}{2}$(pore size). Doing this derivation for a molecule on an edge in the y-direction results in the equation

$$\Delta t \frac{\partial P}{\partial t} = \frac{q}{8}\left(2\Delta x^2 \frac{\partial^2 P}{\partial x^2} + 4\Delta y^2 \frac{\partial^2 P}{\partial y^2} + 2\Delta z^2 \frac{\partial^2 P}{\partial z^2}\right), \tag{3.2}$$

while the derivation for a molecule on an edge in the z-direction results in the equation

$$\Delta t \frac{\partial P}{\partial t} = \frac{q}{8}\left(2\Delta x^2 \frac{\partial^2 P}{\partial x^2} + 2\Delta y^2 \frac{\partial^2 P}{\partial y^2} + 4\Delta z^2 \frac{\partial^2 P}{\partial z^2}\right). \tag{3.3}$$

Recall that if a tPA molecule moves, it *must* move onto an edge oriented in one of the other two directions. So there is biased movement away from fibers oriented in the same direction as the fiber with tPA. But because this is true for fibers oriented in all three principal directions, the overall diffusion is given by the average of Equations (3.1) - (3.3). This gives

$$\frac{\partial P}{\partial t} = D\nabla^2 P,$$

where $D = \frac{q}{12\Delta t}(\text{pore size})^2$ is the diffusion coefficient for tPA. Rearranging gives the macroscale time step:

$$\frac{\Delta t}{q} = \frac{(\text{pore size})^2}{12D}. \tag{3.4}$$

We do not explicitly know q, the probability of a molecule moving to a neighboring edge, but it does not matter since the ratio $\frac{\Delta t}{q}$ is fixed. As long as we choose a q that makes Δt small enough that our method converges, the actual choice of q does not matter. For the macroscale results presented in this chapter we use q=0.2, $D = 5 \times 10^{-7}$ cm^2/s so $\Delta t \approx 6.72 \times 10^{-4}$ s for a fine clot and 2.69×10^{-3} s for a coarse clot.

Because binding events occur continuously and independently, every time a tPA molecule unbinds or diffuses to a new edge, we use an exponential distribution to choose the time at which the molecule will bind to the edge:

$$t_{\text{bind}} = t - \frac{\ln(\hat{r}_1)}{k_{\text{on}}^{\text{tPA}} b} - \frac{\Delta t}{2},$$

where t is the current time, $\hat{r}_1$ is a random variable uniformly distributed on [0,1] ($\hat{r}_1 \in U[0,1]$), $k_{\text{on}}^{\text{tPA}}$ is the binding rate of tPA to fibrin, and b is the concentration of available tPA binding sites. We bind a molecule at time t (a multiple of Δt) if $t_{\text{bind}} \leq t$. The subtraction of a half time step, $\frac{\Delta t}{2}$, in the definition of t_{bind} eliminates bias in the algorithm and implies that binding actually occurs at the time t closest to t_{bind}. For the same reason, we also subtract $\frac{\Delta t}{2}$ from the degradation and unbinding times selected from the microscale model distributions.

The macroscale model is expressed algorithmically as follows:

1. Determine the clot geometry and Δt, set $t = 0$, fix t_{final} (a prescribed final time), and initialize the degradation times of all edges to 0.

2. Randomly place a specified number of tPA molecules in the fibrin-free region.

3. For $t \leq t_{\text{final}}$:

    a. set $t = t + \Delta t$.

    b. degrade any edges with nonzero degradation times $\leq t$, and unbind any tPA molecules that were bound to the degraded edges.

    c. check the unbinding times for all bound tPA molecules, unbind any with times $\leq t$.

    d. assign each newly unbound molecule a binding time, t_{bind}.

    e. for each unbound molecule, pick a random number $\hat{r} \in U[0,1]$ and

        i. if $\hat{r} \leq (1-q)$, the molecule does not move.

            A. If $t_{\text{bind}} > t$ or the edge has already been degraded, the tPA molecule remains unbound.

            B. If $t_{\text{bind}} \leq t$ and the edge the molecule is on has not been degraded, bind the molecule and use the microscale distributions to find the new unbinding time, the number of plasmin molecules produced, and the degradation time for that fiber.

        ii. if $\hat{r} > (1-q)$, the molecule has the opportunity to move, but may bind before it can do so.

            A. If $t_{\text{bind}} > t$ or the edge has already been degraded, randomly move the tPA to a neighboring edge and calculate a new binding time for the tPA to that edge.

B. If $t_{\text{bind}} \leq t$ and the edge the molecule is on has not been degraded, pick a random number, $\hat{r}_2 \in U[0,1]$.

I. If $\hat{r}_2 > \frac{(t-t_{\text{bind}})}{\Delta t}$, then movement happens before the tPA binds. Randomly move the tPA to a neighboring edge and calculate a new binding time for the tPA to that edge.

II. If $\hat{r}_2 \leq \frac{(t-t_{\text{bind}})}{\Delta t}$, the molecule binds and therefore cannot move. Use the microscale model distributions to calculate a new unbinding time, the number of plasmin molecules produced, and the degradation time for the fiber.

f. return to step **a.**

3.2 Results

3.2.1 Microscale model results

To explore the range of model behavior (and because not all parameter values have been measured), we use four different parameter sets, shown in Table 3.1. Since this is a stochastic model, we report the statistics of many independent simulations. The microscale model results presented in this section are given as median (first quartile Q1, third quartile Q3) of 600 simulations, and the macroscale model results are mean $\pm$ standard deviation of 10 simulations. In some instances of the microscale simulation, lysis of an individual fiber did not occur because tPA unbound before creating any plasmin. These failed runs are excluded from single fiber lysis time data since they would yield an infinite lysis time; the microscale results presented are therefore the average lysis times conditional upon successful lysis.

3.2.1.1 tPA leaving time

From the microscale model we obtain distributions of the tPA leaving time (the time at which tPA diffuses away from the cross section), the number of plasmin molecules produced, and the single fiber lysis time for thin and thick fibers for all parameter sets (Table 3.2). As expected, the thick fiber takes longer to degrade. Unexpectedly, for Case A and B parameters, tPA stays bound to the thick fiber slightly longer than it stays bound to the thin fiber, even though the same tPA binding and unbinding rates are used. The tPA unbinding rate in Cases A and B is small enough that tPA rarely unbinds. Instead, tPA

Table 3.1. Parameter sets used in the model. Case A is the baseline parameter set. tPA binding and unbinding rates are changed in Cases C and D, but the dissociation constant ($k_{\mathrm{D}}^{\mathrm{tPA}} = k_{\mathrm{off}}^{\mathrm{tPA}}/k_{\mathrm{on}}^{\mathrm{tPA}}$) remains fixed. The dissociation constant for PLG is different depending on whether fibrin is intact or nicked, and the dissociation constant for tPA is different depending on whether tPA is bound to a doublet with PLG or without PLG. k_{on}^{i} and k_{off}^{i} are the binding rate of species i to fibrin and the unbinding rate of species i from fibrin, respectively, for i=tPA, PLG, or plasmin (PLi). $k_{\mathrm{cat}}^{\mathrm{ap}}$ is the catalytic rate constant for activation of PLG to plasmin, $k_{\mathrm{cat}}^{\mathrm{n}}$ is the catalytic rate constant for plasmin-mediated exposure of cryptic binding doublets, and k_{deg} is the plasmin-mediated rate of fibrin degradation. We know the dissociation constants for tPA and PLG, but not the individual rates, so references in the table are for k_{D}. * Estimated.

Parameters	Case A	Case B	Case C	Case D	Reference
k_{deg} (s^{-1})	10	1	10	1	
$k_{\mathrm{off}}^{\mathrm{PLG}}$ (s^{-1})	3.8	3.8	3.8	3.8	[?, ?]
$k_{\mathrm{on}}^{\mathrm{PLG}}$, intact ($\mu\mathrm{M}^{-1}\mathrm{s}^{-1}$)	0.1	0.1	0.1	0.1	[?]
$k_{\mathrm{on}}^{\mathrm{PLG}}$, nicked ($\mu\mathrm{M}^{-1}\mathrm{s}^{-1}$)	1.7273	1.7273	1.7273	1.7273	[?]
$k_{\mathrm{off}}^{\mathrm{PLi}}$ (s^{-1})	38	38	38	38	[?]*
$k_{\mathrm{off}}^{\mathrm{tPA}}$, with PLG ($\mathrm{s}^{-1}$)	0.0002	0.0002	0.02	0.02	[?]
$k_{\mathrm{off}}^{\mathrm{tPA}}$, without PLG ($\mathrm{s}^{-1}$)	0.0036	0.0036	0.36	0.36	[?]
$k_{\mathrm{on}}^{\mathrm{tPA}}$ ($\mu\mathrm{M}^{-1}\mathrm{s}^{-1}$)	0.01	0.01	1.0	1.0	[?, ?]
$k_{\mathrm{cat}}^{\mathrm{ap}}$ (s^{-1})	50	50	50	50	
$k_{\mathrm{cat}}^{\mathrm{n}}$ (s^{-1})	10	1	10	1	

is released from the fiber when plasmin degrades the doublet to which it is bound. For plasmin to force the release of tPA, the two molecules must be sharing a doublet when a plasmin-mediated degradation event is chosen by the Gillespie algorithm. With the given parameter values, plasmin molecules can crawl many times between degradation events. Thick fibers have more doublets that the plasmin molecules can crawl to, so plasmin shares a doublet with tPA less frequently in thick fibers than in thin; this is responsible for the increased tPA residence time on thick fibers. With Case C and D parameters, the tPA unbinding rate is larger than in Cases A and B, and tPA almost always unbinds before it encounters plasmin. The tPA leaving times in thin and thick fibers are very similar in these cases since the dynamics are dominated by the tPA kinetic rates, which do not depend on fiber size.

Table 3.2. Microscale model results. Entries are median (Q1, Q3) of 600 independent simulations, except for lysis time, which is the result of only those simulations that produced a plasmin molecule. The "Number of PLi" column gives data about the average total number of plasmin molecules produced in one run. The column labeled "Runs with PLi" gives the number of runs, out of 600, that resulted in production of plasmin. † Q1 and the median are both 0 because the majority of the runs generated no plasmin. * To generate enough lysis time data, 1800 runs were used instead of 600.

Parameters	Fiber diameter (nm)	tPA leaving time (s)	Number of PLi	Lysis time (min)	Runs with PLi
Case A	100	7.98 (3.26, 14.90)	2 (1, 3)	1.59 (1.12, 2.73)	587
	200	8.46 (3.34, 16.80)	2 (1, 3)	5.98 (4.06, 11.05)	594
Case B	100	37.60 (19.40, 69.39)	7 (4, 13)	3.19 (2.30, 5.61)	589
	200	42.35 (17.79, 73.64)	7 (4, 14)	11.38 (6.99, 21.53)	586
Case C	100	1.60 (0.64, 3.13)	0 (0, 1)†	2.64 (2.47, 2.77)	701*
	200	1.63 (0.66, 3.19)	0 (0, 1)†	10.93 (10.29, 11.45)	713*
Case D	100	1.94 (0.77, 3.87)	0 (0, 1)†	20.87 (10.88, 21.53)	732*
	200	1.90 (0.85, 3.92)	0 (0, 1)†	84.15 (42.82, 85.75)	690*

3.2.1.2 Degradation and single fiber lysis

Since there are four times as many binding doublets in a thick fiber as a thin fiber, it would be reasonable to expect that a thick fiber would take four times as long to degrade. The model results support this hypothesis (Figure 3.4). Because we do not know the exact percentage of doublets that must be degraded before the fiber can be considered lysed, we vary our definition of lysis from 1% of total doublets degraded to 95% of total doublets degraded and see how median lysis times are affected. As Figure 3.4(a) shows, thin fibers lyse four times faster than thick fibers, on average, regardless of how we define lysis. Normalized single fiber lysis time distributions for Case C parameters are shown in Figures 3.4(b), 3.4(c), for lysis defined as degradation of 2/3 of the total doublets. The thick and thin single fiber lysis time distributions look very similar when the thin fiber lysis times are multiplied by a factor of 4.1. This is close to the factor of 4 that relates the medians of the data, as seen in Figure 3.4(a).

Insight into how the degradation rate k_{deg} affects lysis is gained by comparing Case A to Case B. With baseline parameter values (Case A), plasmin attempts to degrade a doublet 10 times per second, on average. In the case with low degradation rate (Case B), plasmin does this once per second. For thick fibers, 3.5 times more plasmin is produced in Case B than in Case A on average (7 vs. 2 molecules, respectively). While it seems reasonable that

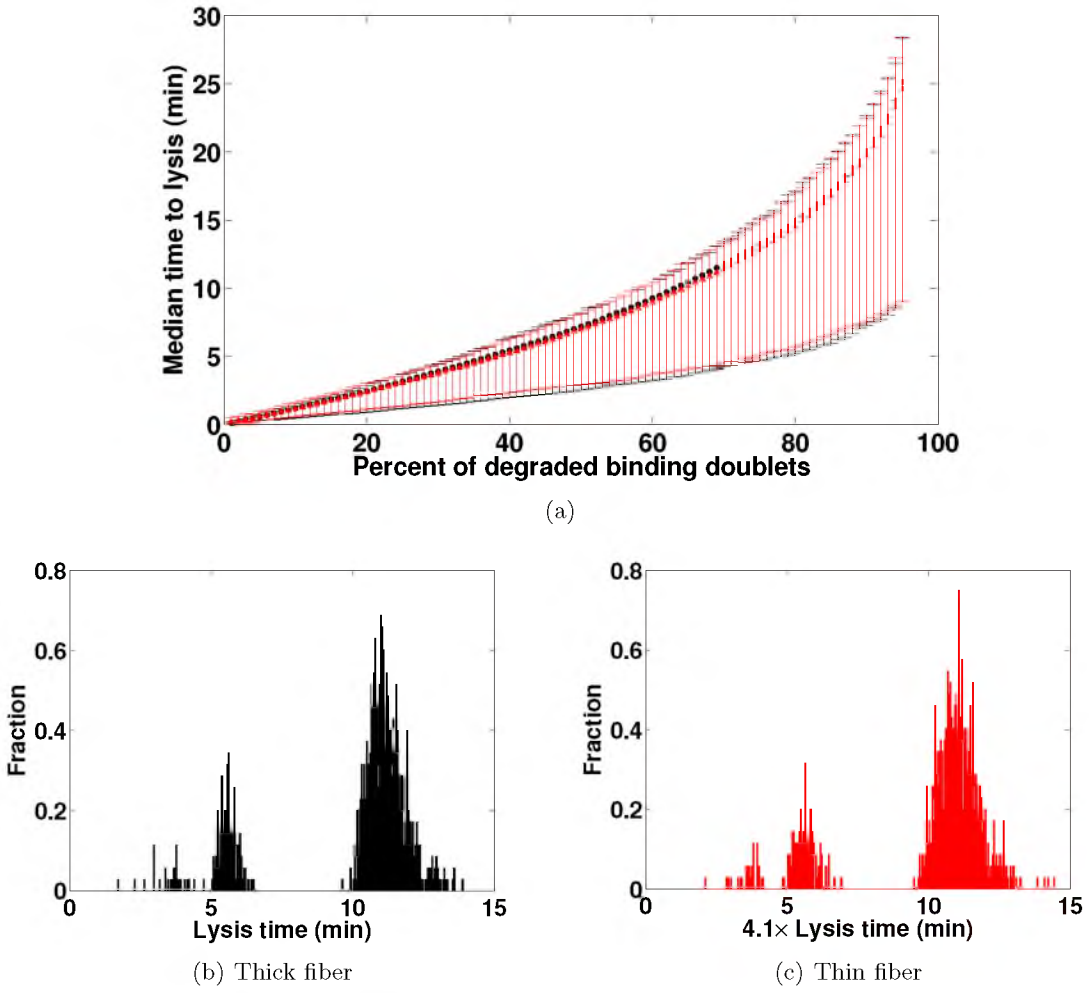

(a)

(b) Thick fiber

(c) Thin fiber

Figure 3.4. Single fiber lysis time data for Case C parameters. (a) Single fiber lysis times as a function of the percentage of binding doublets that must be degraded for lysis to be complete. Black circles denote median lysis time, top error bar (black) represents the 95th percentile and bottom error bar (black) represents the 5th percentile, for a thick fiber. Red triangles denote 4×(median lysis time), with top and bottom error bars (red) 4×(95th percentile) and 4×(5th percentile), respectively, for a thin fiber; thick fiber lysis times are approximately four times longer than thin fiber lysis times. (b), (c) Normalized single fiber lysis time distributions for a thick fiber and a thin fiber, respectively, with lysis defined as degradation of 2/3 of the total number of doublets. The thin fiber lysis times are scaled by a factor of 4.1, showing that the range of the thick fiber lysis time distribution is approximately four times larger than the range of the thin fiber lysis time distribution. The distributions have several peaks because the lysis times directly correlate to the number of plasmin molecules produced, which is discrete. For example, the large, right-most peak corresponds to runs when only one plasmin molecule was created.

more plasmin would result in faster lysis, lysis times are actually about 1.9 times longer with lower degradation rates because the plasmin is less efficient (11.38 min for Case B vs. 5.98 min for Case A). A similar result is seen for thin fibers. If plasmin degrades only once per second, approximately ten times more plasmin is needed to get the same lysis time as Case A. Clearly lysis depends on plasmin efficiency, not solely on the number of plasmin molecules produced.

The degradation rate, k_{deg}, affects not only the lysis time, but also the pattern of lysis. With a higher degradation rate, lysis is localized and moves like a wave through the cross section (Figure 3.5(a)). Plasmin molecules are created on the doublet with tPA, and they cannot move very far between degradation events. Therefore, plasmin degrades the area around the tPA doublet first. The plasmin molecules slowly move away from the tPA doublet, systematically spreading lysis as they go. Contrast this with Case B, where $k_{\text{deg}} = 1\ \text{s}^{-1}$. Here, plasmin can crawl a considerable distance between degradation events and start lysis in many locations throughout the cross section (Figure 3.5(b)). Further investigation is required to determine whether the pattern of microscale lysis is important, or if the single fiber lysis time alone is important for macroscale degradation.

3.2.1.3 Microscale model data used in macroscale model

The microscale data is incorporated into the macroscale model as follows. Running 600 independent simulations of the microscale model with each fiber diameter, 100 nm and 200 nm, generates the data in Figure 3.6. First we obtain an empirical cumulative distribution function for tPA leaving times (Figure 3.6(a)). This distribution is used in the macroscale model to randomly pick a tPA leaving time every time a tPA molecule binds to a fiber. Next, we bin the number of plasmin molecules produced into tPA leaving time intervals. For tPA leaving times ranging from 0-30 seconds, we create 5-second intervals in which to bin the plasmin data. For tPA leaving times greater than 30 seconds, we create 10-second intervals in which to bin the plasmin data. We find the mean of the data in each bin and fit a line to these means, weighted by the number of data points in each bin (Figure 3.6(b)). In the macroscale model, we use this line to determine the number of plasmin molecules produced for a given tPA leaving time. Unsurprisingly, more plasmin is produced for larger tPA leaving times. Finally, we fit a power function to the scatter plot of lysis time versus plasmin number data and use it to determine the lysis time (Figure 3.6(c)). As expected, lysis times are long when only a few plasmin molecules are created, and shorter when there

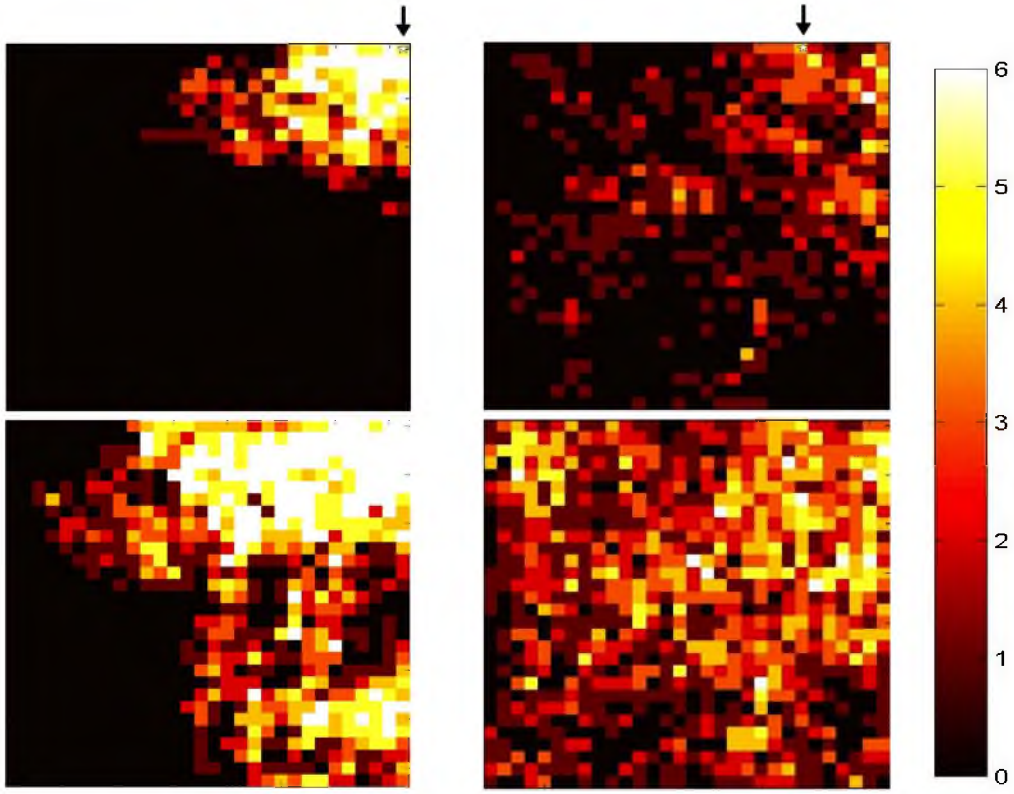

(a) $k_{\text{deg}} = 10\ \text{s}^{-1}$ (b) $k_{\text{deg}} = 1\ \text{s}^{-1}$

Figure 3.5. Fibrin degradation in a cross section of a 200 nm diameter fiber. Each pixel represents a binding location that contains 6 doublets. The color bar indicates level of degradation, with lighter colors denoting higher levels of degradation. The pixel ranges from black if none of the doublets at a particular binding location have been degraded, to white if all 6 binding doublets have been degraded. Top images show cross sections with one-tenth of binding doublets degraded, and bottom images are cross sections with one-third of binding doublets degraded. The arrows point to a white star in the top images, which indicates the location of tPA. (a) Case A parameters. With $k_{\text{deg}} = 10\ \text{s}^{-1}$, lysis is localized because plasmin is not able to move very far between degradation events. Top image at $t = 33.91$ s, bottom image at $t = 72.42$ s. (b) Case B parameters. With $k_{\text{deg}} = 1\ \text{s}^{-1}$, lysis happens throughout the cross section because plasmin can move a considerable distance between degradation events. Top image at $t = 84.74$ s, bottom image at $t = 188.82$ s.

is more plasmin. The data displayed in Figure 3.6 is all the microscale model information needed for the macroscale model.

3.2.2 Macroscale model results

3.2.2.1 Qualitative observations

Depending on the tPA binding site concentration per fiber, macroscale lysis can proceed as a front with a high accumulation of tPA molecules at the front (Figure 3.7(a), 3.7(b)), or lysis can occur throughout the clot in no particular pattern (Figure 3.7(c), 3.7(d)). We imagine that tPA binding sites are distributed throughout the fibrin fibers, but only those binding sites on the surface of the fiber are available to tPA as it diffuses through the clot. The thick fibers have half as many available binding sites per unit volume as the thin fibers. The argument is as follows. The binding site concentration, b, we use to calculate macroscale binding of tPA is the number of available binding sites per volume, which is the number of fibers per volume times the available binding sites per fiber. The former scales like $\frac{1}{r^3}$ and the latter is proportional to surface area per fiber, and so scales like r^2.

Because the radius of our thick fiber is twice the radius of our thin fiber, $b_{\text{coarse}} = \frac{1}{2} b_{\text{fine}}$. The average length of time it takes for a tPA molecule to bind to a fiber is $(k_{\text{on}}^{\text{tPA}} b)^{-1}$. So for a given binding rate, $k_{\text{on}}^{\text{tPA}}$, the time to bind is shorter for a higher b. A long tPA binding time means that the molecule can diffuse farther between binding events, effectively distributing the tPA more evenly throughout the clot. If tPA binds to fibers located throughout the clot, then it also initiates lysis on fibers located throughout the clot. Macroscale lysis in this case is not front-like (Figure 3.7(c), 3.7(d)). On the other hand, a short binding time means that the molecule is not able to diffuse very far between binding events, effectively localizing tPA at the clot front. In this case, lysis proceeds as a front (Figure 3.7(a), 3.7(b)).

3.2.2.2 Lysis front velocity and degradation rate

Besides the qualitative conclusions drawn above, we also obtain quantitative results about macroscale lysis. We use two measures of macroscale lysis: front velocity and degradation rate. We measure front velocity of a given column of the lattice by tracking in time the y-position (same axes as Figure 3.2(b)) of the first edge oriented in the y-direction that contains fibrin. This gives position vs. time data from which we can estimate a front velocity. We do this for each of the columns extending above the N nodes on the bottom row of the lattice. So we have N front velocities, which we average to obtain the overall

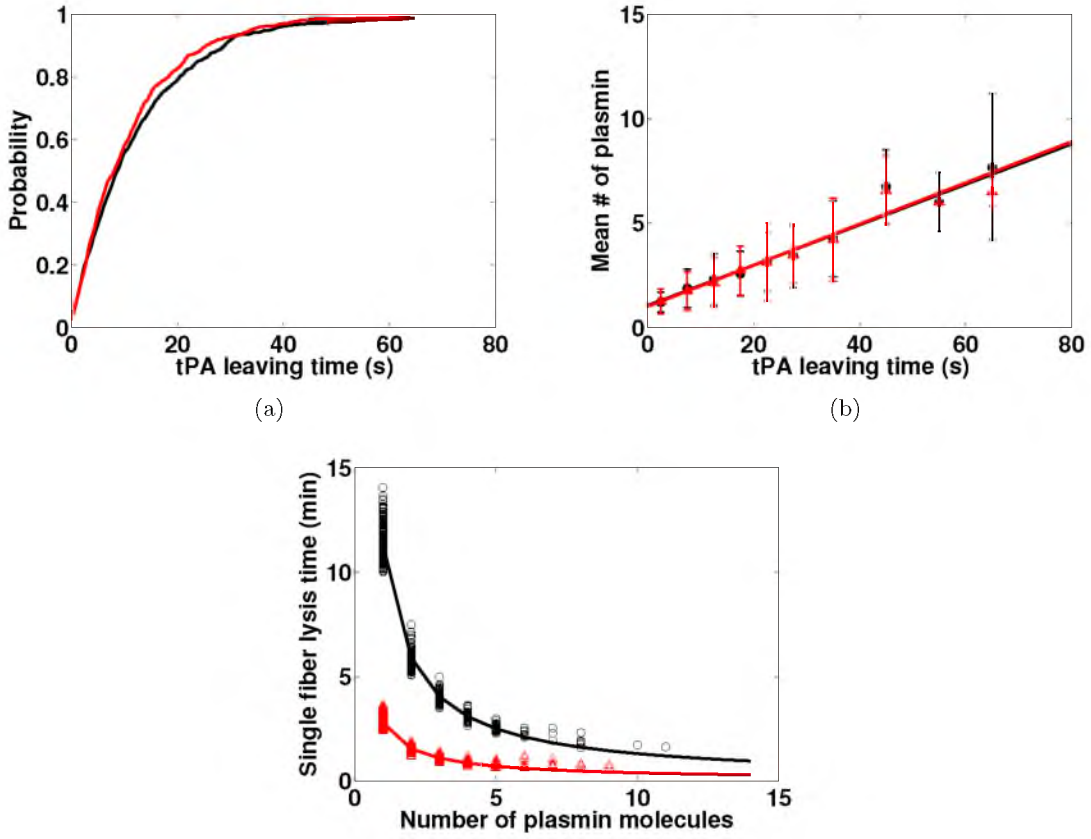

Figure 3.6. Microscale model results for 100 nm fiber (red) and for 200 nm fiber (black) with Case A parameters. Red triangles indicate thin fiber data, black circles indicate thick fiber data. (a) Empirical cumulative distribution function of tPA leaving times. (b) The best fit lines of the data relating tPA leaving time to the number of plasmin molecules produced. The raw data is binned in 5 second intervals from 0 to 30 s (e.g., 0-5 s, 5-10 s, etc.), and 10 second intervals from 30 s onward. Means of each bin are plotted at the interval midpoint. A line is then fit to the means, weighted by the number of data points in each bin. (c) The best fit curves of the data relating number of plasmin molecules to single fiber lysis time.

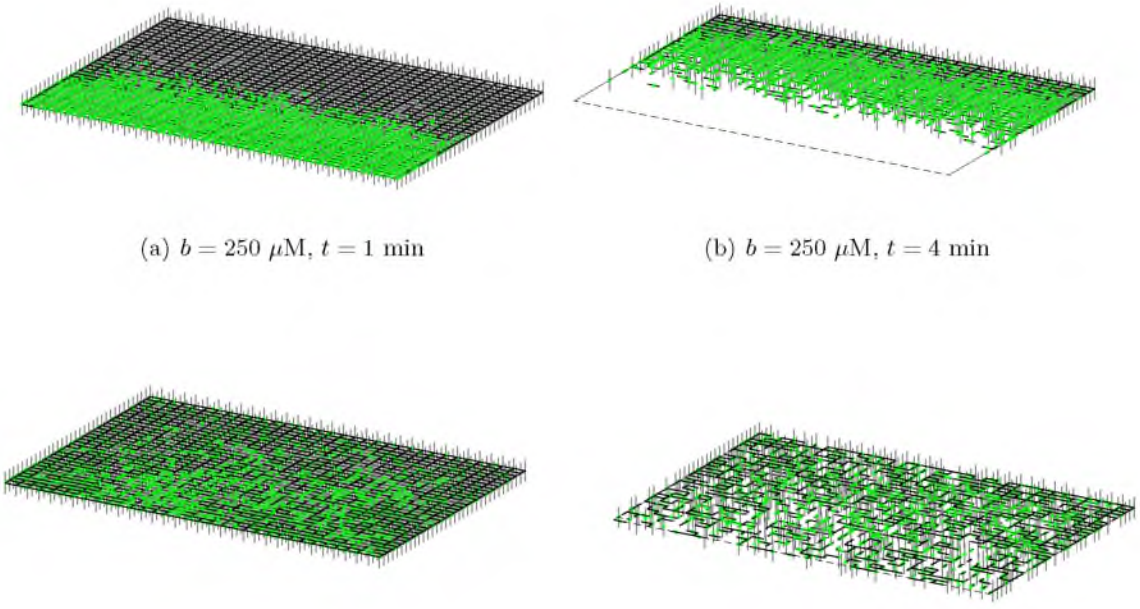

(a) $b = 250$ μM, $t = 1$ min

(b) $b = 250$ μM, $t = 4$ min

(c) $b = 1$ μM, $t = 1$ min

(d) $b = 1$ μM, $t = 4$ min

Figure 3.7. The 3-D distribution of tPA and state of degradation for a coarse clot with Case A parameters. Approximately 44,200 tPA molecules (a 5 nM concentration) were randomly distributed in the $51.68 \times 100 \times 3.04$ μm^3 fibrin-free region abutting the clot. Green asterisks denote bound tPA; unbound tPA is not plotted. Black segments represent fibrin fibers. The dashed lines in (b) and (d) indicate the border of the initial clot. The physical distance between lattice nodes is 3.04 μm. (a), (b) State of the clot approximately 1 min and 4 min, respectively, after the introduction of tPA. The tPA binding site concentration per fiber is $b = 250$ μM. (c), (d) State of the clot approximately 1 min and 4 min, respectively, after the introduction of tPA. The tPA binding site concentration per fiber is $b = 1$ μM.

Table 3.3. Macroscale model results for Case A parameters with a 5 nM tPA concentration. Entries are mean ± standard deviation of 10 independent simulations. Front velocity calculations do not make sense for simulations in which lysis was not front-like, hence the "–" in some entries. b is the concentration of available tPA binding sites and H is the height of the fibrin-free region abutting the clot.

Clot type	b **(**μ**M)**	H **(**μ**m)**	**Front velocity (**μ**m/min)**	**Degradation rate (% fibers**$\times 10^{-1}$**/s)**
fine	2	51.68	–	4.29 ± 0.083
coarse	1	51.68	–	4.11 ± 0.101
fine	500	51.68	18.39 ± 0.47	3.03 ± 0.017
coarse	250	51.68	16.83 ± 1.00	2.64 ± 0.048
fine	500	3.04	10.02 ± 0.43	1.69 ± 0.015
coarse	250	3.04	10.76 ± 0.90	1.75 ± 0.025

lysis front velocity for the given simulation. We also calculate the standard deviation. We do 10 independent simulations, so the results presented in Table 3.3 are means of the 10 means ± means of the 10 standard deviations. Front velocity calculations begin when the first fiber degrades, not when the bolus of tPA is added to the fibrin-free region. We could instead have tracked how the position of fibers oriented in the z- or x-direction changes in time, but results would not be significantly different.

Degradation rate is a useful measure of lysis speed when the pattern of lysis is not front-like. To calculate degradation rate, we plot the percentage of fibers degraded as a function of time. Lysis begins sometime after the addition of tPA, and lysis of the last few fibers takes a bit longer, but the plot is linear in the middle range of times from shortly after lysis begins to shortly before lysis ends. Fitting a line to the linear part of this plot allows us to estimate a (percent degraded)/s degradation rate. We identify the linear part of the plot as the region between the first and last times that the slope between consecutive data points is $\geq 1 \times 10^{-3}$ (% degraded)/s. This eliminates the slowly changing initial and final data from the degradation rate calculation. Because we do 10 independent simulations, results presented in Table 3.3 are means of the 10 independent degradation rates ± the standard deviation of the 10 degradation rates.

The macroscale lysis results presented in Table 3.3 are for Case A parameters with a bolus of 5 nM tPA solution added to the fibrin-free region. The volume of 5 nM solution added varies, since we change the height of the fibrin-free region in some of the simulations. For a fibrin-free region that is approximately half the height of the clot, 51.68 μm, lysis is not front-like and fine clots lyse faster than coarse (as measured by degradation rate) when

$b = 2$ μM for the fine clot and 1 μM for the coarse clot. When $b = 500$, 250 μM for fine and coarse clots, respectively, lysis proceeds as a front and fine clots lyse faster than coarse clots. However, if we keep the larger binding site concentrations and simply change the height of the fibrin-free region to 3.04 μm (i.e., change the volume of tPA solution we add), then lysis is still front-like, but coarse clots lyse faster than fine.

3.2.2.3 Effect of tPA on lysis front velocity

It is not simply the number of fibers that determines which type of clot lyses faster; the number of tPA molecules in the system relative to the surface area of the clot abutting the fibrin-free region has a strong influence on lysis speeds. Figure 3.8 shows fine and coarse front velocities as a function of this tPA-to-surface-area ratio for Case A parameters. Several different tPA concentrations and fibrin-free volumes were used, but these values on

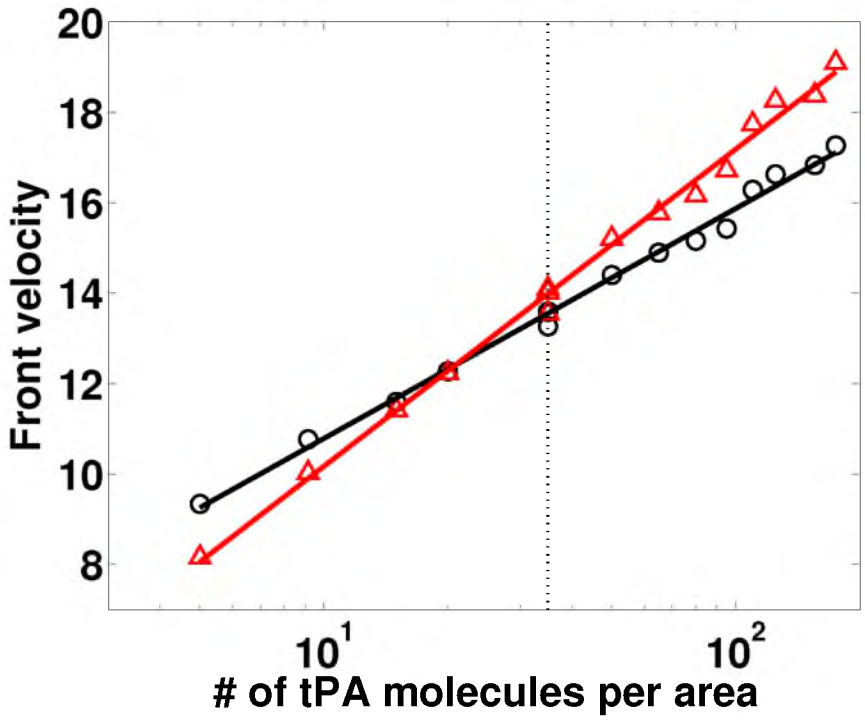

Figure 3.8. Lysis front velocity for fine clot (red triangles) and coarse clot (black circles) as functions of the ratio of number of tPA molecules to surface area of clot exposed to the fibrin-free region. Symbols are means of 10 runs. Dashed line indicates 3 runs with fixed tPA-to-surface-area ratio. Velocities are measured in μm/min. 15 different experiments were run with tPA-to-surface-area ratios varying from 5 to 175 molecules/μm^2, and corresponding front velocities were calculated.

their own do not matter; it is the total number of tPA molecules relative to the surface area (which we fix at 100 μm $\times$ pore size) that affects lysis rate. As the tPA-to-surface-area ratio increases, so does the front velocity. Since we keep the surface area of the clot fixed, we can only increase the ratio by increasing the number of tPA molecules in the system. The way we do so, however, does not matter, as long at the fibrin-free region is not too big. We can keep the size of the fibrin-free region fixed and use a larger tPA concentration, or we can fix the tPA concentration and increase the size of the fibrin-free region. Both methods increase the number of tPA molecules used in the simulation. The dotted line in Figure 3.8 represents this. We ran three different simulations of the macroscale model using the same number of tPA molecules, but three different fibrin-free volumes and tPA concentrations. For a fine clot, the two upper triangles are almost indistinguishable – they look like one triangle. For these two runs, we used tPA concentrations of 19.12 nM and 6.37 nM, and fibrin-free heights of 3.04 μm and 9.12 μm, respectively. This shows that the same tPA-to-surface-area ratio produces the same front velocity, as long as the fibrin-free region is not too big. When we took a fibrin-free height of 51.68 μm and a 1.12 nM tPA concentration (the lower triangle), we got a slightly slower front velocity, even though the ratio was the same as in the other two simulations. This is because there is so much fibrin-free space into which the tPA molecules can diffuse, that they encounter the clot, and consequently begin lysis, less frequently.

The coarse front velocities respond similarly to the tPA-to-surface-area ratio (Figure 3.8). By fitting a line to the data for both coarse and fine front velocities and calculating the point at which the two lines intersect, we estimate 25.09 molecules/μm^2 to be the tPA-to-surface-area ratio below which coarse clots lyse faster than fine. As the tPA-to-surface-area ratio increases, so does the fine-to-coarse front velocity ratio. With a fixed surface area, this means that as the number of tPA molecules increases, so does the fine front velocity relative to the coarse. This makes sense, because if the system were to contain enough tPA to bind to all the fibers at the front of the fine clot, the disadvantage of having more fibers would be erased. Lysis would be started on all the fibers at the lysis front, and since individual thin fibers lyse faster than thick fibers, the fine clot would degrade more quickly. On the other hand, if there are sufficiently few tPA molecules, then lysis could not begin on all thin fibers at once. In this case, coarse clots would have the advantage of containing fewer fibers. There would be more tPA molecules per fiber in the coarse clots, *and* there would be fewer fibers. Lysis would begin on a higher percentage of thick fibers

than thin and, if that percentage were sufficiently high, this would cause the coarse clot to lyse faster than the fine one.

3.3 Discussion

In this chapter we have described a model of fibrinolysis that includes several new and important features: multiple dimensions, multiple scales, and stochasticity. Detailed treatment of the biochemistry of lysis occurs in a microscale model of a single fiber cross section. Treatment of the overall clot lysis, including transport of the lysis-initiating enzyme tPA, occurs in a macroscale model which uses data obtained from microscale model simulations. We have shown that our 3-dimensional, stochastic model exhibits behavior that is qualitatively consistent with the literature. Lysis proceeds as a front, with a high accumulation of tPA at the front. Individual thin fibers lyse more quickly than individual thick fibers, and under certain conditions coarse clots composed of thick fibers lyse more quickly than fine clots composed of thin fibers. The faster degradation of coarse clots is based on the number of tPA molecules relative to the surface area of the clot, and the fact that in a given clot volume there are fewer fibers to cut. When the tPA-to-surface-area ratio is small enough (for our parameters and clot geometries, < 25.09 molecules/μm^2), there is not enough tPA to start lysis on all the thin fibers at the front of the fine clot. However, there *is* enough tPA to start lysis on all the thick fibers at the front of the coarse clot because there are fewer fibers. Despite the longer single fiber lysis times, coarse clots made of thick fibers lyse faster than fine clots in these situations because lysis must be started fewer times. However, for the same parameters and clot structures, if there is enough tPA at the clot edge to bind to all the thin fibers at the front of the fine clot, fine clots lyse faster than coarse. So it is not simply fiber number that determines relative front velocities, but rather fiber number in conjunction with the number of tPA molecules exposed to the clot. For any tPA concentration, if the height of the fibrin-free region is small enough, then almost all the tPA molecules bind to fibers at the clot front within the first minute. Hence, the number of tPA molecules added to the system, and not the tPA concentration, matters. The overall lysis time is determined by the combination of individual fiber lysis time, the number of fibers in the clot needing to be cut, and the number of tPA molecules per unit surface area of the clot front (which influences how many individual fiber lysis processes occur concurrently).

Rigorous comparisons of our multiscale model with published quantitative data remain

a challenge. Comparing our results to experiments, we appear to get reasonable single fiber lysis times. The lysis times for our baseline parameters (Case A) are on the same order as experimentally observed times: the model predicts thin fibers lyse in 1.59 minutes and thick fibers lyse in 5.98 minutes, while Collet et al. measure thin fibers to lyse in 3.1 ± 1.1 minutes, and thick fibers to lyse in 5.4 ± 1.4 minutes [?]. The definition of single fiber lysis in the Collet et al. experiment is unclear, however. Presumably the fiber is considered lysed when it is no longer visible by the confocal microscope, but this is obviously different than our definition in which the fiber is lysed when it is cut by plasmin-mediated degradation of fibrin within a cross section. Further, it is not clear when the experimental clock starts to run because it is not possible to see when a tPA molecule binds to a fibrin fiber. More similar to the criterion in our model, Blinc et al. use atomic force microscopy (AFM) to obtain single fiber transection times of 7.6 ± 3.7 and 6.4 ± 4.2 minutes for thin and thick fibers, respectively, which according to the authors do not differ significantly [?]. A fiber that was continuous in the previous AFM image but laterally split in the current image is considered lysed, but a single image takes 2-8 minutes to acquire so time resolution is a serious issue. Additional data are necessary to verify our single fiber lysis results, but our numbers appear to be in a reasonable range.

The predicted lysis front velocities in fine and coarse clots are not as different as the measured rates. Collet et al. find coarse clots lyse at a rate of 31 μm/min and fine clots lyse at a rate of 2.15 μm/min [?]. The fastest coarse front velocity we obtain is 17.27 μm/min, the slowest fine front velocity is 8.15 μm/min, and the largest coarse-to-fine front velocity ratio is about 1.15. Wootton et al. measure lysis speeds ranging from 8.4 μm/min to 18.6 μm/min, under various flow conditions (which we do not include in the model), but do not distinguish between clot structures [?]. In a different experiment where 10 nM urokinase (a plasminogen activator that unlike tPA can activate unbound PLG) was added to the edge of a fibrin clot formed in buffer, the fine front velocity was about 12 μm/min while the coarse front velocity was about 25 μm/min [?]. If PLG is not pre-equilibrated with a fibrin clot, and instead is first introduced to the clot with the bolus of tPA (tPA 69.4 nM, PLG 2.4 μM), lysis speed is slower: 2.92 ± 0.57 μm/min for an unspecified clot structure [?]. Not only are all these experiments (with the exception of Collet et al. [?]) different from the situation we model, it also is unclear how the experimental front velocities are measured, which makes comparisons to our model difficult. We measure front velocities from the time the first fiber degrades, but measurements could also be taken from the time tPA is first

introduced into the system or from some arbitrary time after lysis begins. Due to the wide range of lysis rates measured experimentally, it will be beneficial to have additional data with which to compare our model.

In a recent study, Longstaff et al. showed that when tPA variant delF-tPA was added to the edge of a clot, after an initial transient front of lysis with localized delF-tPA, delF-tPA diffused ahead of the front and was distributed throughout a larger region of the clot [?]. Lysis rates, estimated from changes in clot turbidity, were slower for lysis initiated by delF-tPA than by normal tPA. By lowering the concentration of available tPA binding sites in our model, we can eliminate the accumulation of tPA at the clot edge and the resulting front-like pattern of lysis. However, unlike Longstaff et al., distribution of tPA throughout the clot yields significantly faster lysis than tPA localized at the front. This suggests that therapeutics should be aimed at preventing tPA from accumulating at the lysis front. However, dispersal of tPA throughout the clot should be accomplished by minimal change to tPA structure, as Longstaff et al. showed that a tPA variant missing a key binding domain results in slower lysis [?].

The microscale model is able to predict the efficiency of individual molecules – something that is currently unattainable experimentally, since single molecules cannot be counted. Figure 3.6 nicely illustrates how many plasmin molecules can be produced by a single tPA molecule, and how the number of plasmin molecules determines lysis time. The microscale model predicts that for small tPA unbinding rates, a tPA molecule stays bound to a thick fiber slightly longer than it does to a thin fiber because plasmin is slower to encounter and degrade the doublet with tPA. We are not aware of any single-molecule experiments addressing this phenomenon (or if the experiments are even possible with current technology); this is an example of how mathematical models can be used to propose new avenues of research for laboratory scientists. Our prediction is a product of the assumptions we made about microscale degradation and movement of plasmin (i.e., that tPA is released when plasmin degrades the fibrin to which tPA is bound, and that plasmin crawls to neighboring binding sites inside a fiber); an experiment to measure the length of time tPA stays bound to fibers of varying thickness would be worthwhile. If tPA stays bound to thick fibers longer, our model provides a hypothesis for why; if tPA does not stay bound to thick fibers longer, this suggests that either the physiological rate of tPA unbinding is large (Case C, D) or that one or more of our model assumptions needs modification. For instance, perhaps tPA remains bound to the fiber, even after the doublet has been degraded.

Either way, we obtain useful information by comparing the model to experiments.

We find that the degradation rate affects both the time and pattern of single fiber lysis. Lower degradation rates produce slower lysis times and lead to degradation occurring throughout the cross section. Higher degradation rates result in faster lysis that moves as a wave across the fiber cross section.

Macroscale model results depend on single fiber lysis times, but we do not know what the lysis criteria for a single fiber should be. We assume that the fiber is cut when 2/3 of the binding doublets in a cross section are degraded. We justify this assumption with a plausible argument about fibers under tension. However, we could also have defined lysis to occur when a given number of doublets remain. If a fiber is cut when all but 100 binding doublets are degraded, lysis of the thick fiber will take longer, relative to lysis of the thin fiber, because the thick fiber has four times as many binding doublets. Even if lysis is dependent on percentage of doublets degraded rather than number, macroscale front velocities differ for varying values of this percentage. As Figure 3.4(a) shows, single fiber lysis times increase nonlinearly as the percentage of doublets required for lysis increases from 1% to 95%. Choosing a percentage other than 66.67% changes the magnitude of the thin and thick lysis times, but the thin-to-thick lysis time ratio remains unchanged. Until there is more evidence for a "correct" criterion for single fiber lysis, we believe our assumption is reasonable.

Analysis of our model results suggests several possible experiments. The hypothesis that the number of tPA molecules relative to the surface area of the clot exposed to those molecules determines which clot structure lyses faster should be testable in the lab. Also, current technology is such that individual fibrin fibers can be isolated and observed at shorter time intervals, meaning that more accurate single fiber lysis experiments should now be possible. The prediction of the model is that a thick fiber with diameter twice the thin fiber diameter will take four times longer to degrade. If the thick fiber experimental degradation time is longer than four times the thin fiber degradation time, this could suggest that the criteria for complete lysis is not that a certain *percentage* of doublets are lysed, but rather that a given *total number* of doublets remains, below which lysis is almost certain to occur. On the other hand, if the thick fiber lysis time is less than four times the thin fiber lysis time, this suggests that the unbinding of tPA by plasmin has a significant effect; tPA could be forced to unbind by plasmin-mediated degradation less frequently in thick fibers because of the additional space for plasmin to crawl. If tPA stays bound longer to

a thick fiber than a thin fiber, more plasmin can be produced, and lysis can happen faster than expected. As explained above, an experiment that tests the length of time tPA stays bound to fibers of various diameters would be interesting, but we are unsure if this type of experiment is currently feasible. Finally, our modeling suggests that a potential target for new therapeutics should be a tPA variant that has much of the same structure as tPA, but binds less strongly to the clot front. Understanding conditions which increase the lysis rates of clots of varying structure is important for improved blood clot therapies. The broad question of how to safely increase lysis rates clinically is ongoing motivation for our work. Our multiscale model is one step toward a better understanding of what influences fibrinolysis rates. Laboratory experiments to test our hypotheses will provide even more insight, and direct future modeling efforts.

CHAPTER 4

APPLICATIONS OF A MODIFIED MULTISCALE MODEL

In this chapter we present modifications of the stochastic multiscale model (described in Chapter 3) that make it more amenable to biologically meaningful experimentation. Model modifications are explained in detail in Section 4.1 and results are presented in Section 4.2 and discussed in Section 4.3.

4.1 Model modifications

We make several modifications to the multiscale model presented in Chapter 3. Many of these changes are motivated by biology: the microscale and macroscale domains are adjusted so that model fibrin concentrations are similar to physiological fibrin concentrations (Section 4.1.1); the physical size of PLG is taken into account so that tPA-mediated activation of PLG and plasmin-mediated degradation of fibrin occur on a more biologically reasonable spatial scale (Section 4.1.2); and additional published parameter values are used (Section 4.1.3). Finally, the microscale data are input into the macroscale model in a more appropriate way (Section 4.1.4).

4.1.1 Geometry

The first major change to the model presented in Chapter 3 is to adjust the microscale model domain to better reflect biologically realistic fibrin volumes and concentrations within a fiber. Fibrin fibers are approximately 20% protein and 80% water and have a fibrin concentration of about 824 μM [?, ?]. Consider a thin fiber with diameter 97.5 nm and a thick fiber with diameter 195 nm (in Chapter 3 the diameters were 100 nm and 200 nm, respectively). For the thin fiber, instead of using 15 binding locations along one row of the square cross section, we now use 9 (calculations in Appendix A). For the thick fiber we now use 18 binding locations along one row instead of 30. This results in 19.63% of the fiber being protein (Equation 4.1), and an 800.95 μM fibrin concentration per fiber

(Equation 4.2).

$$\text{Percent protein per fiber} = \frac{9^2 \text{ protofibrils}}{22.5\pi(48.75)^2 \text{ nm}^3} \times \frac{22.5\pi(2.4)^2 \text{ nm}^3}{1 \text{ protofibril}} = 19.63\%. \tag{4.1}$$

$$\text{Fibrin concentration per fiber} = \frac{9^2 \text{ monomers}}{22.5\pi(48.75)^2 \text{ nm}^3} \times \frac{10^6\,\mu\text{mol}}{6.02 \times 10^{23} \text{ monomers}} \times \frac{10^{24} \text{ nm}^3}{1\text{L}} = 800.95\,\mu\text{M}. \tag{4.2}$$

In performing these calculations, each binding location is assumed to represent a protofibril. The calculations require volumes, so we assume that the "length" of a cross section is 22.5 nm – the distance between binding sites along a fiber. In a 22.5 nm length of protofibril there is 1 fibrin monomer, because the half-staggering arrangement of monomers results in one half of two separate fibrin monomers coming together to form the protofibril.

The new microscale domain is more accurate with respect to fibrin volume and concentration, and also with respect to protofibril spacing. When we calculated that 15 protofibrils would fit in one row of the thin fiber cross section in Section 3.1.1, we measured from one protofibril midpoint to the neighboring protofibril midpoint, and essentially packed protofibrils very close together. The new geometry, with protofibrils spaced 4.8 nm apart, is more realistic than abutting protofibrils and results in a far more accurate protein percentage (about 20% vs. 56%).

Because the microscale model domain is different, we must also adjust the macroscale model geometry. We take the fibrin concentration per fiber to be 800.95 μM (Equation 4.2) and the fibrin concentration averaged over the clot to be 8.8 μM [?]. Given a fixed fiber diameter and assuming the clot is formed in a small chamber with dimensions 100 μm$\times$ 100 μm$\times$ depth μm, we find the number of lattice nodes and pore size necessary to keep these concentrations fixed. The new number of nodes in one row of the fine (coarse) lattice is 69 (35), with pore size 1.37 μm (2.74 μm). This results in a fine (coarse) clot with 14145 (3605) fibers. To calculate the node number, N, notice that the number of edges in a 3-D square lattice (that is one fiber deep in one direction) is $N^2+2N(N-1)$. To enforce concentrations, node number and pore size (p.s.) are found by solving the system of equations given by Equations 4.3 and 4.4.

$$\text{Fibrin conc. in clot} = \frac{\text{volume of fibers}}{\text{volume of clot}} \times \text{ fibrin conc. per fiber}$$

$$8.8\,\mu\text{M} = \frac{[N^2 + 2N(N-1)]\pi \text{r}^2 \text{ p.s.}}{100^2 \text{p.s.}} \times 800.95\,\mu\text{M}. \tag{4.3}$$

$$\text{Length of lattice} = (\text{nodes in one row}) \times \text{diameter} + (\text{pores in one row}) \times \text{p.s.}$$

$$100\,\mu\text{m} = N \times \text{diameter} + (N-1) \times \text{ p.s.} \tag{4.4}$$

The final change to the macroscale model is the parameter which describes the concentration of fibrin on the fiber surface available for tPA binding, b. The number of protofibrils on the fiber surface is the number of binding locations along the edge of the square cross section. For a thin (thick) fiber, 32 (68) of the 81 (324) protofibrils are on the surface of the fiber, or 39.51% (20.99%) of the total fibrin. This means that the fibrin concentration on the surface of a fiber available for tPA binding is $b = 316$ μM in fine clots, and $b = 168$ μM in coarse clots. As before, the time that tPA binds to a fiber in the macroscale model is calculated from an exponential distribution with rate parameter $b \cdot k_{\text{on}}^{\text{tPA}}$.

4.1.2 tPA activation and plasmin-mediated degradation

In the microscale model described in Section 3.1.1, tPA could only convert PLG to plasmin if tPA and PLG were bound to the same doublet. Physiologically, however, the size of PLG (9-11 nm in diameter) suggests that a PLG molecule bound anywhere in a 5-nm diameter protofibril cross section should be accessible to a tPA molecule in the same cross section. Therefore, we relax the constraint that tPA and PLG must share a doublet for conversion to plasmin to occur, and instead allow tPA to convert *any* PLG at the same binding location to plasmin. In practice, this amounts to the consideration of additional reactions in the Gillespie algorithm: now tPA can convert PLG on any of the 6 doublets at its location to plasmin (Appendix F). Similarly, we now allow plasmin to degrade any doublet at the same binding location, not just the doublet it occupies. This implies that plasmin is large enough to reach, and degrade, any of the 6 chains of the protofibril to which it is bound. If there is more than one degradable doublet at the same binding location as plasmin, we assume the rate of degradation for each doublet is the same, so there is no bias in which doublet is chosen for degradation. Similarly, the rate of conversion of PLG to plasmin is the same for each PLG molecule at the binding location containing tPA.

4.1.3 Parameter values

We adjust multiscale model parameters to reflect additional references from the literature. Table 4.1 contains the new Case A parameters with the corresponding references. We still have not found experimental measures of tPA and PLG binding and unbinding rates, only dissociation constants. We use binding rates from the modeling paper by Wootton et al. [?], and choose unbinding rates to satisfy the measured dissociation constants. In section 4.2.3 we allow plasmin to unbind from the microscale model, so we now have a rate of plasmin crawling ($k^{\mathrm{PLi}}_{\mathrm{crawl}}$, which was $k^{\mathrm{PLi}}_{\mathrm{off}}$ in Chapter 3) and a rate of plasmin fully unbinding ($k^{\mathrm{PLi}}_{\mathrm{unbind}}$).

The rates of plasmin unbinding from fibrin presented in the literature range from 0.05 s^{-1} to 57.6 s^{-1} [?, ?]. In our simulations we use $k^{\mathrm{PLi}}_{\mathrm{unbind}} = 0.05\ \mathrm{s}^{-1}$ as the unbinding rate and

Table 4.1. Baseline (Case A) parameter set used in the modified microscale model. $k^{\mathrm{PLG}}_{\mathrm{on}}$ and $k^{\mathrm{PLG}}_{\mathrm{off}}$ are the binding rate of PLG to fibrin and the unbinding rate of PLG from fibrin, respectively, with dissociation constant $k^{\mathrm{PLG}}_{D} = k^{\mathrm{PLG}}_{\mathrm{off}}/k^{\mathrm{PLG}}_{\mathrm{on}}$. The tPA rates have similar meanings. k^{PLG}_{D} is different depending on whether fibrin is intact or nicked, and k^{tPA}_{D} is different depending on whether tPA is bound to a doublet with PLG or without PLG. $k^{\mathrm{ap}}_{\mathrm{cat}}$ is the catalytic rate constant for activation of PLG to plasmin, $k^{\mathrm{n}}_{\mathrm{cat}}$ is the catalytic rate constant for plasmin-mediated exposure of cryptic binding doublets, and k_{deg} is the plasmin-mediated rate of fibrin degradation. $k^{\mathrm{PLi}}_{\mathrm{crawl}}$ and $k^{\mathrm{PLi}}_{\mathrm{unbind}}$ are the crawling rate and unbinding rate of plasmin, respectively. We know the dissociation constants for tPA and PLG, but not the individual rates, so references in the table are for k_{D}. We assume that $k^{\mathrm{n}}_{\mathrm{cat}} = k_{\mathrm{deg}}$, since we have not found any references for the rate of plasmin-mediated exposure of binding sites.

Parameters	Case A	Reference
k_{deg} (s^{-1})	5	[?, ?]
$k^{\mathrm{PLG}}_{\mathrm{off}}$ (s^{-1})	3.8	[?, ?]
$k^{\mathrm{PLG}}_{\mathrm{on}}$, intact ($\mu\mathrm{M}^{-1}\mathrm{s}^{-1}$)	0.1	[?]
$k^{\mathrm{PLG}}_{\mathrm{on}}$, nicked ($\mu\mathrm{M}^{-1}\mathrm{s}^{-1}$)	1.7273	[?]
$k^{\mathrm{PLi}}_{\mathrm{crawl}}$ (s^{-1})	57.6	[?]
$k^{\mathrm{PLi}}_{\mathrm{unbind}}$ (s^{-1})	0.05	[?]
$k^{\mathrm{tPA}}_{\mathrm{off}}$, with PLG ($\mathrm{s}^{-1}$)	0.0002	[?]
$k^{\mathrm{tPA}}_{\mathrm{off}}$, without PLG ($\mathrm{s}^{-1}$)	0.0036	[?]
$k^{\mathrm{tPA}}_{\mathrm{on}}$ ($\mu\mathrm{M}^{-1}\mathrm{s}^{-1}$)	0.01	[?, ?]
$k^{\mathrm{ap}}_{\mathrm{cat}}$ (s^{-1})	0.1	[?, ?]
$k^{\mathrm{n}}_{\mathrm{cat}}$ (s^{-1})	5	

$k_{\text{crawl}}^{\text{PLi}} = 57.6\ \text{s}^{-1}$ as the crawling rate. In order for plasmin to crawl, the rate of unbinding must be much less than the rate of crawling (Appendix G).

4.1.4 Using microscale data in the macroscale model

In Section 3.2.1.3 we described how the microscale data was incorporated in the macroscale model. Briefly, when a tPA molecule bound to a fiber in the macroscale model we generated a random number and used it with the empirical CDF of tPA leaving times to determine when to unbind the tPA molecule. We then found the mean number of plasmin molecules generated in the chosen tPA leaving time. Finally, we used a power function fit to a scatter plot of the lysis time vs. plasmin number data to determine the lysis time associated with the given number of plasmin molecules.

With the modifications made to the microscale model, we no longer have nice relationships (between tPA leaving time and number of plasmin molecules produced, and between number of plasmin molecules produced and lysis time) to exploit in the macroscale model. Instead of approximating relationships by simple linear or power functions, we now directly use distributions. We record the tPA leaving times and lysis times from 10,000 microscale model simulations. If lysis does not occur in a given run, a placeholder lysis time of 9000 seconds is assigned. The tPA leaving time data are sorted in ascending order, and the lysis time data are rearranged accordingly to keep the lysis times in the same position as their corresponding tPA leaving times. We represent the 10,000 tPA leaving times by 100 discrete times (corresponding to the 100 percentiles of the original 10,000 tPA leaving times) and use this data to make an empirical tPA leaving time CDF. When a tPA molecule binds to a fiber in the macroscale model, a uniformly distributed random number, r_1, is generated and used to interpolate a tPA leaving time from the CDF.

To determine when the fiber will degrade based on the tPA leaving time, we put the sorted 10,000 lysis times into 100 bins and select the $\lceil r_1 \times 100 - 0.5 \rceil^{\text{th}}$ bin. Sorting the entries of this bin allows us to generate an empirical lysis time CDF for the chosen tPA leaving time. We then generate a second uniformly distributed random number and use it to interpolate a lysis time from the CDF. During the interpolation, if we access a lysis time of 9000 s (the placeholder time for when lysis does not occur), then tPA does not initiate lysis. The fiber to which tPA is bound will not degrade until another tPA molecule binds and a lysis time less than 9000 seconds is chosen from the CDF.

4.2 Results

The microscale model results presented in this section are given as median (first quartile Q1, third quartile Q3) of 10,000 simulations, and the macroscale model results are mean ± standard deviation of 10 simulations. Unless otherwise stated, macroscale simulations were run for 30 minutes of simulation time. We start by verifying that the main result from Chapter 3 – that the number of tPA molecules exposed to the surface of the clot determines relative lysis speeds – still holds following the model adjustments described in Section 4.1. Using Case A parameters (Table 4.1), we set up 10 macroscale experiments with tPA-to-surface-area ratios varying from 8 to 450 molecules/μm^2. We obtain these ratios by varying both the tPA concentration and the height of the fibrin-free region. As in Figure 3.8, we find that the number of tPA molecules in the system relative to the surface area of the clot abutting the fibrin-free region has a strong influence on lysis speeds. Figure 4.1 shows front velocities in fine and coarse clots as a function of the tPA-to-surface-area ratio for Case

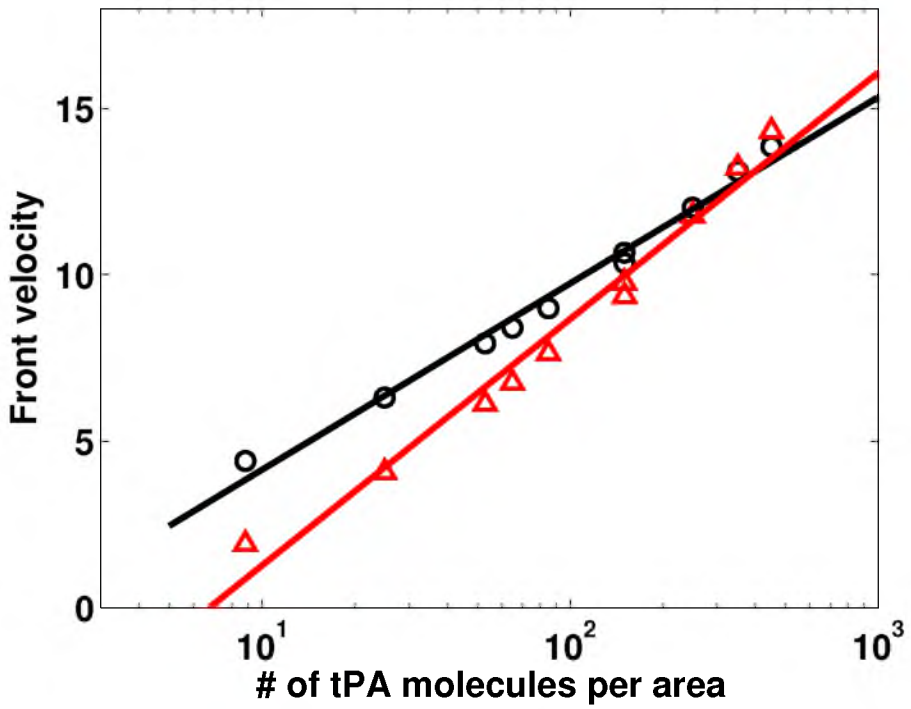

Figure 4.1. Lysis front velocity of a fine clot (red triangles) and a coarse clot (black circles) as a function of the ratio of the number of tPA molecules to the surface area of clot exposed to the fibrin-free region. Experiments were run with ten different tPA-to-surface-area ratios varying from 8 to 450 molecules/μm^2. Each symbol is the mean of ten independent simulations.

A parameters. As the tPA-to-surface-area ratio increases, so does the front velocity. By fitting a line to the data for both coarse and fine front velocities and calculating the point at which the two lines intersect, we estimate 287 molecules/μm^2 to be the tPA-to-surface-area ratio below which coarse clots lyse faster than fine. This number is much higher than the estimate of 25 molecules/μm^2 that we found in Chapter 3, indicating that with these modifications, there is a wider range of conditions for which coarse clots will lyse more quickly than fine.

4.2.1 Parameter variation

Many of the parameter values the multiscale model requires have been characterized experimentally (Table 4.1). However, there are no reliable estimates of binding and unbinding rates for lytic proteins. Moreover, it is possible to engineer tPA variants that have different dissociation constants. To test these unknown and adjustable parameters, we experiment with different parameter values. We either vary tPA and PLG binding and unbinding rates while keeping the dissociation constants fixed (Section 4.2.1.1) or vary the tPA dissociation constant (Section 4.2.1.2).

4.2.1.1 Varying binding and unbinding rates

It is not simply the tPA and PLG dissociation constants that affect the multiscale model (and physiological lysis); the individual binding and unbinding rates also play a role, but are much harder to measure experimentally. The only estimates in the literature, $k_{\text{off}}^{\text{tPA}} = 6.658 \times 10^{-5}$ s^{-1}, $k_{\text{on}}^{\text{tPA}} = 1.148 \times 10^{-4}$ μM^{-1}s^{-1}, $k_{\text{off}}^{\text{PLG}} = 4.131 \times 10^{-3}$ s^{-1}, and $k_{\text{on}}^{\text{PLG}} = 1.087 \times 10^{-4}$ μM^{-1}s^{-1}, are from Diamond and Anand [?]. However, a more recent paper claims that measuring binding and unbinding rates is very hard to do and that no good estimates have been made for these rates [?]. We use our model to investigate how lysis depends on binding and unbinding rates (for fixed dissociation constants) and to estimate a range of plausible parameter values. The different parameter cases we study are displayed in Table 4.2.

- ***Case B*** First, consider Case B parameters, which are identical to the baseline parameters (Case A) except that the tPA binding and unbinding rates are two orders of magnitude smaller (and therefore similar to Diamond and Anand's values). The smaller rates cause an increase in tPA leaving time and the number of runs that result in lysis (Table 4.3). The longer tPA leaving time makes sense since tPA has a much smaller unbinding rate. In fact, only about 0.8% of the runs result in tPA unbinding on its own; tPA

Table 4.2. Parameter sets with varying binding and unbinding rates. Parameter values that differ from baseline Case A parameter values are underlined. $k_{\text{on}}^{\text{PLG}}$ and $k_{\text{off}}^{\text{PLG}}$ are the binding rate of PLG to fibrin and the unbinding rate of PLG from fibrin, respectively, with dissociation constant $k_D^{\text{PLG}} = k_{\text{off}}^{\text{PLG}}/k_{\text{on}}^{\text{PLG}}$. The tPA rates have similar meanings. k_D^{PLG} is different depending on whether fibrin is intact or nicked, and k_D^{tPA} is different depending on whether tPA is bound to a doublet with PLG or without PLG. $k_{\text{cat}}^{\text{ap}}$ is the catalytic rate constant for activation of PLG to plasmin (PLi), $k_{\text{cat}}^{\text{n}}$ is the catalytic rate constant for plasmin-mediated exposure of cryptic binding doublets, and k_{deg} is the plasmin-mediated rate of fibrin degradation. $k_{\text{crawl}}^{\text{PLi}}$ and $k_{\text{unbind}}^{\text{PLi}}$ are the crawling rate and unbinding rate of plasmin, respectively.

Parameters	**Case B (small tPA rates)**	**Case C (large tPA rates)**	**Case D (intermediate PLG rates)**	**Case E (small PLG rates)**	**Case F (small tPA and PLG rates)**
k_{deg} (s^{-1})	5	5	5	5	5
$k_{\text{off}}^{\text{PLG}}$ (s^{-1})	3.8	3.8	<u>0.038</u>	<u>0.0038</u>	<u>0.0038</u>
$k_{\text{on}}^{\text{PLG}}$, intact ($\mu\text{M}^{-1}\text{s}^{-1}$)	0.1	0.1	<u>0.001</u>	<u>0.0001</u>	<u>0.0001</u>
$k_{\text{on}}^{\text{PLG}}$, nicked ($\mu\text{M}^{-1}\text{s}^{-1}$)	1.7273	1.7273	<u>0.017273</u>	<u>0.0017273</u>	<u>0.0017273</u>
$k_{\text{crawl}}^{\text{PLi}}$ (s^{-1})	57.6	57.6	57.6	57.6	57.6
$k_{\text{unbind}}^{\text{PLi}}$ (s^{-1})	0.05	0.05	0.05	0.05	0.05
$k_{\text{off}}^{\text{tPA}}$, with PLG ($\text{s}^{-1}$)	<u>2×10^{-6}</u>	<u>0.02</u>	0.0002	0.0002	<u>2×10^{-6}</u>
$k_{\text{off}}^{\text{tPA}}$, without PLG ($\text{s}^{-1}$)	<u>3.6×10^{-5}</u>	<u>0.36</u>	0.0036	0.0036	<u>3.6×10^{-5}</u>
$k_{\text{on}}^{\text{tPA}}$ ($\mu\text{M}^{-1}\text{s}^{-1}$)	<u>0.0001</u>	<u>1.0</u>	0.01	0.01	<u>0.0001</u>
$k_{\text{cat}}^{\text{ap}}$ (s^{-1})	0.1	0.1	0.1	0.1	0.1
$k_{\text{cat}}^{\text{n}}$ (s^{-1})	5	5	5	5	5

Table 4.3. Microscale model results for varying binding and unbinding rates. Entries are median (Q1, Q3) of 10,000 independent simulations. The column labeled "Time to first PLi" gives data about the time the first plasmin molecule was created. The column labeled "Runs with PLi" gives the number of runs, out of 10,000, in which plasmin was produced and single fiber lysis occurred. The columns labeled "Forced" and "Unbound" give the number of runs out of 10,000 for which tPA was forced to unbind by plasmin and for which tPA unbound on its own, respectively. The "Number of PLi" and "Max PLi" columns give data about the average total number of plasmin molecules produced in one run, and the maximum number of plasmin molecules produced in any of the 10,000 runs, respectively.

Parameters	**Fiber diameter (nm)**	**tPA leaving time (s)**	**Forced**	**Unbound**	**Time to first PLi (s)**	**Number of PLi**	**Max PLi**	**Runs with PLi**
Case A	97.5	90.80 (44.01, 173.18)	4760	4383	80.89 (33.88, 159.48)	1 (1, 2)	7	5956
	195	104.63 (46.44, 198.31)	4895	4834	84.21 (35.40, 170.07)	2 (1, 3)	10	5892
Case B	97.5	161.69 (76.08, 299.69)	8316	74	143.79 (59.27, 283.63)	1 (1, 2)	8	9935
	195	193.42 (95.81, 336.88)	9054	80	139.77 (58.23, 278.44)	2 (1, 3)	13	9939
Case C	97.5	2.05 (0.85, 4.09)	37	9963	2.29 (1.02, 4.15)	1 (1, 1)	2	148
	195	2.04 (0.86, 4.06)	43	9957	1.73 (0.70, 3.97)	1 (1, 1)	4	145
Case D	97.5	133.88 (53.04, 273.79)	2729	6776	104.38 (21.25, 235.06)	1 (1, 2)	6	3406
	195	139.93 (55.15, 277.77)	2722	7103	92.73 (18.22, 224.67)	1 (1, 2)	10	3369
Case E	97.5	155.97 (52.83, 337.87)	1126	8664	14.04 (4.67, 102.48)	1 (1, 2)	6	1413
	195	165.36 (62.58, 333.32)	1061	8864	13.44 (4.97, 85.01)	1 (1, 2)	9	1367
Case F	97.5	2657.6 (891.11, 5714.6)	7017	1486	2566.6 (796.51, 5649.5)	1 (1, 2)	7	8520
	195	2739.7 (891.05, 5682.5)	7555	1412	2649.3 (785.09, 5611.4)	1 (1, 2)	11	8605

is forced to unbind by plasmin-mediated degradation of the doublet to which it is bound in the overwhelming majority of runs. With Case B parameters, 99% of the runs result in lysis, while only about 59% of the Case A runs result in lysis. Because tPA is not likely to unbind on its own when Case B parameters are used, longer lysis times can occur than in Case A. These long lysis times are a result of slow creation of the first plasmin molecule; tPA likely will not unbind unless it is forced to unbind by plasmin, so if the creation of plasmin takes a long time, then tPA will stay bound for a long time, and lysis times will be long. Figure 4.2 shows lysis time CDFs for the different parameter cases. The Case B distribution (red curve) is virtually indistinguishable from the Case A distribution (black curve) up to about 6 minutes. The difference in Cases A and B is that Case B has more long lysis times, resulting in the higher, but otherwise similar, CDF.

Macroscale lysis with Case B parameters (small tPA rates) is not front-like because tPA can diffuse through the clot easily due to the small binding rate to fibrin (Table 4.4). Figure 4.3 shows the number of successful independent tPA binding events as a function of time ("successful" meaning that the binding event resulted in the initiation of lysis, and "independent" meaning that no other tPA had previously begun lysis on that edge). For coarse clots, the enhanced diffusion of tPA through the clot results in faster lysis with Case B parameters (red curve), compared to Case A (black curve). For fine clots, Case B parameters display slower lysis compared to Case A. This is because of the large number of fibers in the fine clot and the longer tPA leaving time for Case B parameters. It takes a while for the 1211 tPA molecules to access all 14145 fibers in the fine clot, so when tPA leaving times are longer (as in Case B), it will take even longer for the tPA to reach all the different fibers. This is not an issue in coarse clots; the 2422 tPA molecules can make it to all 3605 fibers without much trouble. Hence, Case B parameters slow down fine clot lysis, but speed up coarse clot lysis.

- ***Case C*** Increasing baseline tPA binding and unbinding rates by two orders of magnitude (Case C), results in tPA quickly unbinding from the fiber cross section and lysis only occurring in 1.5% of the runs (Table 4.3). When lysis *does* occur, single fiber lysis times are very short (Figure 4.2, green curve) because degradation requires tPA to create plasmin within the first few seconds of the simulation, before the tPA unbinds (Table 4.3). In fact, lysis results are very similar to those with only one plasmin molecule (instead of one tPA molecule) at the start of the simulation, which gives an estimate of how long it takes one plasmin molecule to degrade a single fiber (results not shown). The similarity of

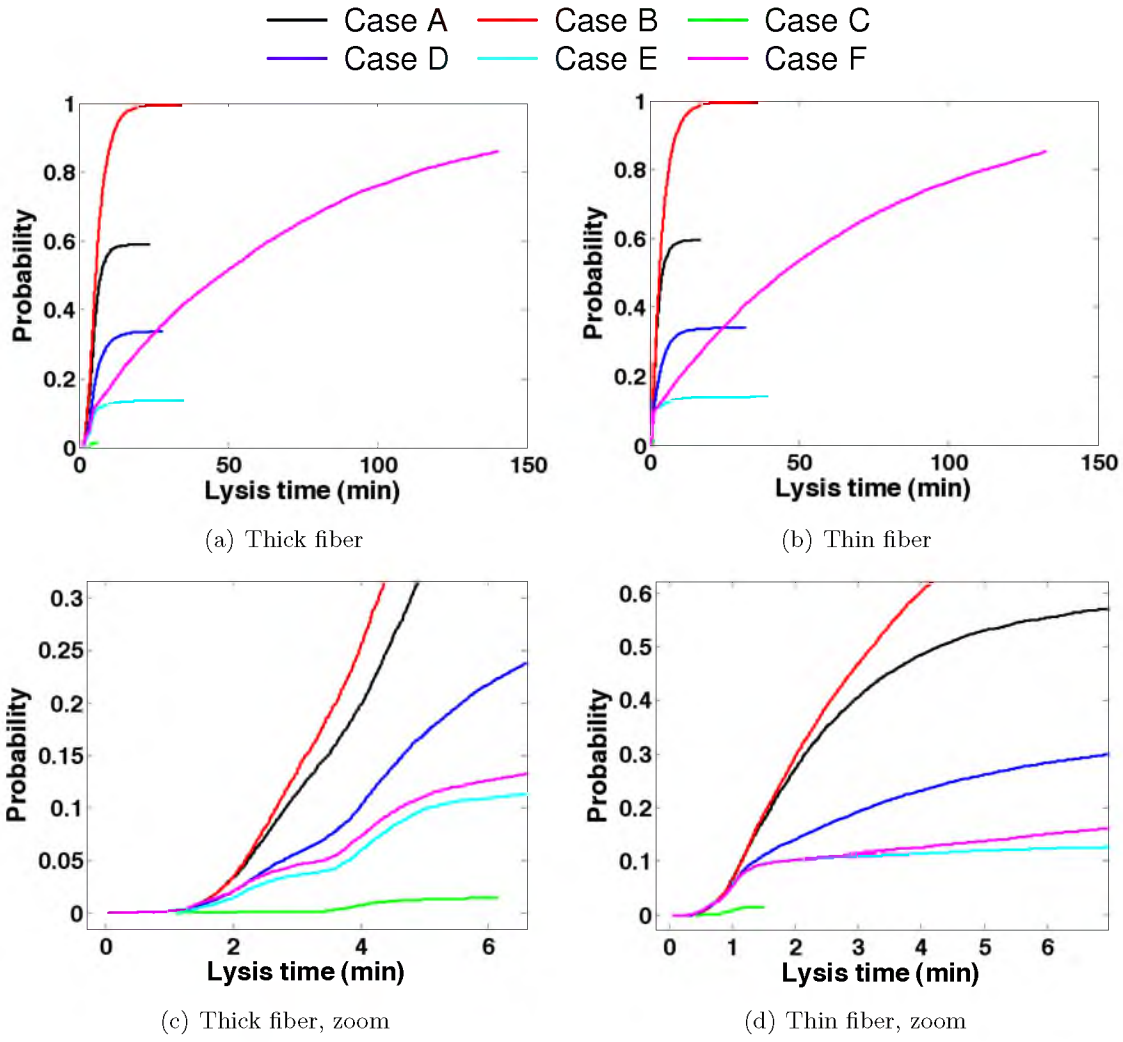

(a) Thick fiber

(b) Thin fiber

(c) Thick fiber, zoom

(d) Thin fiber, zoom

Figure 4.2. Lysis time cumulative distribution functions from the microscale model for varying binding and unbinding rates. The CDFs do not asymptote to 1 because we define "Probability" as the fraction of 10,000 runs. In all simulations, fewer than 10,000 runs resulted in lysis, so there are fewer than 10,000 lysis times. (a) Thick fiber. (b) Thin fiber. (c) Zoomed in view of the first 6 minutes of the thick fiber CDF. (d) Zoomed in view of the first 6 minutes of the thin fiber CDF.

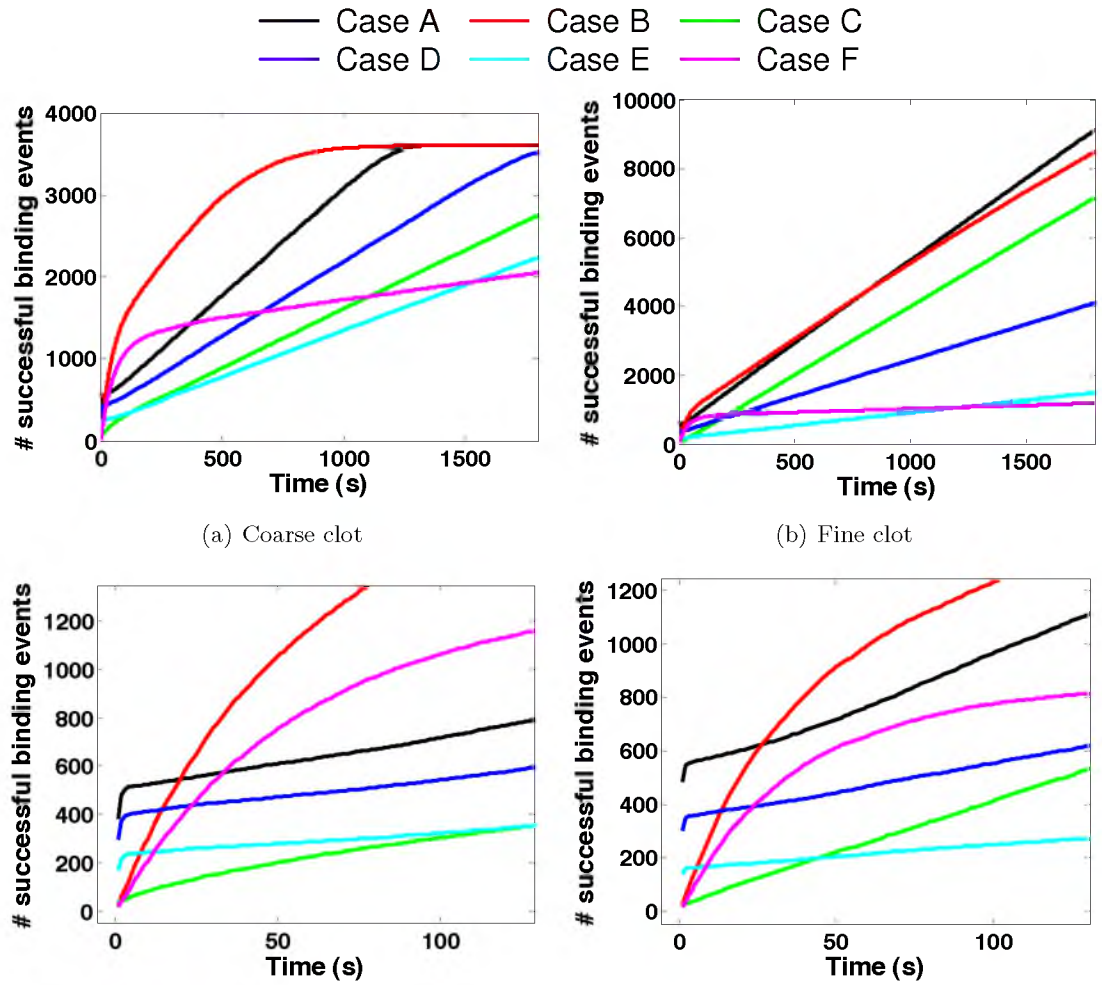

(a) Coarse clot

(b) Fine clot

(c) Coarse clot, zoom

(d) Fine clot, zoom

Figure 4.3. Number of successful tPA binding events as a function of time for varying binding and unbinding rates. Plots are averages of 10 independent simulations. (a) Coarse clot with 3605 total fibers (and 3605 possible successful binding events). (b) Fine clot with 14145 total fibers. (c) Zoomed in view of the first 125 seconds of the coarse clot data. (d) Zoomed in view of the first 125 seconds of the fine clot data.

Table 4.4. Macroscale model results for varying binding and unbinding rates. The experiments involved a 5 nM tPA concentration added to a fibrin-free region with height 2.935 μm. Entries are mean $\pm$ standard deviation of 10 independent simulations. Front velocity calculations do not make sense for simulations in which lysis was not front-like, hence the "$-$" in some entries. * Lysis is front-like (tPA strongly binds to the front), but so slow that it is computationally challenging to measure front velocity.

Parameters	**Clot type**	**Front velocity (μm/min)**	**Degradation rate (% fibers/min)**
Case A	fine	1.97 ± 0.10	1.99 ± 0.016
	coarse	4.40 ± 0.24	4.22 ± 0.061
Case B	fine	$-$	1.61 ± 0.007
	coarse	$-$	6.11 ± 0.004
Case C	fine	1.67 ± 0.09	1.68 ± 0.016
	coarse	2.43 ± 0.10	2.41 ± 0.017
Case D	fine	0.75 ± 0.28	0.87 ± 0.015
	coarse	3.04 ± 0.23	3.06 ± 0.016
Case E	fine	$0.52 \pm 1.38^*$	0.31 ± 0.011
	coarse	1.78 ± 0.36	1.89 ± 0.039
Case F	fine	$-$	0.11 ± 0.007
	coarse	$-$	0.95 ± 0.029

the results in the two cases indicates that when Case C parameters (large tPA rates) result in lysis, plasmin is produced almost immediately. This suggests that the main determinant of lysis time is the time it takes for the first plasmin molecule to be created. With all of the parameter sets tested, only 1-2 plasmin molecules are created, on average. Since the plasmin-mediated degradation rate is the same in all cases, once plasmin is formed, it will degrade at the same rate. Hence, the difference in lysis times must come from the difference in times to first plasmin production. For a given parameter set, the time to produce the first plasmin molecule is roughly the same for both thin and thick fibers. This makes sense, since fiber diameter does not play a role in the initial production of plasmin.

Despite the fast single fiber lysis times, macroscale lysis with Case C parameters is slower than with Case A (Table 4.4) for two main reasons: very rapid binding localizes tPA to a narrow region of fibrin at the front of the clot, preventing tPA diffusion farther into the clot and initiation of lysis on other fibers; and tPA initiates lysis only 1.5% of the time it binds to fibrin. Figure 4.3 illustrates these points; Case C (green curve) results in fewer successful tPA binding events as a function of time than Case A (black curve).

- ***Case D*** With the baseline tPA binding and unbinding rates but with PLG binding and unbinding rates two orders of magnitude smaller (Case D), tPA stays bound to the cross

section longer because it is less likely to be forced to unbind by plasmin (Table 4.3). tPA is less likely to be forced to unbind by plasmin because it takes longer to create plasmin when the PLG binding rate is so low. Unless tPA starts bound to a doublet containing PLG, creation of plasmin cannot occur until a PLG molecule binds, which can take a long time ($\mathcal{O}(10^3$ s)). Because of this, lysis times are slower (Figure 4.2, blue curve). Macroscale lysis is also slower than Case A (Table 4.4, Figure 4.3), because of the slower single fiber lysis times and the fact that only 34% of the time tPA binds will it start lysis (compared to 59% in Case A).

- ***Case E*** PLG binding and unbinding rates three orders of magnitude smaller than baseline rates (Case E) fall within the range of values presented by Diamond and Anand [?]. With Case E parameters, we still find that tPA stays bound longer than when Case A parameters are used, and even fewer simulations result in lysis than in Case D (Table 4.3). This is because the majority of runs for which lysis occurs are runs in which tPA starts bound to a doublet with PLG. If tPA starts on an empty doublet, it is far more likely to unbind before a PLG molecule binds, never initiating lysis. A quasi-steady state approximation shows a 9.5% probability that an initially exposed doublet contains one bound PLG molecule (Appendix D). If the only simulations that result in lysis are those for which tPA starts on a doublet with PLG, we would expect only about 9.5% of the simulations to result in lysis. Since lysis occurred in 14% of the Case E simulations, tPA must occasionally start on an empty doublet which later binds a PLG molecule. This results in long lysis times, as tPA waits for PLG to bind (Figure 4.2). The CDFs of Case E (cyan curve) and Case A (black curve) are similar for very short lysis times (when tPA starts bound to a doublet with PLG and quickly creates a plasmin molecule), but ultimately Case E can yield much longer lysis times than Case A. For a thin fiber, the largest Case E lysis time is roughly 40 min, while the largest Case A lysis time is roughly 20 min. Macroscale lysis is even slower than Case D (Table 4.4, Figure 4.3).

- ***Case F*** Finally, when binding and unbinding rates of both tPA *and* PLG are smaller than baseline Case A parameters (Case F, reflecting Diamond and Anand's estimates), tPA stays bound for a very long time. The tPA leaving time is so long because tPA rarely unbinds on its own due to a small unbinding rate, and is slow to produce a plasmin molecule to force the tPA to unbind (Table 4.3). Single fiber lysis times are very slow (Figure 4.2, magenta line) and consequently macroscale lysis is severely retarded. Figure 4.3 shows that there are many successful tPA binding events early in the simulation when Case F parameters

are used (magenta line). Yet, due to the incredibly long tPA leaving times, after the first round of tPA binding it takes a long time for tPA to unbind and start lysis on a new fiber.

4.2.1.2 Varying tPA dissociation constants

To test potential therapeutics for lysing blood clots, we experimentally vary the tPA dissociation constant, k_D^{tPA}. It is possible to engineer tPA variants that maintain key features of tPA-mediated fibrinolysis, but that have different binding or unbinding rates. We conduct experiments with k_D^{tPA} (for tPA binding to fibrin without bound PLG) ranging from 0.036 μM to 36 μM (Table 4.5). The dissociation constant for tPA binding to fibrin in the presence of PLG is scaled by the same factor. All other parameter values are kept the same as Case A, but either the tPA binding rate or the tPA unbinding rate is changed to alter the dissociation constant to some value other than the physiological value of 0.36 μM.

The value of the dissociation constant does not affect microscale results; only the unbinding rate of tPA from fibrin influences microscale lysis (Table 4.6). When the tPA dissociation constant is varied by fixing the unbinding rate and varying the binding rate,

Table 4.5. Parameter sets with varying k_D^{tPA}. Parameter values that differ from baseline Case A parameter values are underlined. Parameter descriptions are the same as in Table 4.2.

Parameters	**Case G** ($k_D^{\mathbf{tPA}}$**=3.6, small** $k_{\mathbf{on}}^{\mathbf{tPA}}$)	**Case H** ($k_D^{\mathbf{tPA}}$**=3.6, large** $k_{\mathbf{off}}^{\mathbf{tPA}}$)	**Case J** ($k_D^{\mathbf{tPA}}$**=36**)	**Case K** ($k_D^{\mathbf{tPA}}$**=0.036**)
k_{deg} (s^{-1})	5	5	5	5
$k_{\mathrm{off}}^{\mathrm{PLG}}$ (s^{-1})	3.8	3.8	3.8	3.8
$k_{\mathrm{on}}^{\mathrm{PLG}}$, intact ($\mu\mathrm{M}^{-1}\mathrm{s}^{-1}$)	0.1	0.1	0.1	0.1
$k_{\mathrm{on}}^{\mathrm{PLG}}$, nicked ($\mu\mathrm{M}^{-1}\mathrm{s}^{-1}$)	1.7273	1.7273	1.7273	1.7273
$k_{\mathrm{crawl}}^{\mathrm{PLi}}$ (s^{-1})	57.6	57.6	57.6	57.6
$k_{\mathrm{unbind}}^{\mathrm{PLi}}$ (s^{-1})	0.05	0.05	0.05	0.05
$k_{\mathrm{off}}^{\mathrm{tPA}}$, with PLG ($\mathrm{s}^{-1}$)	0.0002	<u>0.002</u>	0.0002	0.0002
$k_{\mathrm{off}}^{\mathrm{tPA}}$, without PLG ($\mathrm{s}^{-1}$)	0.0036	<u>0.036</u>	0.0036	0.0036
$k_{\mathrm{on}}^{\mathrm{tPA}}$ ($\mu\mathrm{M}^{-1}\mathrm{s}^{-1}$)	<u>0.001</u>	0.01	<u>0.0001</u>	<u>0.1</u>
$k_{\mathrm{cat}}^{\mathrm{ap}}$ (s^{-1})	0.1	0.1	0.1	0.1
$k_{\mathrm{cat}}^{\mathrm{n}}$ (s^{-1})	5	5	5	5

Table 4.6. Microscale model results for varying tPA dissociation constants. Baseline Case A parameters are included for comparison. Entries are median (Q1, Q3) of 10,000 independent simulations. The column labeled "Time to first PLi" gives data about the time the first plasmin molecule was created. The column labeled "Runs with PLi" gives the number of runs, out of 10,000, in which plasmin was produced and single fiber lysis occurred. The columns labeled "Forced" and "Unbound" give the number of runs out of 10,000 for which tPA was forced to unbind by plasmin and for which tPA unbound on its own, respectively. The "Number of PLi" and "Max PLi" columns give data about the average total number of plasmin molecules produced in one run, and the maximum number of plasmin molecules produced in any of the 10,000 runs, respectively.

Parameters	**Fiber diameter (nm)**	**tPA leaving time (s)**	**Forced**	**Unbound**	**Time to first PLi (s)**	**Number of PLi**	**Max PLi**	**Runs with PLi**
Case A	97.5	90.80 (44.01, 173.18)	4760	4383	80.89 (33.88, 159.48)	1 (1, 2)	7	5956
	195	104.63 (46.44, 198.31)	4895	4834	84.21 (35.40, 170.07)	2 (1, 3)	10	5892
Case G	97.5	95.87 (45.61, 179.85)	4683	4441	85.11 (36.21, 170.05)	1 (1, 2)	7	5874
	195	106.39 (48.55, 195.06)	4807	4933	83.37 (34.32, 163.45)	2 (1, 3)	12	5808
Case H	97.5	18.67 (7.93, 36.53)	821	9132	17.32 (7.10, 34.98)	1 (1, 2)	6	1275
	195	19.34 (8.18, 38.21)	691	9309	18.04 (7.34, 36.06)	1 (1, 2)	9	1214
Case J	97.5	92.53 (43.55, 175.12)	4683	4451	80.56 (33.13, 163.86)	1 (1, 2)	7	5853
	195	107.01 (47.99, 198.05)	4811	4918	86.31 (34.53, 170.25)	2 (1, 3)	11	5820
Case K	97.5	95.32 (44.51, 179.71)	4672	4430	83.20 (35.19, 167.38)	1 (1, 2)	7	5883
	195	104.23 (47.31, 196.24)	4804	4932	81.18 (33.87, 165.90)	2 (1, 3)	9	5835

the microscale lysis CDFs are indistinguishable (Figure 4.4, Cases A, G, J and K). The CDFs are the same because the simulation begins with tPA bound, so the binding rate only enters the model via the rebinding probability calculation. Decreasing the binding rate (Cases G and J) decreases the rebinding probability, so tPA does not rebind. Increasing the binding rate (Case K) increases the rebinding probability, but only to $\mathcal{O}(10^{-5})$, so tPA still effectively does not rebind. Therefore, microscale results with fixed unbinding rates but variable binding rates are no different than results with the baseline Case A parameters.

On the other hand, if the dissociation constant is varied by fixing the binding rate and varying the unbinding rate (Case H), there is an effect on microscale lysis. Setting $k_D^{\text{tPA}} = 3.6\ \mu\text{M}$ (an order of magnitude bigger than the physiological value) by an order of magnitude decrease in binding rate (Case G) had no effect on microscale lysis, but setting $k_D^{\text{tPA}} = 3.6\ \mu\text{M}$ by an order of magnitude increase in unbinding rate (Case H) slows down microscale lysis (compare Cases A and G to Case H in Table 4.6 and Figure 4.4). A larger unbinding rate results in longer lysis times because tPA unbinds more quickly, produces less plasmin, and consequently slows lysis. On the macroscale level, because tPA unbinds more quickly with Case H parameters, tPA molecules are able to start lysis on other fibers more quickly, resulting in more successful tPA binding events as a function of time (compare red

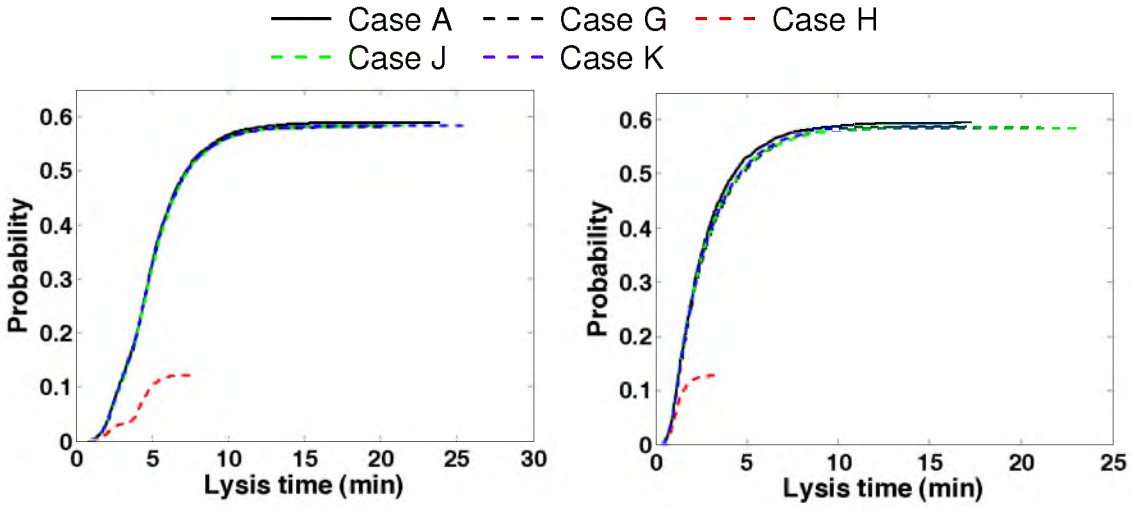

(a) Thick fiber (b) Thin fiber

Figure 4.4. Lysis time cumulative distribution functions from the microscale model for varying tPA dissociation constants. The CDFs do not asymptote to 1 because we define "Probability" as the fraction of 10,000 runs. In all simulations, fewer than 10,000 runs resulted in lysis, so there are fewer than 10,000 lysis times. (a) Thick fiber. (b) Thin fiber.

dashed curve to black solid curve in Figure 4.5). Degradation is faster but less front-like than with Case A parameters (Table 4.7).

For the simulations in which k_D^{tPA} is changed by varying the binding rate (Cases G, J, and K), differences become evident on the macroscale. The macroscale degradation rate is faster with Case G parameters than with Case A because the smaller binding rate means that tPA binds less readily to the clot front (Table 4.7). Relative to a larger binding rate, tPA diffuses farther into the clot, where it can start lysis on the interior fibers earlier; there are more successful independent tPA binding events at any given time when Case G parameters are used (Figure 4.5, dashed black curve), compared to Case A parameters (Figure 4.5, solid black curve).

Increasing the dissociation constant an additional order of magnitude (to $k_D^{\mathrm{tPA}} = 36$ μM) by decreasing the binding rate (Case J), has a similar effect on clot lysis as Case B (small tPA rates): lysis of a fine clot is slower than with Case A parameters, but lysis of a coarse clot is faster (Table 4.7). Successful independent tPA binding events occur earlier in coarse clots with Case J parameters (Figure 4.5, dashed green curve) compared to Case A (solid black curve), but the opposite is true in fine clots. As with Case B, this is due to the number of fibers in the different clots. With such a low tPA binding rate, it is difficult for

Table 4.7. Macroscale model results for varying tPA dissociation constants (Cases G-K). Baseline Case A parameters are included for comparison. The experiments involved a 5 nM tPA concentration added to a fibrin-free region with height 2.935 μm. Entries are mean $\pm$ standard deviation of 10 independent simulations. Front velocity calculations do not make sense for simulations in which lysis was not front-like, hence the "$-$" in some entries. *Lysis is front-like (tPA strongly binds to the front), but so slow that it is computationally challenging to measure front velocity.

Parameters	**Clot type**	**Front velocity (μm/min)**	**Degradation rate (% fibers/min)**
Case A	fine	1.97 ± 0.10	1.99 ± 0.016
	coarse	4.40 ± 0.24	4.22 ± 0.061
Case G	fine	$-$	2.12 ± 0.027
	coarse	$-$	7.10 ± 0.002
Case H	fine	1.50 ± 2.35*	2.25 ± 0.018
	coarse	5.57 ± 0.66	5.72 ± 0.055
Case J	fine	$-$	1.70 ± 0.018
	coarse	$-$	5.41 ± 0.004
Case K	fine	1.43 ± 0.06	1.43 ± 0.016
	coarse	2.21 ± 0.08	2.18 ± 0.021

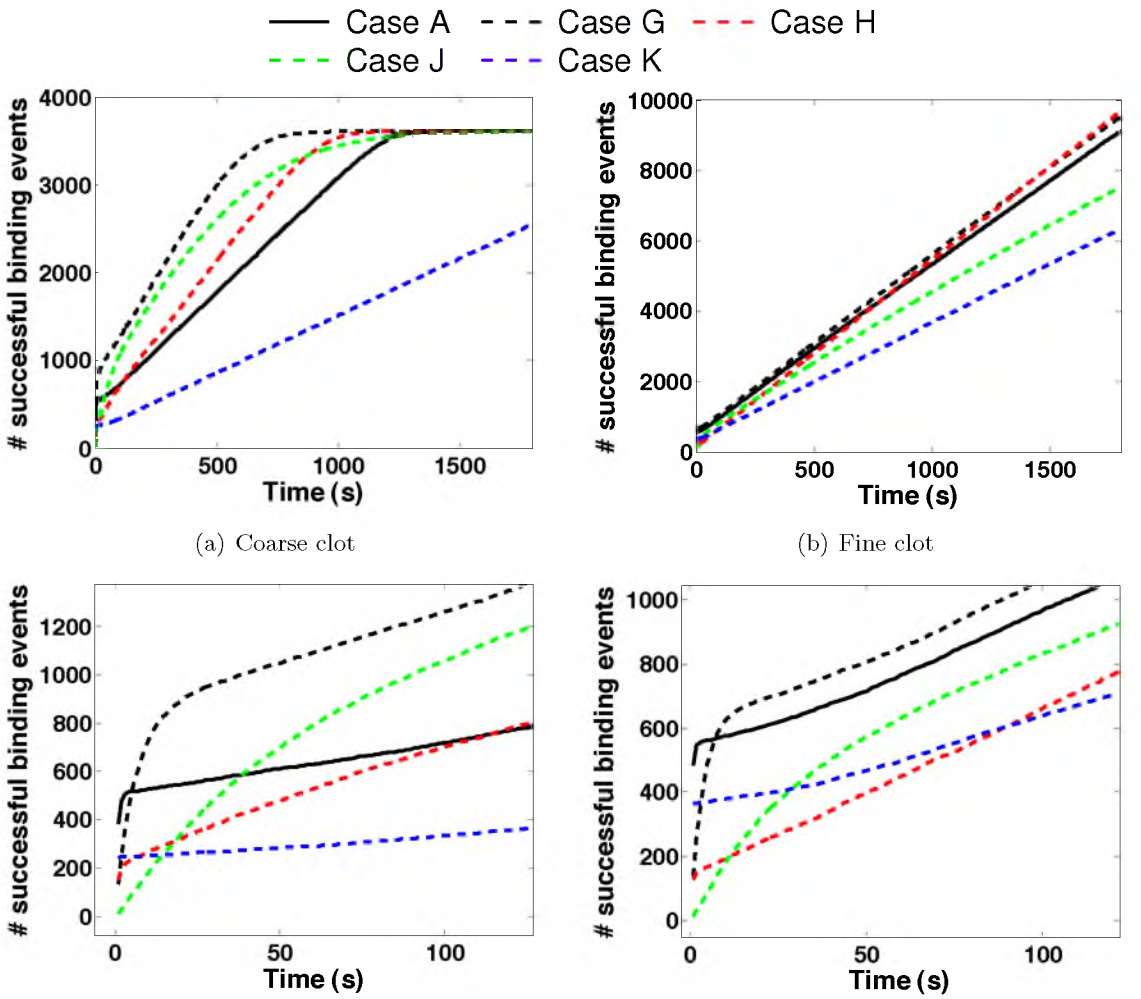

(a) Coarse clot

(b) Fine clot

(c) Coarse clot, zoom

(d) Fine clot, zoom

Figure 4.5. Number of successful tPA binding events as a function of time for varying tPA dissociation constants. Plots are averages of 10 independent simulations. (a) Coarse clot with 3605 total fibers (and 3605 possible successful binding events). (b) Fine clot with 14145 total fibers. (c) Zoomed in view of the first 125 seconds of the coarse clot data. (d) Zoomed in view of the first 125 seconds of the fine clot data.

tPA to start lysis ("successfully" bind) on all the thin fibers in the fine clot, but this is less of an issue in a coarse clot where there are fewer fibers. This appears to be another instance in which the number of fibers in a clot affects lysis rates. In fact, if we look at the raw number of tPA bindings (whether or not they successfully started lysis), we find that about 10000 bindings occur in 1800 seconds in both types of clots (results not shown). These are a sufficient number of binding events to degrade the 3605 thick fibers in the coarse clot, but not nearly enough to degrade the 14145 thin fibers in the fine clot. Lastly, with Case J parameters, fine and coarse clot lysis rates are slower compared to Cases G and H. This suggests there exists a value for the tPA dissociation constant that optimizes lysis speed; increasing k_D^{tPA} from 0.36 μM (physiological) to 3.6 μM speeds up lysis, but increasing it further to 36 μM begins to slow lysis down.

With a dissociation constant an order of magnitude *smaller* than physiological ($k_D^{\text{tPA}} = 0.036$ μM), obtained by using an order of magnitude larger tPA binding rate (Case K), the lysis front velocity is slower than with Case A (Table 4.7). This is because tPA binds more readily to fibrin, and is therefore prevented from diffusing farther into the clot and beginning lysis on internal fibers. As a function of time, there are far fewer successful tPA binding events for Case K (Figure 4.5, dashed blue curve) than for Case A (black solid curve).

4.2.2 tPA rebinding

Given the very low tPA rebinding probability calculated in Appendix E, we conclude that tPA essentially never rebinds to the fiber cross section. The absence of tPA rebinding eliminates the positive feedback caused by plasmin-mediated exposure of new binding sites. Since tPA can never rebind, it does not matter how many new binding sites are exposed – no additional plasmin can be created. It would be possible for a different tPA molecule to bind to one of the newly exposed sites. However, due to the low tPA concentration (only 3 tPA molecules/μm^3 in a 5 nM tPA concentration), this is very unlikely. It is often stated in the literature that there is positive feedback, but direct evidence for this is lacking. In order to explore the effect that positive feedback would have in the model, we must allow tPA to rebind. The microscale model is adjusted so that tPA rebinds with 100% probability if there is an available doublet within two binding locations of the doublet from which it unbound. The constraint that tPA can only rebind up to two binding locations away from where it unbound is motivated by the idea that tPA is more likely to rebind nearby, since the binding

rate for tPA to fibrin is large. If there are multiple doublets available for tPA rebinding, the doublet to which tPA binds is chosen randomly using a uniform distribution. We study tPA rebinding using three representative parameter sets from Section 4.2.1.1: baseline (Case A), small tPA binding and unbinding rates (Case B), and small PLG binding and unbinding rates (Case D).

Results from microscale model simulations with tPA rebinding are presented in Table 4.8 and Figure 4.6. Comparing data from runs *with* tPA rebinding (Table 4.8) to data from runs *without* tPA rebinding (Table 4.3) provides insight into how the presence of tPA affects lysis. Unsurprisingly, for a given set of parameters, tPA stays bound to the cross section for a longer total amount of time when tPA can rebind. In fact, in many cases tPA stays bound for the whole simulation, producing a tPA leaving time equal to the lysis time. Figure 4.6 shows that single fiber lysis is faster when tPA can rebind, but a wider range of lysis times is also possible. The dashed curves represent runs with tPA rebinding, and the solid curves represent runs without tPA rebinding. We see that for all cases, the dashed curves are above the solid curves. With tPA rebinding, 100% of the microscale runs result in lysis, so some longer lysis times are achieved compared to runs without tPA rebinding. These longer lysis times correspond to situations in which tPA unbinds before creating a plasmin molecule (so in the runs without rebinding, these would be failed attempts at lysis), but then rebinds and later produces plasmin.

Adding positive feedback via tPA rebinding to the microscale model increases macroscale lysis rates in coarse clots with Case A or Case D parameters (compare Table 4.9 to

Table 4.8. Microscale model results for tPA rebinding. Entries are median (Q1, Q3) of 10,000 independent simulations. The column labeled "Time to first PLi" gives data about the time the first plasmin molecule was created. The column labeled "Runs with PLi" gives the number of runs, out of 10,000, in which plasmin was produced and single fiber lysis occurred.

Parameters	**Fiber diameter (nm)**	**tPA leaving time (s)**	**Time to first PLi (s)**	**Runs with PLi**
Case A (tPA)	97.5	183.50 (98.46, 323.93)	143.39 (59.91, 283.14)	10000
	195	260.06 (161.02, 406.11)	142.71 (60.45, 287.08)	10000
Case B (tPA)	97.5	180.00 (96.78, 320.86)	145.34 (60.56, 283.71)	10000
	195	251.83 (156.15, 388.91)	142.25 (59.41, 281.96)	10000
Case D (tPA)	97.5	419.07 (172.81, 814.58)	384.92 (138.70, 777.55)	10000
	195	481.51 (244.08, 905.58)	373.72 (134.33, 793.87)	10000

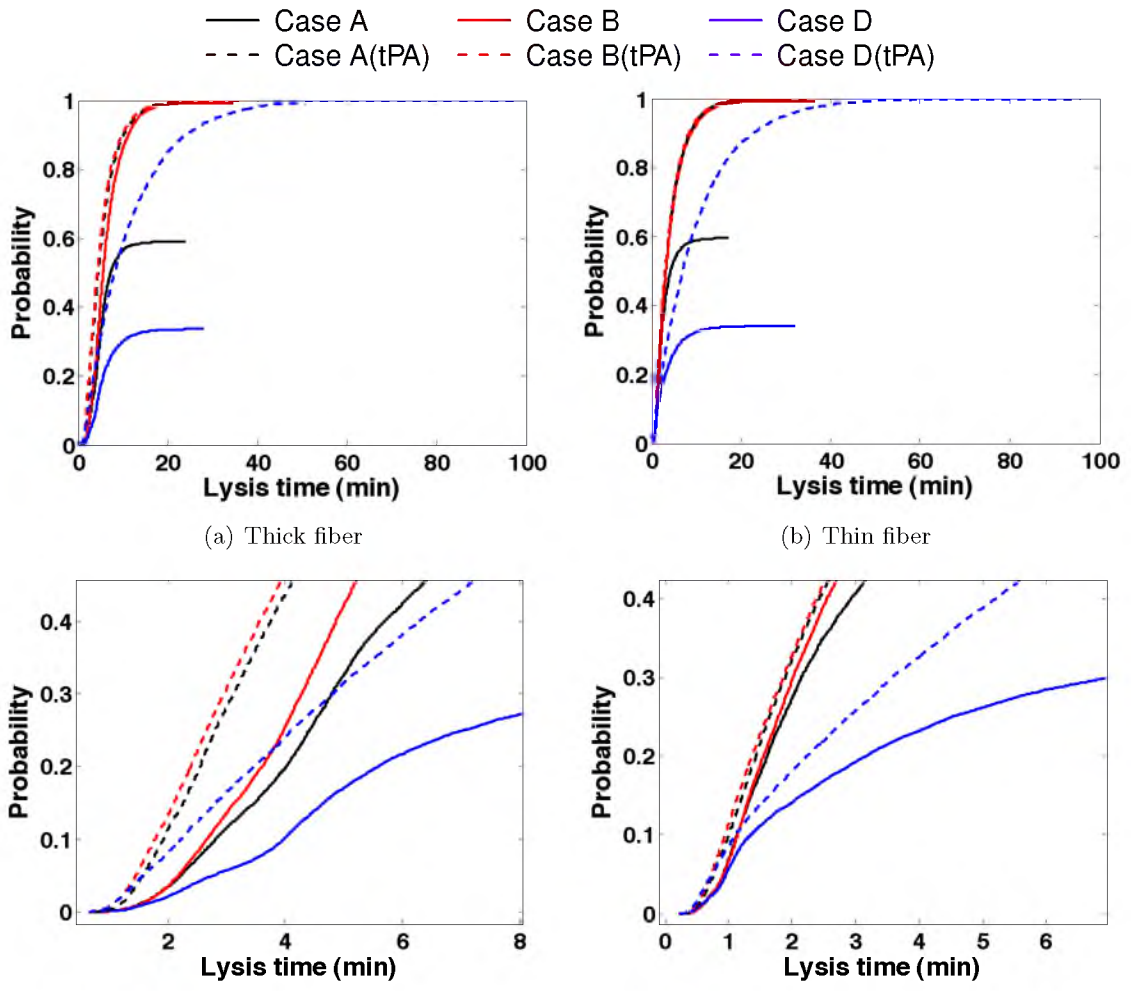

(a) Thick fiber

(b) Thin fiber

(c) Thick fiber, zoom

(d) Thin fiber, zoom

Figure 4.6. Lysis time cumulative distribution functions from the microscale model with tPA rebinding. Dashed curves denote simulations with tPA rebinding. For comparison, solid curves represent simulations without tPA rebinding. The solid curves do not asymptote to 1 because we define "Probability" as the fraction of 10,000 runs. In those simulations, fewer than 10,000 runs resulted in lysis, so there are fewer than 10,000 lysis times. (a) Thick fiber. (b) Thin fiber. (c) Zoomed in view of the first 8 minutes of the thick fiber CDF. (d) Zoomed in view of the first ≈ 7 minutes of the thin fiber CDF.

Table 4.9. Macroscale model results for tPA rebinding. The experiments involved a 5 nM tPA concentration added to a fibrin-free region with height 2.935 μm. Fine clots were run for 60 minutes of simulation time, coarse clots for 30 minutes. Entries are mean ± standard deviation of 10 independent simulations. Front velocity calculations do not make sense for simulations in which lysis was not front-like, hence the "−" in some entries.

Parameters	**Clot type**	**Front velocity (μm/min)**	**Degradation rate (% fibers/min)**
Case A (tPA)	fine	1.77 ± 0.07	1.77 ± 0.009
	coarse	4.78 ± 0.22	4.70 ± 0.024
Case B (tPA)	fine	−	1.57 ± 0.006
	coarse	−	6.09 ± 0.28
Case D (tPA)	fine	0.82 ± 0.09	0.85 ± 0.005
	coarse	3.49 ± 0.17	3.47 ± 0.024

Table 4.4). The number of successful binding events as a function of time is greater when tPA can rebind (blue and black dashed curves are above the solid curves in Figure 4.7), increasing lysis rates. For these parameter cases, allowing tPA to rebind greatly increases the probability that tPA initiates lysis when it binds on the macroscale. For example, with Case A parameters, tPA rebinding increases the likelihood of lysis on the microscale from 59% to 100%. Hence, macroscale lysis rates are increased because tPA is more efficient – every time tPA binds to a fiber, it starts lysis. With Case B parameters, however, macroscale lysis of a coarse clot is virtually unchanged whether or not tPA can rebind. In this case, the plots of the number of successful binding events are almost indistinguishable (solid and dashed red curves in Figure 4.7). Because more than 99% of Case B microscale runs result in lysis even when tPA does not rebind (Table 4.3), allowing tPA to rebind has little effect on macroscale lysis.

Fine clots also have more efficient tPA when tPA can rebind to the fiber cross section (compare "Runs with PLi" columns in Table 4.8 and Table 4.3), but unlike in coarse clots, macroscale lysis is not faster. With tPA rebinding, the higher percentage of successful tPA bindings is outweighed by the longer residence time of tPA on fibers; when tPA is bound, it cannot diffuse and therefore initiation of lysis on other fibers is delayed. The very large ratio of fibers to tPA molecules in a fine clot ($14145/1211 \approx 11.68$ fibers/molecule) means that each tPA molecule must start lysis on many different fibers in order for macroscale degradation to occur. Contrast this with a coarse clot, where the fiber-to-tPA ratio is $3605/2422 \approx 1.49$ fibers/molecule. The longer tPA leaving times are not an issue in coarse clots because there are enough tPA molecules to efficiently start lysis on all fibers. However,

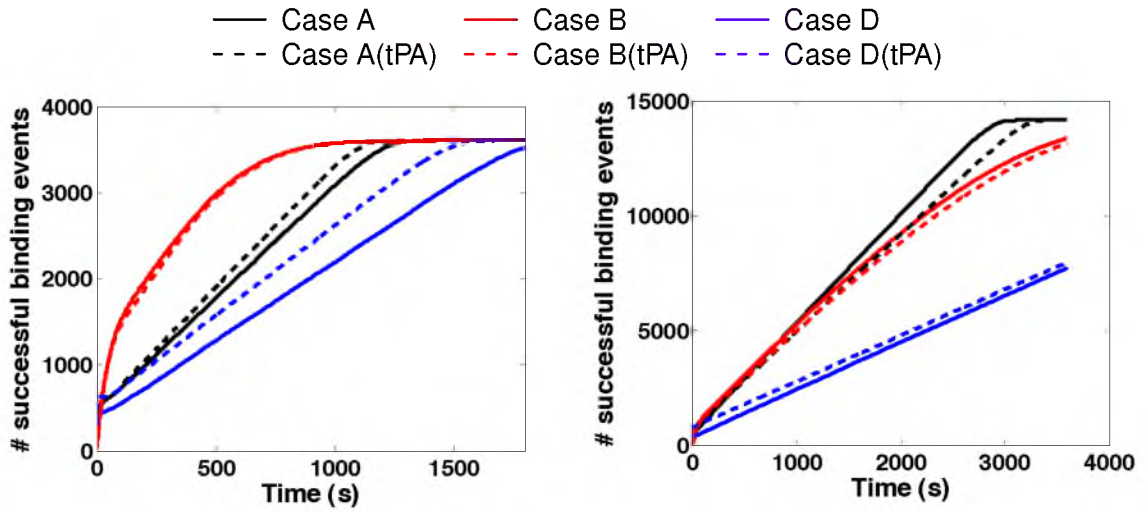

(a) Coarse clot

(b) Fine clot

Figure 4.7. Number of successful tPA binding events as a function of time for tPA rebinding. The dashed curves represent runs with tPA rebinding, and the solid curves represent runs without tPA rebinding. Plots are averages of 10 independent simulations. (a) Coarse clot with 3605 total fibers (and 3605 possible successful binding events). (b) Fine clot with 14145 total fibers.

in fine clots, where each tPA molecule must start lysis on many fibers, preventing tPA from diffusing to new fibers (by keeping it bound longer) can slow lysis. We see this with Case A parameters. Allowing tPA to rebind results in fewer successful binding events as a function of time (dotted black curve is below solid black curve in Figure 4.7), and consequently in slower lysis rates (Table 4.9 and Table 4.4). With Case B and Case D parameters, tPA rebinding does not appreciably change the macroscale lysis rates. As in coarse clots, the reason tPA rebinding does not have an effect with Case B parameters is that every tPA binding event almost certainly initiates lysis, even when tPA cannot rebind. We believe it is serendipitous that tPA rebinding does not have an effect on fine clot lysis with Case D parameters; the prolonged tPA leaving times prevent tPA from diffusing as quickly through the clot, but this is balanced by the higher percentage of successful tPA bindings.

4.2.3 Plasmin unbinding

We now study the effect of the plasmin inhibitor, α_2-antiplasmin (α_2-AP), on our multiscale model. α_2-AP exists in the plasma at a concentration of about 1 μM and binds to plasmin with an association constant of 2×10^7 $M^{-1}s^{-1}$ [?], one of the fastest biological reactions ever characterized [?]. It is believed that plasma-phase α_2-AP directly

inhibits free plasmin. When cross-linked to fibrin, α_2-AP has been shown to inhibit plasmin generated on fibrin [?, ?]. It is believed that α_2-AP inhibits the plasmin once the plasmin unbinds from fibrin; bound plasmin is protected from α_2-AP. Some biological experiments suggest that both fibrin-associated and plasma-phase α_2-AP affect fibrinolysis [?]. However, other experiments seem to imply that free α_2-AP has little effect on clot lysis time [?]. In these experiments, uncross-linked clots showed very little variation in lysis rate, regardless of the α_2-AP concentration in the clotting plasma. Because we do not distinguish between cross-linked and uncross-linked fibrin in our model, we focus on plasma-phase α_2-AP.

To study the effect of α_2-AP on lysis, we allow plasmin to unbind in the microscale model. We assume that unbound plasmin is immediately inhibited by α_2-AP and removed from the system. In this way, we model the *effect* of α_2-AP without directly adding it to the model. We adjust the microscale model by adding plasmin unbinding reactions to the Gillespie algorithm; now plasmin can crawl, degrade fibrin, expose binding sites, and unbind from the cross section.

As expected, allowing plasmin to unbind has no effect on the time required to produce the first plasmin molecule (compare Table 4.10 to Tables 4.9 and 4.3). The tPA leaving time is increased when tPA is usually forced to unbind by plasmin (Case B) relative to when tPA usually unbinds on its own (Cases A and D). Also, single fiber lysis times are slower for all parameters when plasmin is allowed to unbind, with Case B being the most drastically affected (Figure 4.8). Thick fibers degrade less than 1% of the time (0.05-0.89%) when plasmin can unbind, so it is virtually impossible to see the corresponding lysis time CDFs in Figure 4.8(a). Because lysis of thin fibers requires fewer plasmin-mediated degradation events than lysis of thick fibers, a larger percentage of thin fiber simulations result in degradation (6.9-33.61%), but all of these percentages are still lower than when plasmin does not unbind.

Fine clots lyse faster than coarse clots, even though the number of tPA molecules exposed to the clot front is less than 287 molecules/μm^2 (and hence in the range where coarse clots should lyse faster than fine (Figure 4.1)). The fine clots lyse faster because of the drastic difference in successful tPA binding (0.05-0.89% success rate for thick, 6.9-33.61% for thin). This suggests that the number of fibers in the clot, the number of tPA molecules exposed to the clot front, *and* the likelihood of tPA initiating lysis when it binds contribute to relative lysis rates in fine and coarse clots.

When plasmin can unbind *and* tPA can rebind, single fiber lysis times are slower (for

Table 4.10. Microscale model results for plasmin unbinding. Data descriptions are the same as Table 4.8. In the parameter names, "PLi" means that plasmin was allowed to unbind, and "tPA" means that tPA was allowed to rebind.

Parameters	Fiber diameter (nm)	tPA leaving time (s)	Time to first PLi (s)	Runs with PLi
Case A (PLi)	97.5	105.47 (46.08, 209.25)	81.29 (34.31, 166.86)	1517
	195	111.63 (48.49, 222.27)	83.20 (34.84, 167.74)	20
Case B (PLi)	97.5	216.08 (93.52, 416.47)	144.45 (60.35, 283.45)	3361
	195	246.97 (109.44, 489.67)	142.69 (57.02, 282.32)	89
Case D (PLi)	97.5	144.69 (57.74, 302.73)	106.67 (32.01, 241.09)	690
	195	148.77 (58.62, 307.57)	110.97 (33.21, 247.83)	5
Case A (tPA,PLi)	97.5	272.24 (145.21, 475.42)	141.23 (58.24, 279.82)	9911
	195	502.01 (309.67, 783.48)	142.27 (60.90, 284.93)	7608
Case B (tPA,PLi)	97.5	301.05 (150.21, 541.42)	142.27 (57.70, 283.37)	9888
	195	565.81 (332.00, 945.75)	141.57 (58.51, 286.91)	7396
Case D (tPA,PLi)	97.5	619.18 (292.63, 1109.3)	386.21 (142.89, 799.57)	9918
	195	1009.7 (574.94, 1637.9)	386.19 (144.00, 822.56)	7725

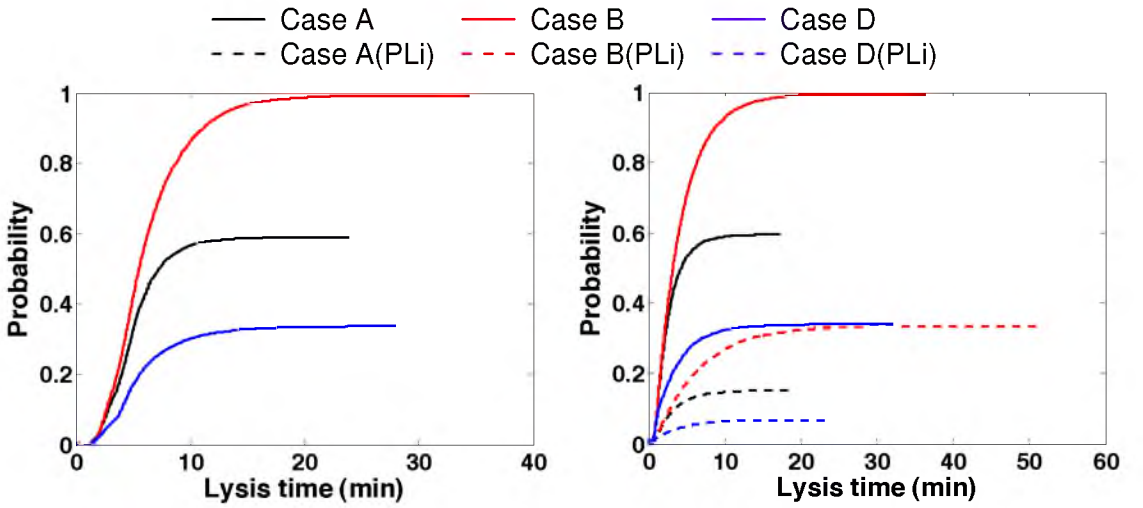

(a) Thick fiber

(b) Thin fiber

Figure 4.8. Lysis time cumulative distribution functions from the microscale model with plasmin unbinding. Dashed curves denote simulations with plasmin unbinding. For comparison, solid curves represent simulations without plasmin unbinding. The CDFs do not asymptote to 1 because we define "Probability" as the fraction of 10,000 runs. (a) Thick fiber. Due to the very low number of runs resulting in lysis when plasmin unbinds, the dashed curves are not visible on this scale. (b) Thin fiber.

all parameter cases tested) than in runs for which plasmin cannot unbind and tPA does not rebind, but lysis occurs more frequently (Figure 4.9(a)). These single fiber lysis times are also slower than those produced by simulations in which plasmin cannot unbind but tPA can rebind (results not shown).

Unsurprisingly, compared to runs in which plasmin does not unbind, clot lysis rates are drastically reduced when plasmin is allowed to unbind, whether or not tPA rebinds (Table 4.11). The number of successful tPA binding events as a function of time is much lower as well (which contributes to the slower lysis rates), since the probability of tPA initiating lysis when it binds is so low (Figures 4.10 and 4.11).

4.3 Discussion

In this chapter we describe biologically motivated modifications of our multiscale model of fibrinolysis. The microscale domain is adjusted so that the fibrin concentration in a single fiber is approximately 800 μM, and the amount of fibrin protein in a fiber is approximately 20% of the fiber volume. The physical size of PLG is accounted for by allowing tPA to activate to plasmin any PLG molecule on the same protofibril, and by allowing plasmin to

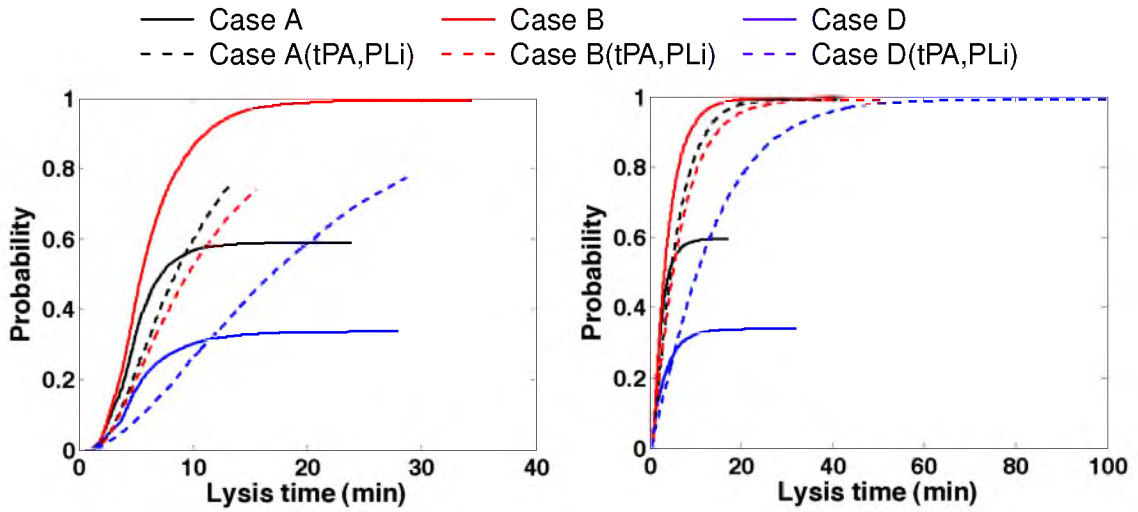

(a) Thick fiber (b) Thin fiber

Figure 4.9. Lysis time cumulative distribution functions from the microscale model with plasmin unbinding and tPA rebinding. Dashed curves denote simulations with plasmin unbinding and tPA rebinding. For comparison, solid curves represent simulations without plasmin unbinding and tPA rebinding. The CDFs do not asymptote to 1 because we define "Probability" as the fraction of 10,000 runs. (a) Thick fiber. (b) Thin fiber.

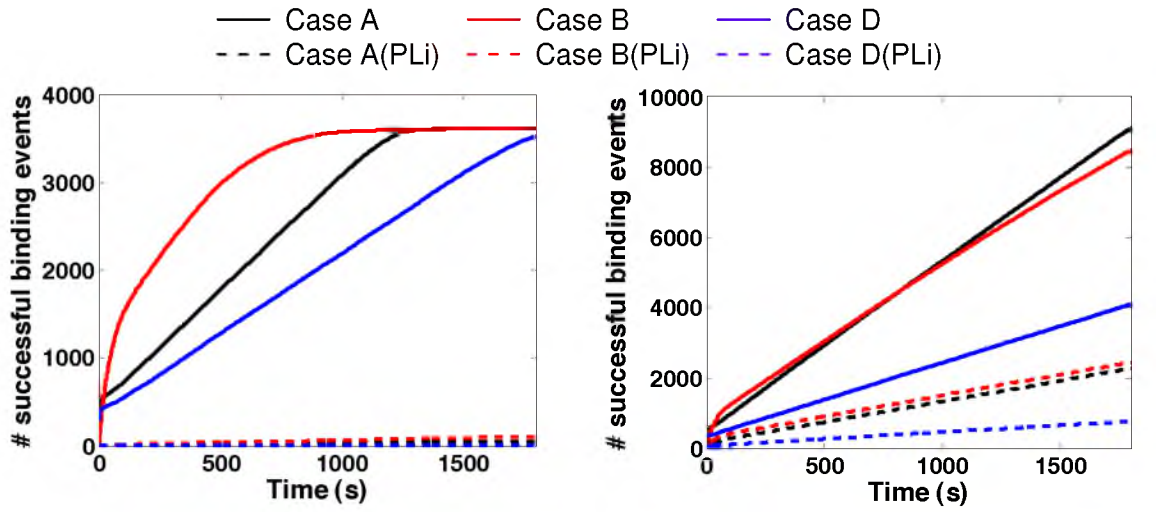

(a) Coarse clot

(b) Fine clot

Figure 4.10. Number of successful tPA binding events as a function of time for plasmin unbinding. The dashed curves represent runs with plasmin unbinding, and the solid curves represent runs without plasmin unbinding. Plots are averages of 10 independent simulations. (a) Coarse clot with 3605 total fibers (and 3605 possible successful binding events). (b) Fine clot with 14145 total fibers.

Table 4.11. Macroscale model results for plasmin unbinding. Data descriptions are the same as Table 4.4. In the parameter names, "PLi" means that plasmin was allowed to unbind, and "tPA" means that tPA was allowed to rebind. * Lysis is front-like (tPA strongly binds to the front), but so slow that it is computationally challenging to measure front velocity.

Parameters	**Clot type**	**Front velocity (μm/min)**	**Degradation rate (% fibers/min)**
Case A (PLi)	fine	0.66 ± 1.60*	0.49 ± 0.012
	coarse	0.04 ± 0.19*	0.045 ± 0.006
Case B (PLi)	fine	–	0.50 ± 0.014
	coarse	–	0.064 ± 0.007
Case D (PLi)	fine	0.25 ± 0.55*	0.16 ± 0.006
	coarse	0.001 ± 0.008*	0.008 ± 0.003
Case A (tPA,PLi)	fine	1.17 ± 0.23	1.24 ± 0.019
	coarse	2.20 ± 0.21	2.21 ± 0.019
Case B (tPA,PLi)	fine	–	1.13 ± 0.014
	coarse	–	2.96 ± 0.030
Case D (tPA,PLi)	fine	0.91 ± 2.52*	0.56 ± 0.014
	coarse	1.25 ± 0.33	1.25 ± 0.018

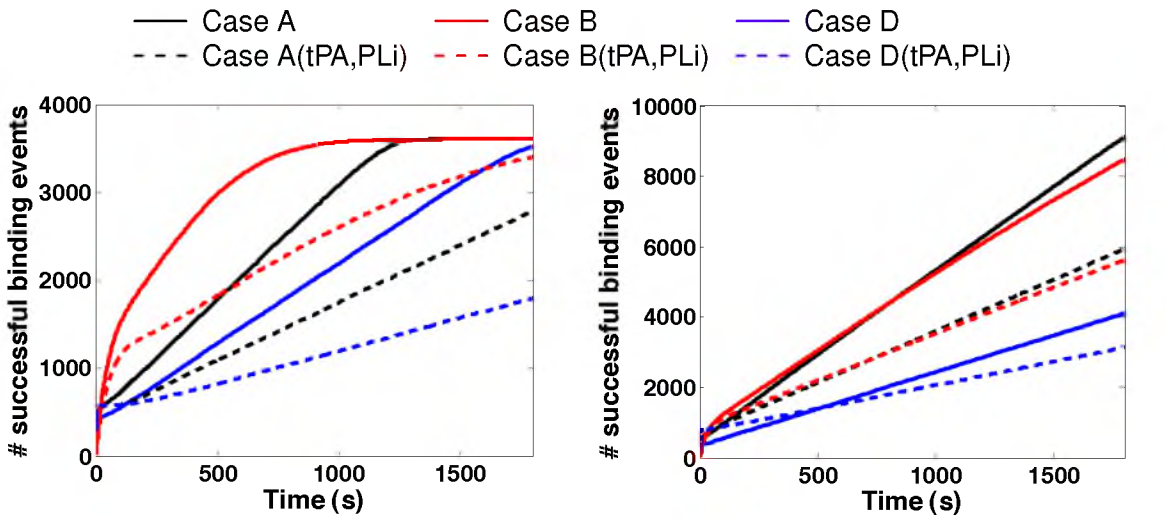

(a) Coarse clot

(b) Fine clot

Figure 4.11. Number of successful tPA binding events as a function of time for plasmin unbinding and tPA rebinding. The dashed curves represent runs with plasmin unbinding and tPA rebinding, and the solid curves represent runs without plasmin unbinding or tPA rebinding. Plots are averages of 10 independent simulations. (a) Coarse clot with 3605 total fibers (and 3605 possible successful binding events). (b) Fine clot with 14145 total fibers.

degrade any doublet on the same protofibril. Since a protofibril is about 5 nm in diameter and a plasminogen (and therefore plasmin) molecule is about 9-11 nm in diameter, it is reasonable that a PLG (or plasmin) molecule bound to one chain of a protofibril would be able to contact the other five protofibril chains.

With model modifications and baseline parameters (Case A), coarse clots lyse faster than fine clots for a wide range of conditions (Figure 4.1). The individual quantities of tPA concentration and volume of fibrin-free region do not matter; as long as the number of tPA molecules exposed to the surface of the clot is less than $287/\mu m^2$, coarse clots will lyse faster than fine. Many experiments show coarse clots lyse faster than fine clots, so this new estimate seems more reasonable than the 25 molecules/μm^2 obtained earlier in Chapter 3; if the threshold number of tPA molecules is larger, presumably many biological experiments will show coarse clots lysing faster than fine.

Since individual binding and unbinding rates for lytic proteins are difficult to measure, we use the multiscale model to hypothesize reasonable ranges for these values. The tPA and PLG binding rates to fibrin in the baseline parameter set (Case A) were suggested

in an earlier mathematical model [?]. The Case A unbinding rates are chosen to enforce the measured dissociation constants. The incredibly slow single fiber and whole clot lysis times for Case F parameters (Figure 4.2, Table 4.4) suggest that the binding and unbinding rates of tPA and PLG should be bigger than those cited in Diamond and Anand [?]. With small tPA rates and baseline PLG rates (Case B), single fiber lysis seems reasonable, but macroscale lysis is not front-like (Figure 4.2, Table 4.4). Since lysis has been observed experimentally to be front-like, tPA (un)binding rates in the absence of PLG are likely larger than these values ($k_{\text{on}}^{\text{tPA}} = 1 \times 10^{-4}$ $\mu\text{M}^{-1}\text{s}^{-1}$, $k_{\text{off}}^{\text{tPA}} = 3.6 \times 10^{-5}$ s^{-1}). Increasing the tPA rates so $k_{\text{on}}^{\text{tPA}} = 1$ $\mu\text{M}^{-1}\text{s}^{-1}$ (Case C) results in infrequent microscale lysis, but produces reasonable macroscale lysis due to the strong binding of tPA to the clot front (Figure 4.2, Table 4.4). With small PLG rates and baseline tPA rates (Cases D and E), only a small fraction of the time tPA binds to fibrin does it start lysis (Table 4.3). Because tPA rarely initiates lysis when it binds *and* because once bound it remains bound for a very long time, macroscale lysis is slowed to what seem to be biologically unreasonable rates (Table 4.4). We conclude that binding rates of tPA and PLG should be in the range $k_{\text{on}}^{\text{tPA}} \in (1 \times 10^{-2}, 1)$ $\mu\text{M}^{-1}\text{s}^{-1}$, $k_{\text{on}}^{\text{PLG}} \in (1 \times 10^{-3}, 1 \times 10^{-1})$ $\mu\text{M}^{-1}\text{s}^{-1}$, with unbinding rates such that the measured dissociation constants are achieved.

To suggest potential targets for new therapeutics aimed at lysing blood clots, we studied model results with varying tPA dissociation constants. The physiological tPA dissociation constant for tPA binding to fibrin in the absence of PLG is 0.36 μM [?]. Decreasing k_D^{tPA} (Case K) slows down macroscale lysis and increasing k_D^{tPA} (Cases G, H, J) speeds up lysis (Table 4.7). It appears that there is an optimum dissociation constant, since lysis is reduced at the highest dissociation constant tested ($k_D^{\text{tPA}} = 36$ μM displays slower lysis than $k_D^{\text{tPA}} = 3.6$ μM). The way that we increase the dissociation constant (either by decreasing the binding rate or increasing the unbinding rate) has a quantitative effect on lysis speed, but lysis is still faster than when the physiological dissociation constant is used. The reason a larger dissociation constant results in faster lysis is because tPA does not bind as strongly to the front and can start lysis on more fibers throughout the clot. So a tPA variant that bound less strongly to fibrin, but retained the full ability to convert PLG to plasmin, would be an ideal target for drug design.

In general, we find that lysis rates are increased when tPA binds less frequently to fibrin. In this case, tPA diffuses more easily and starts lysis on fibers throughout the clot, so lysis is not front-like. The front-like behavior of lysis is dependent on strong binding of tPA to

fibers at the lysis front. If the binding rate of tPA to fibrin is small (Cases B and F in Section 4.2.1.1, Cases G and J in Section 4.2.1.2), or if the concentration of binding sites on fibrin available to tPA is low (Table 3.3 in Section 3.2.2.2), lysis does not proceed as a front. We conclude that in order for a lysis front to exist, tPA must bind strongly to fibrin; the binding rate of tPA to fibrin and the concentration of binding sites available to tPA on fibrin determine whether or not lysis is front-like.

Positive feedback, attained in the model by allowing tPA to rebind to the fiber cross section, has only a small effect on clot lysis. Depending on parameters, positive feedback may or may not affect fine clot lysis rates. Coarse clot lysis rates are increased by positive feedback for all parameter sets that result in inefficient tPA (Cases A and D). If tPA initiates lysis essentially every time it binds to a fiber, then positive feedback has no effect on lysis rates (Case B). The differing effect of positive feedback on the two types of clots is due to the tradeoff between the higher percentage of successful tPA bindings and the longer tPA leaving times. tPA is more efficient on the macroscale when we allow it to rebind on the microscale, but it is also less mobile on the macroscale because it stays bound to fibers for a longer time. In a fine clot with 14145 fibers, the hindered movement of tPA through the clot outweighs the increased efficiency of tPA in starting lysis, and therefore results in slower lysis rates. In a coarse clot with 3605 fibers, the longer tPA leaving times are less important, and the higher efficiency of tPA results in faster lysis rates. In the future, we will more closely examine the potential role of positive feedback in fibrinolysis.

We allow plasmin to unbind from the microscale model to study the effect of α_2-AP on lysis. When plasmin can unbind, there is a significant reduction in the number of microscale runs that result in lysis (Table 4.10). On the macroscale, this results in inefficient tPA (very few of the tPA binding events initiate lysis), and consequently in extremely slow clot lysis rates. The predicted lysis front velocities from the macroscale model (Table 4.11) are up to three orders of magnitude smaller than published experimental lysis front velocities [?, ?, ?]. The slow lysis rates predicted by the model when plasmin unbinds are physiologically unrealistic, though we should not conclude from this observation that plasmin does not unbind. On the contrary, it is highly likely that plasmin unbinds under physiological conditions, so we instead conclude that tPA must rebind. Since whole clot degradation rates increase to more reasonable values if plasmin unbinds and tPA is allowed to rebind to the cross section (Table 4.11), we hypothesize that tPA *does* rebind to fiber cross sections under physiological conditions. This suggests that our rebinding probability

calculation (Appendix E) is not appropriate. The calculation is based on a highly idealized geometry with an idealized definition of binding. Future work will involve a more thorough investigation of the probability of tPA rebinding to a fiber cross section.

CHAPTER 5

FIBRINOLYTIC INHIBITORS

As discussed in Chapter 4, α_2-antiplasmin is a strong inhibitor of plasmin, and consequently of fibrinolysis. In this chapter we discuss two additional fibrinolytic inhibitors: plasminogen activator inhibitor-1 (PAI-1) and thrombin activatable fibrinolysis inhibitor (TAFI). We include these inhibitors in the multiscale model framework described in Chapters 3 and 4 to gain insight into the regulation of fibrinolysis.

5.1 Plasminogen activator inhibitor-1

Plasminogen activator inhibitor-1 (PAI-1) is a potent inhibitor of tPA. The plasma concentration of PAI-1 is about 0.4 nM [?, ?], but continuous production of PAI-1 by activated platelets could greatly increase the PAI-1 concentration in platelet-rich blood clots [?]. PAI-1 binds stoichiometrically to tPA with second order rate constant 35 $\mu M^{-1}s^{-1}$ and is consumed during the inhibition process [?]. Fibrin-bound tPA is inaccessible to PAI-1 [?], providing a mechanism for PAI-1 regulation of fibrinolysis: PAI-1 inhibits plasma-phase tPA, preventing systemic lysis, but developing blood clots provide protection for tPA, leading to the initiation of fibrinolysis.

PAI-1 is present in the blood in both active and latent states [?]. The active state, which interacts with tPA, is unstable (half-life of $\approx$ 10 min) and spontaneously converts into the latent form. However, active PAI-1 may bind to the protein vitronectin, increasing its half-life 2–10-fold while retaining its inhibitory ability [?]. Almost all active PAI-1 in plasma circulates in this vitronectin complex [?].

In this section we investigate the effect of platelets and PAI-1 on clot lysis. The microscale model is unchanged and the macroscale model is adjusted to include the physical presence of platelets and the inhibitory effect of PAI-1. We focus our investigation on coarse clots, but similar results are obtained for fine clots.

5.1.1 Model modifications

Plasma concentrations of PAI-1 are about 0.4 nM, but platelets trapped in the fibrin mesh of blood clots release PAI-1 locally. Measuring the PAI-1 concentration released by platelets is difficult, but an experiment with platelet-rich plasma (in which the platelets had been lysed) showed a concentration of about 5 nM [?]. Another experiment measured a PAI-1 concentration of 210 nM in a whole blood clot reconstituted with 10^{10} purified platelets/mL [?]. In the macroscale model, we assume that regions of clot containing platelets also contain PAI-1 at concentration 5 nM or, for an extreme experiment, 1 μM. The presence of platelets in the macroscale clot is modeled by defining a 9 μm $\times$ 9 μm $\times$ 2.74 μm region of the clot to be undegradable fibrin (we call this undegradable region an "obstacle"). This small region is about the size of a 3×3 clump of platelets. tPA can diffuse into such obstacles, but cannot bind and therefore cannot initiate lysis. We retain the lattice edges in the obstacles for ease of computation, but since the edges are undegradable and tPA cannot bind to them, we can imagine that there are platelets in this region instead of fibrin.

To mimic the inhibitory effect of PAI-1, we remove tPA that enters the obstacles with a probability dependent on the PAI-1 concentration. The second order rate constant for PAI-1 complexing with tPA is 35 $\mu\text{M}^{-1}\text{s}^{-1}$ [?], and the time step used in the macroscale model is about 0.0025 s. We derive the probability of tPA removal during one time step in a region of clot containing 5 nM PAI-1 by,

$$p_{\text{removal}} = 35\ \mu\text{M}^{-1}\text{s}^{-1} \times 0.005\ \mu\text{M} \times 0.0025\ \text{s} = 4.375 \times 10^{-4}.$$

Similarly, the probability of tPA removal in one time step is 0.0875 if the local PAI-1 concentration is 1 μM. This information is included in the macroscale model by checking the location of each tPA molecule at each time step. If a tPA molecule is in a region of clot containing platelets, we generate a uniformly distributed random number, $r \in U[0,1]$. If $r < p_{\text{removal}}$, then the tPA molecule is removed from the simulation. If $r \geq p_{\text{removal}}$, then the tPA molecule is not removed and instead remains unbound at the current edge or diffuses to a neighboring fiber. Because platelets continually produce PAI-1, we assume the PAI-1 concentration remains fixed, even though PAI-1 is consumed as it inhibits tPA. The macroscale algorithm described in Section 3.1.2 is modified as follows (changes in italics):

1. Determine the clot geometry and Δt, set $t = 0$, fix t_{final} (a prescribed final time), *fix*

the tPA removal probability $p_{removal}$, and initialize the degradation times of all edges to 0.

2. Randomly place a specified number of tPA molecules in the fibrin-free region.

3. For $t \leq t_{\text{final}}$:

a. set $t = t + \Delta t$.

b. degrade any edges with nonzero degradation times $\leq t$, and unbind any tPA molecules that were bound to the degraded edges.

c. check the unbinding times for all bound tPA molecules, unbind any with times $\leq t$.

d. assign each newly unbound molecule a binding time, t_{bind}.

e. for each unbound molecule, pick a random number $\hat{r} \in U[0,1]$ and

i. if $\hat{r} \leq (1-q)$, the molecule does not move.

A. *If the tPA molecule is on a degradable edge, the molecule can bind.*

I. If $t_{\text{bind}} > t$ or the edge has already been degraded, the molecule remains unbound.

II. If $t_{\text{bind}} \leq t$ and the edge the molecule is on has not been degraded, bind the molecule and use the microscale distributions to find the new unbinding time and the degradation time for that fiber.

B. *If the tPA molecule is on an undegradable edge, the molecule can be removed. Pick a random number* $\hat{r}_2 \in U[0,1]$.

I. *If* $\hat{r}_2 < p_{removal}$, *remove the tPA molecule from the simulation.*

II. *If* $\hat{r}_2 \geq p_{removal}$, *the tPA molecule remains on its current edge.*

ii. if $\hat{r} > (1-q)$, the molecule has the opportunity to move, but may bind before it can do so.

A. *If the tPA molecule is on a degradable edge, the molecule can bind.*

I. If $t_{\text{bind}} > t$ or the edge has already been degraded, randomly move the tPA to a neighboring edge and calculate a new binding time for the tPA to that edge.

II. If $t_{\text{bind}} \leq t$ and the edge the molecule is on has not been degraded, pick a random number, $\hat{r}_3 \in U[0,1]$.

aa. If $\hat{r}_3 > \frac{(t-t_{\text{bind}})}{\Delta t}$, then movement happens before the tPA binds. Randomly move the tPA to a neighboring edge and calculate a new binding time for the tPA to that edge.

bb. If $\hat{r}_3 \leq \frac{(t-t_{\text{bind}})}{\Delta t}$, the molecule binds and therefore cannot move. Use the microscale model distributions to calculate a new unbinding time and the degradation time for the fiber.

B. *If the tPA molecule is on an undegradable edge, the molecule can be removed. Pick a random number* $\hat{r}_4 \in U[0,1]$.

I. *If* $\hat{r}_4 < p_{removal}$*, remove the tPA molecule from the simulation.*

II. *If* $\hat{r}_4 \geq p_{removal}$*, randomly move the tPA to a neighboring edge and calculate a new binding time for the tPA to that edge.*

f. return to step **a.**

5.1.2 Results

We use the modified macroscale model described above to study the effect of platelets and PAI-1 on lysis. We experiment with different numbers of obstacles in the clot, as well as different distributions of obstacles throughout the clot. Baseline Case A parameters (Table 4.1) without tPA rebinding or plasmin unbinding are used in all experiments, and the investigation is limited to lysis of coarse clots (although we find similar results for fine clots). Unless otherwise noted, experiments were run with fibrin-free height $H = 2.935$ μm. Sets of experiments are run in pairs: once with a tPA removal probability corresponding to a 5 nM PAI-1 concentration ($p_{\text{removal}} = 4.375 \times 10^{-4}$) and another time with a 1 μM PAI-1 concentration ($p_{\text{removal}} = 0.0875$). We use "platelet region" and "obstacle" interchangeably to refer to the region of clot containing undegradable fibrin.

5.1.2.1 Fraction of clot composed of obstacles

We start with one obstacle (9 μm $\times$ 9 μm $\times$ 2.74 μm clump of platelets) in the middle of the coarse clot, corresponding to 0.8% of the domain being undegradable fibrin. A 5 nM tPA concentration is introduced into the fibrin-free region, which has height $H = 2.935$ μm (Figure 3.2). Lysis proceeds more quickly when the tPA removal probability is small ($p_{\text{removal}} = 4.375 \times 10^{-4}$) compared to when the removal probability is larger ($p_{\text{removal}} = 0.0875$) (Figure 5.1). In both cases, however, all the tPA molecules are inhibited eventually. The pattern of lysis is also affected when the removal probability is high ($p_{\text{removal}} = 0.0875$);

lysis is slowed behind the obstacle compared to the rate of lysis away from the obstacle (Figure 5.1). The reduction in lysis behind the obstacle is due to inhibition of tPA as it diffuses through the platelet region. Some of the tPA molecules are removed from the region, hence fewer tPA molecules arrive at the rear edge of the obstacle. This effect is not seen when $p_{\text{removal}} = 4.375 \times 10^{-4}$.

We also study the effect of the number of obstacles on clot lysis. Initially, we evenly space four 9 μm $\times$ 9 μm $\times$ 2.74 μm obstacles throughout the domain (3.2% of the total domain is undegradable fibrin in this case). We then increase the number of evenly spaced obstacles to 9 (7.3% of domain is undegradable fibrin), 16 (13% of domain is undegradable fibrin), and 25 (20.3% of domain is undegradable fibrin) in subsequent experiments. Lysis proceeds at about the same rate regardless of number of obstacles when $p_{\text{removal}} = 4.375 \times 10^{-4}$ (Figure 5.2). When $p_{\text{removal}} = 0.0875$, however, systematically increasing the number of obstacles results in a systematic reduction in lysis. By the time 20% of the domain is undegradable fibrin, hardly any lysis occurs (Figure 5.3).

There is more uninhibited tPA at a given percentage of clot degradation when $p_{\text{removal}} = 4.375 \times 10^{-4}$ than when $p_{\text{removal}} = 0.0875$. However, as a function of time, the number of tPA molecules remaining in the experiment depends on the percentage of undegradable fibrin in the clot. We expect that tPA will be removed more quickly when $p_{\text{removal}} = 0.0875$ compared to $p_{\text{removal}} = 4.375 \times 10^{-4}$, and we do see this in experiments with large numbers (16 or 25) of equally spaced obstacles. In these experiments, tPA encounters the PAI-1 regions very quickly and is completely removed from the experiment more quickly when the removal probability is large ($p_{\text{removal}} = 0.0875$). Interestingly, when there are small numbers (four or nine) of evenly spaced obstacles in the clot, tPA is completely removed from the experiment more quickly when the removal probability is small ($p_{\text{removal}} = 4.375 \times 10^{-4}$), because lysis happens faster and the tPA is not protected from PAI-1. When tPA is bound to fibrin, it cannot diffuse, so it cannot "wander" into the platelet region. Once all the fibrin has been degraded, tPA diffuses and is quickly inhibited.

So far we have considered only situations in which the PAI-1 secreted by platelets remains in the vicinity of the platelets and does not diffuse. We can model diffused, plasma-phase PAI-1 by including in the model the effect of the stable PAI-1–vitronectin complex. We model this effect by assuming a low level of tPA removal on all the edges: we take $p_{\text{removal}} = 3.675 \times 10^{-5}$ (which corresponds to a 0.42 nM PAI-1 concentration) on non-obstacle edges and $p_{\text{removal}} = 4.375 \times 10^{-4}$ on edges in the platelet region. Edges in the platelet region

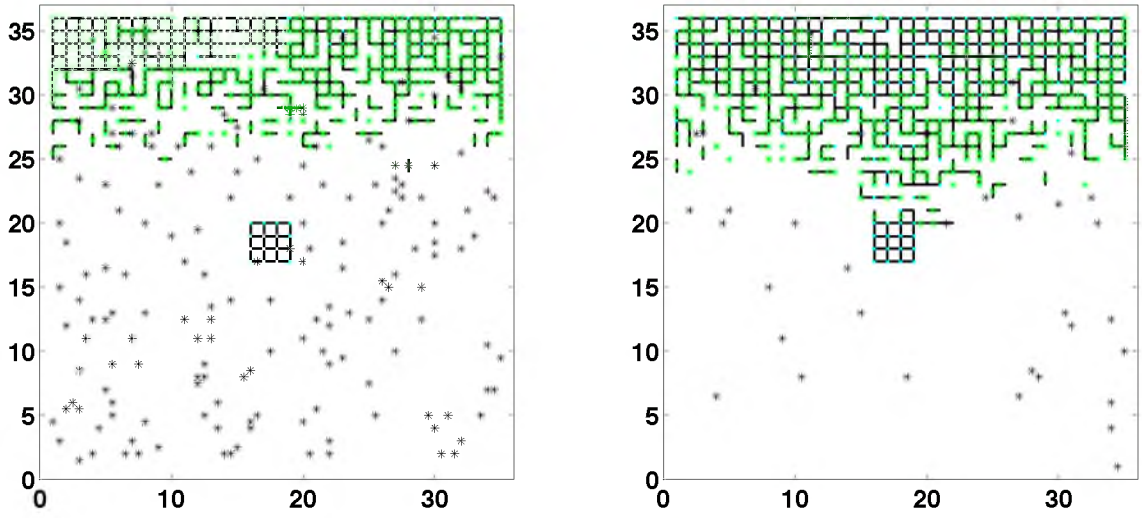

(a) $t = 24$ min

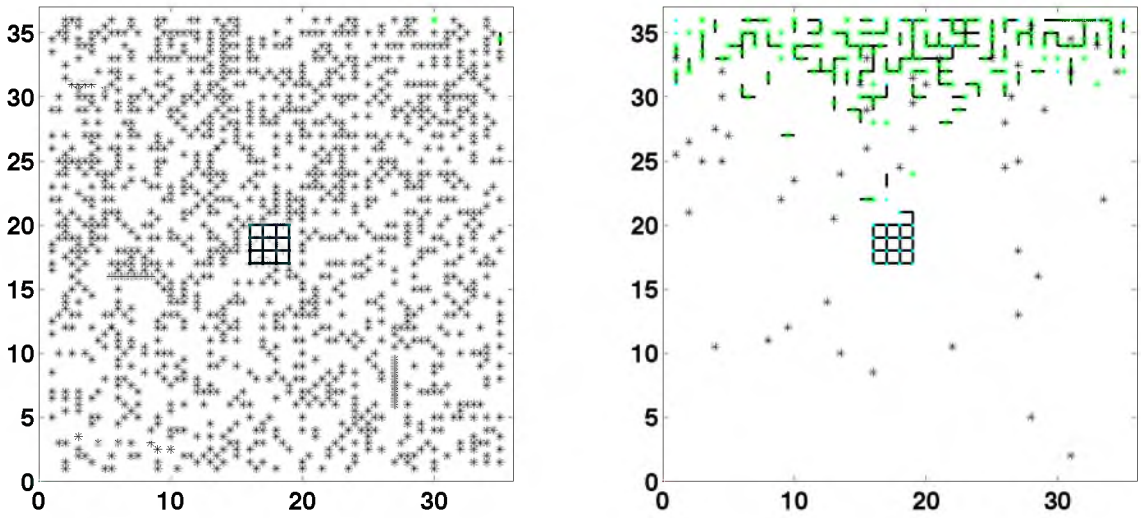

(b) $t = 31$ min

Figure 5.1. Coarse clot lysis around a single obstacle. Figures on left have $p_{\text{removal}} = 4.375 \times 10^{-4}$, and figures on right have $p_{\text{removal}} = 0.0875$. Figures are 2-D projections of the 3-D clot; black lines indicate fibrin fibers in the plane of the page, and blue dots represent fibers extending out of the page. Green asterisks represent bound tPA, and black asterisks represent unbound tPA. Numbers on axes correspond to lattice node number, with a physical distance between lattice nodes of 2.74 μm. (a) Macroscale clot 24 minutes after introduction of the 5nM bolus of tPA. (b) Macroscale clot 31 minutes after introduction of the 5nM bolus of tPA. The small square of fibrin in the center of the clot is the obstacle.

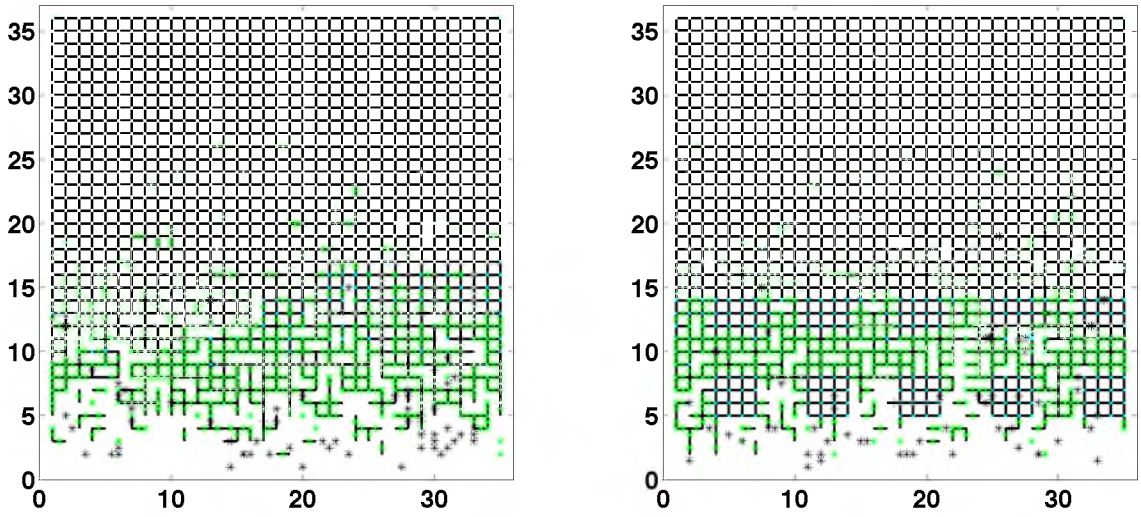

(a) $t = 7$ min

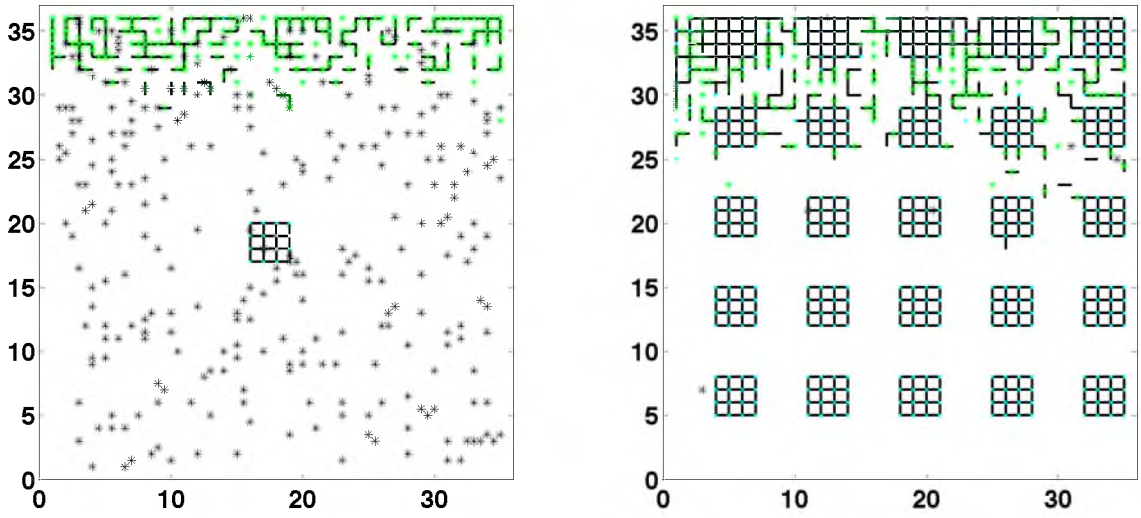

(b) $t = 27$ min

Figure 5.2. Coarse clot lysis around different numbers of obstacles, with tPA removal probability $p_{\text{removal}} = 4.375 \times 10^{-4}$. The clot on the left contains one obstacle, taking up 0.8% of the domain. The clot on the right contains 25 obstacles, accounting for 20% of the domain. Symbols and interpretations are the same as in Figure 5.1. (a) Macroscale clot 7 minutes after introduction of the 5nM bolus of tPA. (b) Macroscale clot 27 minutes after introduction of the 5nM bolus of tPA.

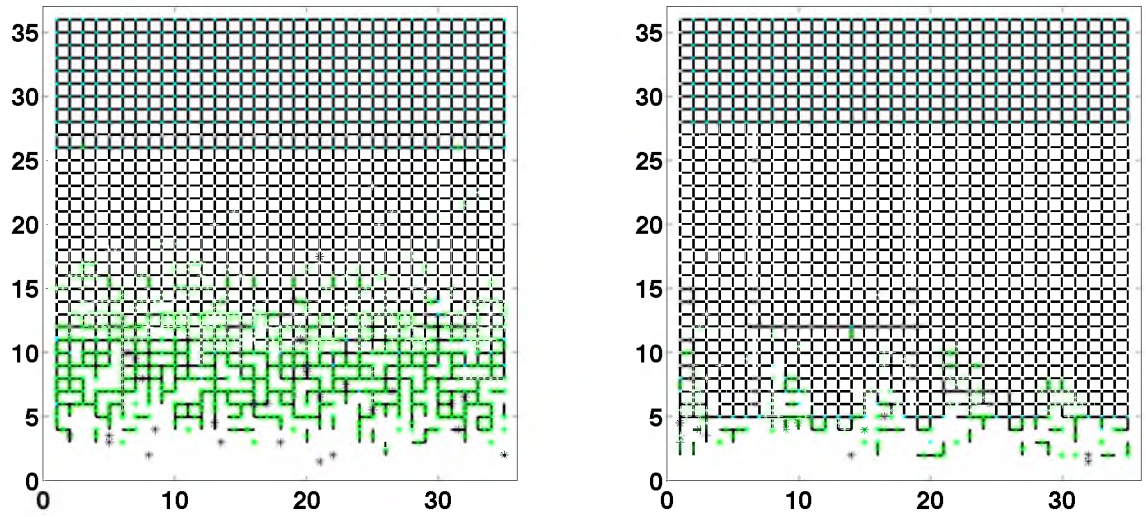

(a) $t = 7$ min

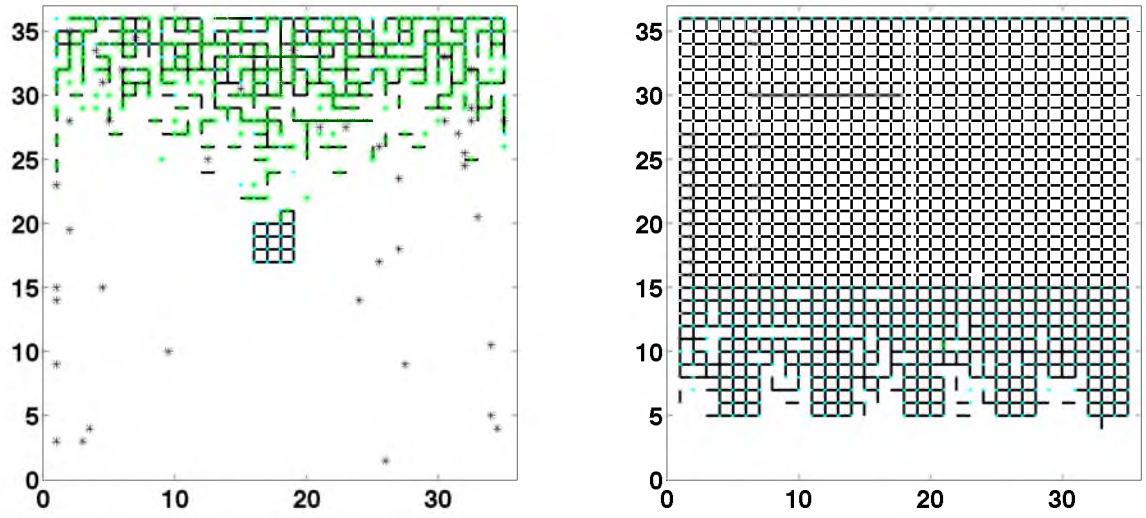

(b) $t = 27$ min

Figure 5.3. Coarse clot lysis around different numbers of obstacles, with tPA removal probability $p_{\text{removal}} = 0.0875$. The clot on the left contains one obstacle, taking up 0.8% of the domain. The clot on the right contains 25 obstacles, accounting for 20% of the domain. Symbols and interpretations are the same as in Figure 5.1. (a) Macroscale clot 7 minutes after introduction of the 5nM bolus of tPA. (b) Macroscale clot 27 minutes after introduction of the 5nM bolus of tPA.

remain undegradable, but all other edges can be degraded. As before, tPA can only be inhibited if it is unbound. We find that the fibrin protects tPA from inhibition; even when tPA can be removed at any edge, lysis proceeds at about the same rate as it does in the case with inhibition only in platelet regions (Figures 5.4(a) and 5.4(b)). However, if there is a low level of tPA removal on all edges and bound tPA *is* accessible to PAI-1, then all tPA is inhibited very quickly and virtually no lysis occurs (Figure 5.4(c)).

5.1.2.2 Distribution of obstacles

As seen in Section 5.1.2.1, the fraction of clot containing platelets has an effect on macroscale lysis with a large tPA removal probability ($p_{\text{removal}} = 0.0875$) and obstacles that are evenly spaced throughout the clot. Here we show how the distribution of these obstacles within the clot affects lysis. We use nine obstacles, and distribute them throughout the clot in two distinct ways: in the first configuration, obstacles are evenly spaces as in the previous section; in the second configuration, all nine obstacles are placed one fiber-length apart, and this mass of tightly-packed obstacles is centered in the clot.

When $p_{\text{removal}} = 4.375 \times 10^{-4}$, lysis occurs at about the same rate regardless of how the nine obstacles are distributed (results not shown). When $p_{\text{removal}} = 0.0875$, lysis is faster and more complete when the obstacles are placed close together as compared to when the obstacles are evenly spaced throughout the clot (Figure 5.5). When the obstacles are placed only one fiber-length apart, most of the clot is degraded except for the fibers connecting the nine obstacles. The explanation for why the two distinct obstacle configurations (that have the same percentage of total platelets) produce such different lysis patterns involves the surface area of obstacles abutting the rest of the clot, which is very different in the two configurations. The surface area of a single obstacle that contacts the surrounding clot is 36 μm $\times$ 2.74 μm = 98.64 μm^2, so when there are nine evenly spaced obstacles, 9 $\times$ 98.64 = 887.76 μm^2 is directly exposed to the bulk fibrin clot. However, when the obstacles are closely packed together, only 108 μm $\times$ 2.74 μm = 295.92 μm^2 of platelet region is directly exposed to the bulk clot. With a smaller surface area exposed to the rest of the clot, tPA is less likely to contact the platelet region and be inhibited. With more tPA around, more lysis can occur, which is why we see a greater extent of lysis in the clot with closely packed obstacles.

When the obstacles are placed close together in the center of the clot, another effect of platelets on lysis is observed: when $p_{\text{removal}} = 4.375 \times 10^{-4}$, the tPA binding front moves

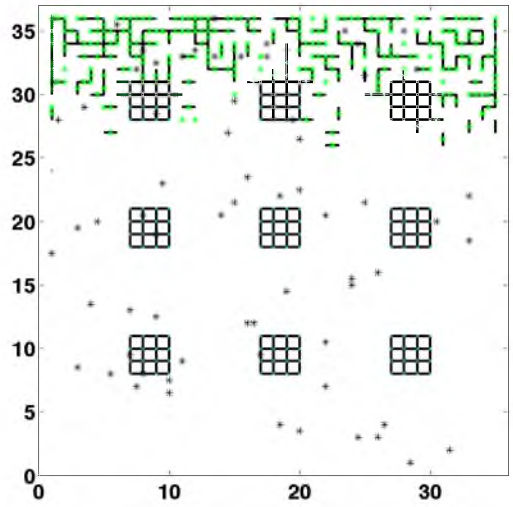

(a) tPA removal only in obstacles

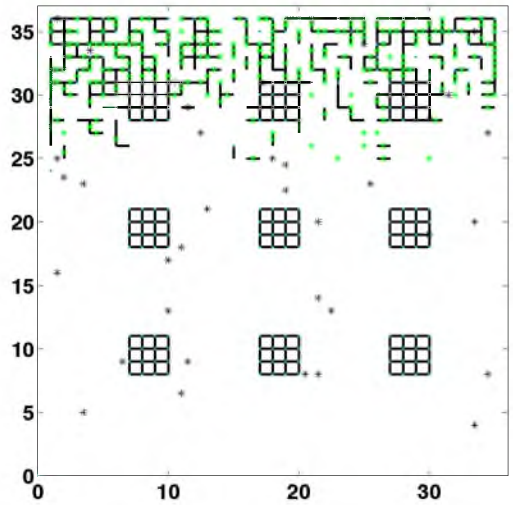

(b) unbound tPA removal on all edges

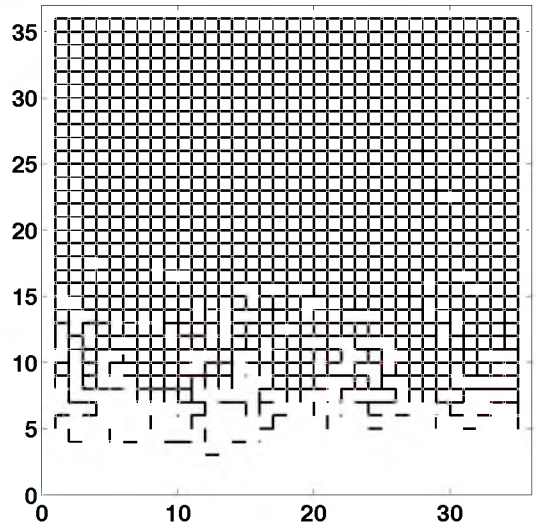

(c) bound and unbound tPA removal on all edges

Figure 5.4. Coarse clot lysis around nine obstacles with a low level of tPA removal on all edges. Symbols and interpretations are the same as in Figure 5.1. All figures show the state of the macroscale clot 27 minutes after introduction of the 5nM bolus of tPA. (a) $p_{\text{removal}} = 4.375 \times 10^{-4}$ on edges in the obstacles. (b) $p_{\text{removal}} = 3.675 \times 10^{-5}$ on *all* edges in the clot, and $p_{\text{removal}} = 4.375 \times 10^{-4}$ on edges in the obstacles. Only unbound tPA can be inhibited. (c) $p_{\text{removal}} = 3.675 \times 10^{-5}$ on *all* edges in the clot, and $p_{\text{removal}} = 4.375 \times 10^{-4}$ on edges in the obstacles. All tPA can be inhibited, not just unbound molecules.

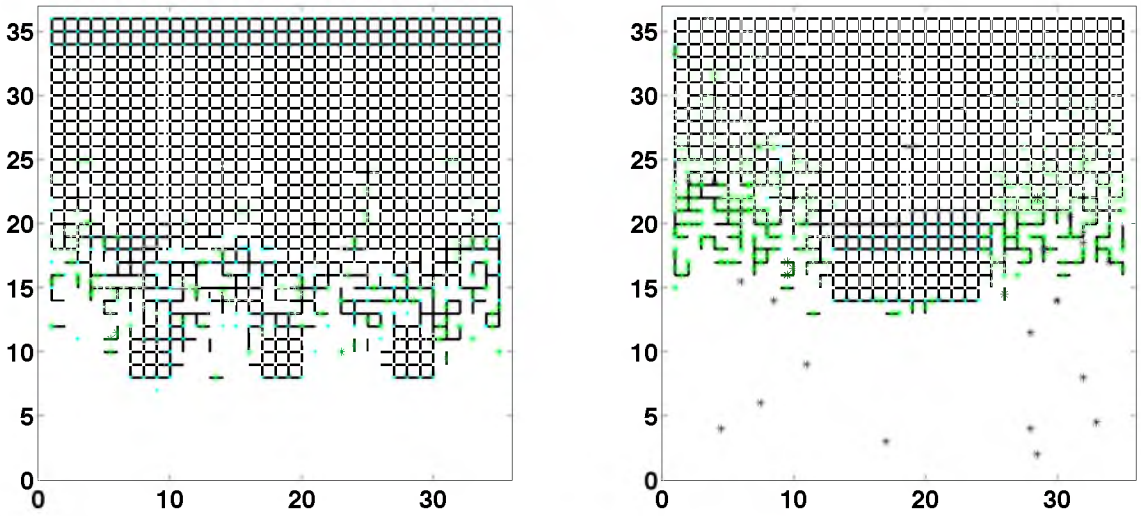

(a) $t = 17$ min

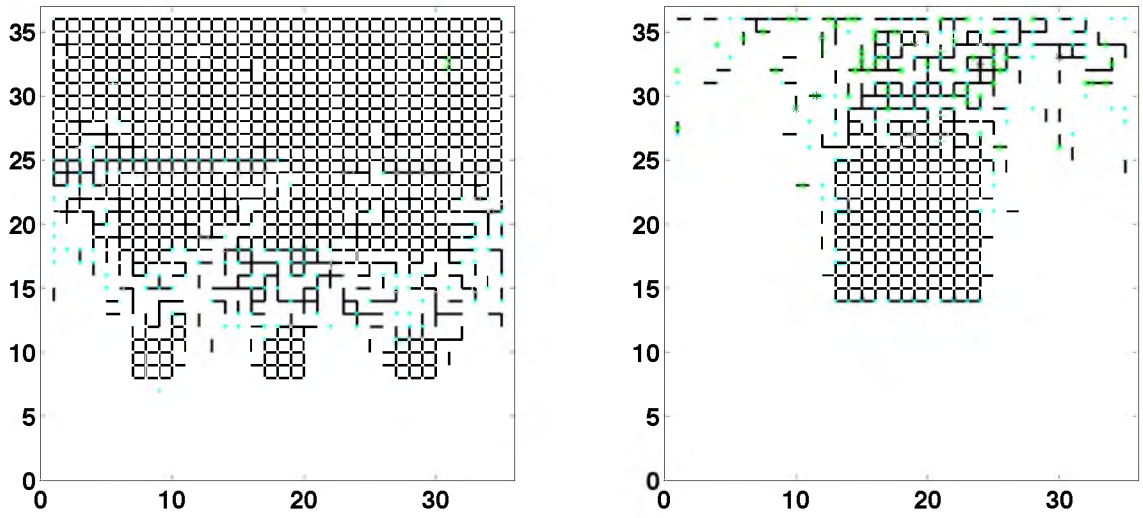

(b) $t = 47$ min

Figure 5.5. Coarse clot lysis around nine obstacles that are distributed in different ways. The figures on the left have the nine obstacles spaced evenly throughout the clot. The figures on the right have the nine obstacles spaced one fiber apart in the center of the clot. Symbols and interpretations are the same as in Figure 5.1. (a) Macroscale clot 17 minutes after introduction of the 5nM bolus of tPA. (b) Macroscale clot 47 minutes after introduction of the 5nM bolus of tPA.

through the platelet region more quickly than it does in other parts of the clot (Figure 5.6). Because tPA cannot bind to fibrin in a platelet region, its diffusion is not impeded. tPA freely diffuses through the region and, therefore, travels a greater distance in a given time than the tPA molecules away from the obstacle, which bind to fibrin and are prevented from diffusing. However, if $p_{\text{removal}} = 0.0875$, the effect is reversed; the tPA binding front moves more quickly in regions of the clot away from the obstacles. The removal probability is high enough that it is very unlikely that a tPA molecule diffuses through the obstacle without being inhibited. The described effect occurs with a 5 nM tPA concentration added to a fibrin-free region with height 2.935 μm (not shown), but is more evident when the 5 nM tPA concentration is added to a fibrin-free region with height 17.61 μm (Figure 5.6).

5.2 Thrombin activatable fibrinolysis inhibitor

In this section, we discuss the indirect fibrinolytic inhibitor, TAFIa. Thrombin activatable fibrinolysis inhibitor (TAFI) is a carboxypeptidase that cleaves lysine residues when activated. Because tPA and PLG bind to lysine residues, TAFI plays a role in fibrinolysis. Activated TAFI (TAFIa) cleaves the tPA and PLG binding sites that become exposed as lysis progresses, preventing the accumulation of PLG on partially degraded fibrin [?]. PLG

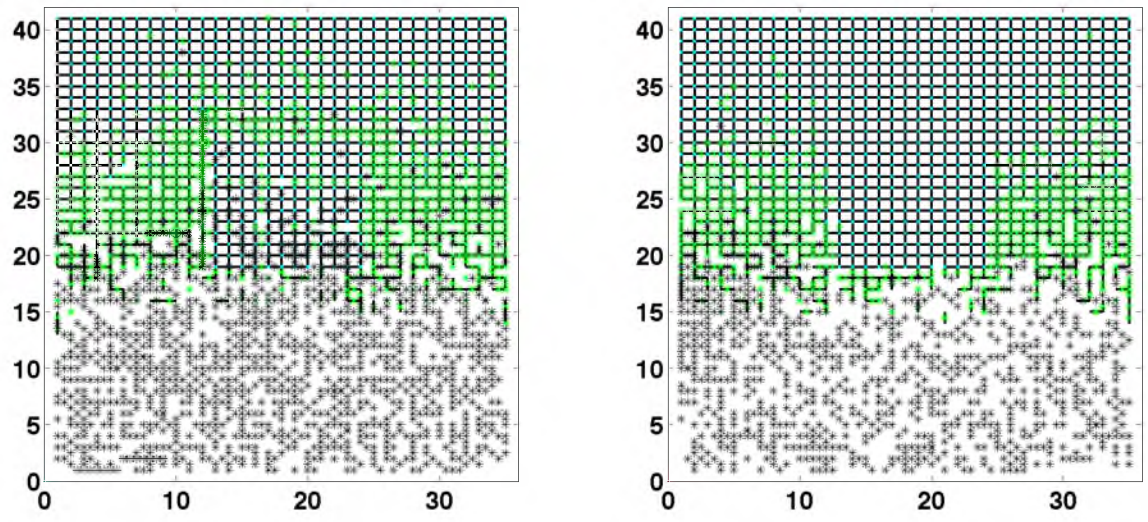

Figure 5.6. tPA diffusion through the platelet region of coarse clots. The clot on the left has $p_{\text{removal}} = 4.375 \times 10^{-4}$ and the clot on the right has $p_{\text{removal}} = 0.0875$. Both clots are shown 8 minutes after introduction of the 5nM bolus of tPA. Symbols and interpretations are the same as in Figure 5.1. The height of the fibrin-free region is $H = 17.61$ μm.

circulates in plasma in its native form, Glu-PLG, but in the presence of partially degraded fibrin can be converted by plasmin to the more active Lys-PLG [?]. Lys-PLG is more easily activated to plasmin by tPA (K_M = 19 μM, k_{cat} = 0.2 s^{-1} for Lys-PLG compared to K_M = 65 μM, k_{cat} = 0.06 s^{-1} for Glu-PLG) [?]. Thus, TAFIa not only slows lysis by inhibiting the activation of PLG to plasmin, but also by inhibiting the conversion of Glu-PLG to Lys-PLG [?]. TAFIa attenuates lysis in these indirect ways, however, and does not directly inhibit plasmin activity [?].

TAFI is activated to TAFIa by plasmin (K_M = 55 nM, k_{cat} = 0.00044 s^{-1}), thrombin (K_M = 0.5 − 2.14 μM, k_{cat} = 0.0021 s^{-1}), and the thrombin-thrombomodulin complex (K_M = 1.01 μM, k_{cat} = 0.4 − 1.24 s^{-1}) [?, ?, ?]. While the thrombin-thrombomodulin complex is the fastest activator, activation by plasmin occurs for a more physiological TAFI concentration (K_M = 55 nM instead of 1.01 μM). The plasma concentration of TAFI ranges from 75-275 nM [?, ?], and plasma levels of TAFIa have been measured to be about 12 pM [?]. However, local physiological TAFIa concentrations in blood clots during lysis are unknown, and are especially hard to measure since TAFIa is unstable (the half-life of TAFIa at 37°C is 8-15 minutes [?]). In TAFI-deficient plasma experiments, it is found that the peak TAFIa concentration is only about 0.2% of the total added TAFI concentration (e.g., when 66 nM TAFI is added, the peak TAFIa concentration is 0.11 nM) [?]. As far as we know, this is the only published measurement of TAFIa during lysis. It seems reasonable that significantly more TAFIa could be produced since there are so many activators of TAFI (plasmin, thrombin, thrombin-thrombomodulin), but we know of no other measurements in the literature.

The interplay between the plasmin inhibitor α_2-AP and TAFIa is complicated. The observed rate of inhibition of plasmin by α_2-AP is much higher in the presence of TAFIa, and the rate increases with increasing initial TAFIa concentrations [?]. This is presumably because TAFIa cleaves binding sites, preventing the protection of plasmin by releasing it into the plasma where it can be inhibited by α_2-AP. In the absence of α_2-AP, TAFIa does not appreciably prolong lysis of a purified fibrin clot; there is virtually no change in the lysis time (it remains about 0.2 hours) for TAFIa concentrations ranging from 0-200 nM in the absence of α_2-AP, but in the presence of 1 μM α_2-AP, lysis times increase from about 3.8 hours (no TAFIa) to 5 hours (200 nM TAFIa) [?]. The results of this experiment are perplexing: why is α_2-AP necessary for TAFIa to prolong lysis? If TAFIa exerts its influence mainly by cleaving PLG binding sites, thus preventing both the accumulation of

PLG and the increase in the rate of PLG activation, at what step would the α_2-AP be required?

We add TAFIa to the microscale model, with and without the effect of α_2-AP (which is modeled by allowing plasmin to unbind, as described in Section 4.2.3), to investigate the interplay between TAFIa and α_2-AP. Model results allow us to suggest an explanation for how TAFIa is effective in delaying lysis only in the presence of α_2-AP.

5.2.1 Model modifications

For the purpose of our investigation, we assume that TAFI has already been activated to TAFIa, and hence we do not model the activation process. TAFIa is included in the microscale model (described in Sections 3.1.1 and 4.1), where it is able to cleave initially-cryptic doublets when they become exposed. We assume TAFIa is present in high enough concentration that we can consider it to be in quasi-steady state, and treat it deterministically as we do PLG – using probabilities of TAFIa being on doublets – rather than explicitly tracking large numbers of individual TAFIa molecules. In the notation of Figure 3.3, we use "4" to represent TAFIa. So N_{14} is a doublet with one tPA molecule and one TAFIa molecule bound. Now N_{PLG} can be N_{22}, N_{02}, N_{00} (as before), or N_{04}, N_{24}, or N_{44}. The probability of N_{PLG} being in any of these 6 states is calculated using the quasi-steady state approximation (Appendix H). In addition to the change in N_{PLG}, four new states are added to the model: a doublet with tPA and TAFIa bound (N_{14}), a doublet with plasmin and TAFIa bound (N_{34}), a doublet that has been cleaved by TAFIa (C), and a cleaved doublet with a plasmin molecule bound (C_3).

With the new states come new reactions, so that now the Gillespie algorithm chooses from 54 reactions (Appendix I). The TAFIa rate constants are listed in Table 5.1. For all experiments described in this section, we use a 20 nM TAFIa concentration, which corresponds to about 10% of the plasma TAFI having been activated to TAFIa. To cleave, TAFIa must be bound to a doublet. It is assumed that TAFIa can bind to and cleave only exposed doublets that were initially cryptic, and that once a doublet is cleaved, no tPA or PLG may bind to it. All bound tPA and PLG molecules on a doublet are released upon its cleavage by TAFIa. Plasmin can bind to cleaved doublets for the same reason it can bind to degraded doublets: we assume plasmin uses the frayed ends of nearby protofibrils to crawl, and therefore can reside on a cleaved doublet by being bound to a frayed protofibril. Cleaved doublets, like all undegraded doublets, can be degraded by any plasmin molecule

at the same binding location.

TAFIa does not directly affect the macroscale model – it appears indirectly via the tPA leaving time and lysis time distributions computed with the microscale model. In all macroscale experiments in this section, a 5 nM tPA concentration is introduced into a fibrin-free region abutting the clot that is 2.935-μm high. The experiments are run for 30 minutes of simulation time.

5.2.2 Results

For each experiment, we run the microscale model with TAFIa 10,000 times with Case A parameters (Tables 4.1 and 5.1). In one experiment, plasmin is not allowed to unbind and therefore is not inhibited by α_2-AP. In another experiment, we model the effect of α_2-AP by allowing plasmin to unbind and immediately be inhibited. Finally, we model positive feedback by running experiments in which tPA rebinds to the fiber cross section, both with and without plasmin unbinding. Microscale model results are presented as median (first quartile Q1, third quartile Q3) of 10,000 simulations, and macroscale model results are presented as mean $\pm$ standard deviation of 10 simulations.

With no tPA rebinding and no plasmin unbinding, adding TAFIa to the microscale model slightly slows down single fiber lysis (compare the dashed and solid black curves in Figure 5.7). The median tPA leaving time is about 5 seconds longer, for both thin and thick fibers, when TAFIa is included in the model (compare "TAFIa" in Table 5.2 to "Case A" in Table 4.3). The time to first plasmin production is very similar for Case A parameters with and without TAFIa. Since single fiber lysis is slower when TAFIa is included in the model, and because TAFIa does not affect the time it takes to produce the first plasmin molecule, TAFIa must reduce the total number of plasmin molecules created. Indeed, we find that the median (Q1, Q3) number of plasmin molecules created in a thick fiber drops

Table 5.1. TAFIa parameters. k_{cleave} is the rate at which TAFIa cleaves binding sites. $k_{\text{on}}^{\text{TAFI}}$ and $k_{\text{off}}^{\text{TAFI}}$ are the TAFIa binding rate to fibrin and the TAFIa unbinding rate from fibrin, respectively. These individual on and off rates have not been measured, but we were able to estimate a dissociation constant from [?].

Parameter	Value	Reference
k_{cleave} (s^{-1})	2.34	[?]
$k_{\text{on}}^{\text{TAFI}}$ ($\mu\text{M}^{-1}\text{s}^{-1}$)	54.9	[?]
$k_{\text{off}}^{\text{TAFI}}$ (s^{-1})	5.49	[?]

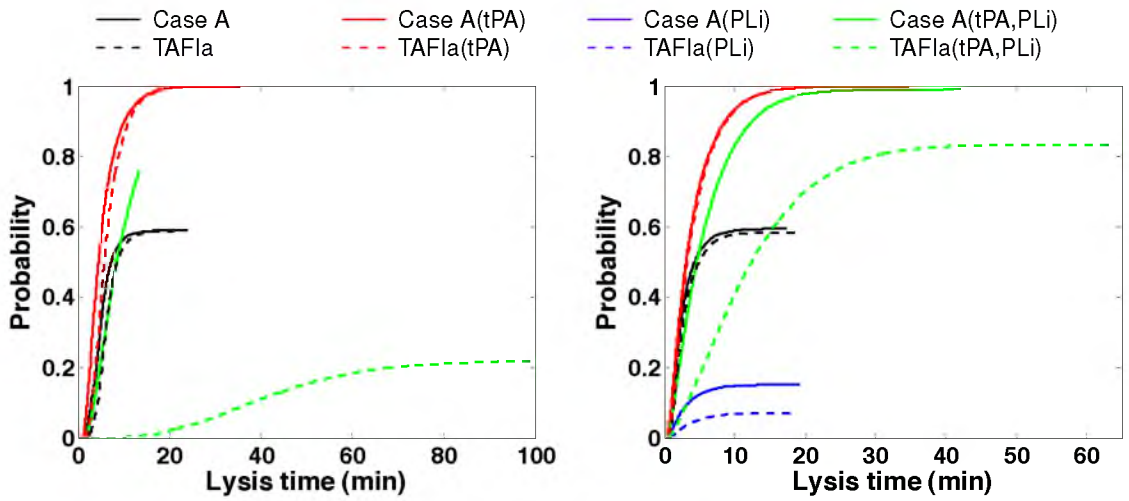

(a) Thick fiber

(b) Thin fiber

Figure 5.7. Empirical lysis time cumulative distribution functions from the TAFIa microscale model with Case A parameters. Solid curves denote simulations without TAFIa, dashed curves denote simulations with TAFIa. "tPA" means tPA was allowed to rebind and "PLi" means plasmin was allowed to unbind. Most of the CDFs do not asymptote to 1 because we define "Probability" as the fraction of 10,000 runs. In most situations, fewer than 10,000 runs resulted in lysis, so there are fewer than 10,000 lysis times. (a) Thick fiber. Only 20 runs out of 10,000 resulted in lysis for "Case A (PLi)" simulation, so the corresponding CDF is not visible on this scale. For the "TAFIa (PLi)" simulation only 1 run out of 10,000 resulted in lysis, so there is no corresponding CDF. (b) Thin fiber.

from 2 $(1, 3)$ to 1 $(1, 2)$ in the presence of TAFIa, and the maximum number of plasmin molecules produced in any run drops from 10 to 6. Similarly, for a thin fiber with TAFIa, the median (Q1, Q3) number of plasmin molecules is 1 $(1, 1)$ (down from 1 $(1, 2)$ without TAFIa), and the maximum number of plasmin molecules produced in any run is 5 (down from 7). The reduced plasmin production causes the increased tPA leaving times in runs with TAFIa; tPA is less likely to be forced to unbind by plasmin when there are fewer plasmin molecules in the cross section, allowing tPA to stay bound longer.

When tPA is allowed to rebind in the TAFIa microscale model but plasmin still does not unbind (denoted "TAFI (tPA)" in tables and figures), single fiber lysis is slightly slower than in the same situation without TAFIa (solid and dashed red curves Figure 5.7). Also, the tPA leaving time is increased and the first plasmin molecule is created at about the same time (compare "Case A (tPA)" in Table 4.8 to "TAFIa (tPA)" in Table 5.2). As in the case without tPA rebinding, the slower single fiber lysis times and longer tPA leaving times are a result of the fewer plasmin molecules that are produced (on average) when TAFIa is

Table 5.2. Microscale model results for Case A parameters with TAFIa. Entries are median (Q1, Q3) of 10,000 independent simulations. The column labeled "Time to first PLi" gives data about the time the first plasmin molecule was created. The column labeled "Runs with PLi" gives the number of runs, out of 10,000, in which plasmin was produced and single fiber lysis occurred. Our standard experiment (denoted "TAFIa" in table) does not allow plasmin to unbind, nor does tPA ever rebind. In different experiments plasmin was allowed to unbind (denoted "PLi" in table), and tPA was allowed to rebind (denoted "tPA" in table).

Parameters	**Fiber diameter (nm)**	**tPA leaving time (s)**	**Time to first PLi (s)**	**Runs with PLi**
TAFIa	97.5	95.38 (44.89, 177.52)	83.02 (35.61, 164.29)	5852
	195	110.26 (47.83, 209.67)	84.34 (34.39, 174.63)	5887
TAFIa (tPA)	97.5	191.03 (108.54, 334.51)	140.74 (57.75, 284.53)	10000
	195	310.73 (211.41, 450.75)	139.47 (56.44, 280.12)	10000
TAFIa (PLi)	97.5	114.73 (49.73, 227.07)	83.96 (34.73, 169.50)	708
	195	121.93 (50.39, 243.49)	84.94 (36.38, 169.06)	1
TAFIa (tPA, PLi)	97.5	583.57 (314.78, 959.90)	139.88 (58.52, 274.80)	8340
	195	1544.9 (894.75, 2335.4)	140.61 (57.43, 280.81)	2189

present.

To study the effect of α_2-AP we allow plasmin to unbind. When plasmin unbinds it is assumed to be inhibited immediately by α_2-AP, and is removed from the simulation. If tPA does not rebind, but plasmin can unbind, adding TAFIa to the microscale model greatly increases the single fiber lysis times (solid and dashed blue curves Figure 5.7). Lysis happens very infrequently; when TAFIa is present and plasmin can unbind, only 1 run out of 10,000 results in lysis of a thick fiber, and 708 runs out of 10,000 result in lysis of a thin fiber. tPA leaving times are slightly increased when TAFIa is included in the model, and the first plasmin molecule is created at about the same time (compare "Case A (PLi)" in Table 4.10 to "TAFIa (PLi)" in Table 5.2).

As illustrated in Figure 5.7, adding plasmin unbinding alone (i.e., α_2-AP) has a greater effect on lysis time than does adding TAFIa alone. The standard Case A parameter results (no TAFIa, no plasmin unbinding) are depicted by the solid black curve. Adding TAFIa slightly slows down lysis (dotted black curve is below solid black curve), but adding plasmin unbinding noticeably slows lysis (solid blue curve, only visible in Figure 5.7(b)). Including TAFIa *and* plasmin unbinding slows lysis even more (dotted blue curve, only visible in Figure 5.7(b)). In fact, adding TAFIa and plasmin unbinding to the microscale model

slows lysis even more than the sum of the effects of adding each alone. For example, with no plasmin unbinding and without TAFIa, the median lysis time of a thin fiber is 2.32 min. Allowing plasmin to unbind increases the median lysis time by 0.17 min (7.33%), while adding TAFIa increases the time by 0.07 min (3.02%). Adding plasmin unbinding and TAFIa together, however, increases the median lysis time by 0.81 min (35.91%). This is because plasmin and TAFIa do not work independently of each other; TAFIa cleaves doublets, causing fewer plasmin molecules to be produced. If those fewer plasmin molecules can also unbind, the result is a significant increase in lysis time.

For completeness, we study the effect of adding TAFIa to the microscale model when tPA can rebind and plasmin can unbind. tPA stays bound over twice as long compared to runs without TAFIa, but the first plasmin molecule is still produced at about the same time (compare "Case A (tPA,PLi)" in Table 4.10 to "TAFIa (tPA,PLi)" in Table 5.2). Single fiber lysis times are much longer (the dotted green curve is substantially below the solid green curve in Figure 5.7), for the same reason described above: there is a much greater effect when TAFIa and α_2-AP are combined than when either acts independently.

The presence of TAFIa in the microscale model results in slower macroscale lysis in all experiments (compare Table 5.3 to Tables 4.4, 4.9, and 4.10). Macroscale lysis proceeds

Table 5.3. Macroscale model results for Case A parameters with TAFIa. The experiments involved a 5 nM tPA concentration added to a fibrin-free region with height 2.935 μm. Entries are mean ± standard deviation of 10 independent simulations. Front velocity calculations do not make sense for simulations in which lysis was not front-like, hence the "–" in some entries. No lysis occurred in the coarse "TAFIa (PLi)" experiment, hence the "–" in both columns. Our standard experiment (denoted in table as "TAFIa") does not allow plasmin to unbind, nor does tPA ever rebind. In different experiments, plasmin was allowed to unbind (denoted in table "PLi") and tPA was allowed to rebind (denoted in table "tPA"). Front velocity and degradation rate were calculated as described in Section 3.2.2.2.

Parameters	**Clot type**	**Front velocity (μm/min)**	**Degradation rate (% fibers/min)**
TAFIa	fine	1.74 ± 0.24	1.90 ± 0.018
	coarse	3.56 ± 0.20	3.55 ± 0.037
TAFIa (tPA)	fine	1.61 ± 0.18	1.69 ± 0.010
	coarse	3.44 ± 0.16	3.42 ± 0.017
TAFIa (PLi)	fine	–	0.22 ± 0.014
	coarse	–	–
TAFIa (tPA, PLi)	fine	–	0.50 ± 0.011
	coarse	–	0.21 ± 0.033

through the clot as a front, except when plasmin is allowed to unbind. In this case, the lack of front-like behavior is likely a result of the very long single fiber lysis times, which result in very little macroscale lysis and hinder accurate measurement of a lysis front. Comparing the dashed curves to the solid curves in Figure 5.8 shows that for all four of the situations tested, TAFIa decreases the number of successful tPA binding events as a function of time. This makes sense for the runs in which plasmin unbinds ("TAFIa (PLi)" and "TAFIa (tPA,PLi)") because the probability that a tPA molecule initiates lysis when it binds in these cases is much lower than the same probability in the runs without TAFIa ("runs with PLi" column in Table 5.2). Additionally, since tPA stays bound longer in the runs with TAFIa, its progression through the clot is slower, which also decreases the number of successful binding events as a function of time. In runs in which plasmin does not unbind ("TAFIa" and "TAFIa (tPA)"), the probability of tPA initiating lysis when it binds is very similar in the presence and absence of TAFIa. The decrease in the number of successful binding events in these cases is due to the reduced movement of tPA through the clot. tPA leaving times are longer in the TAFIa runs, causing tPA to remain on edges for a longer time, which delays the diffusion of tPA molecules to new edges.

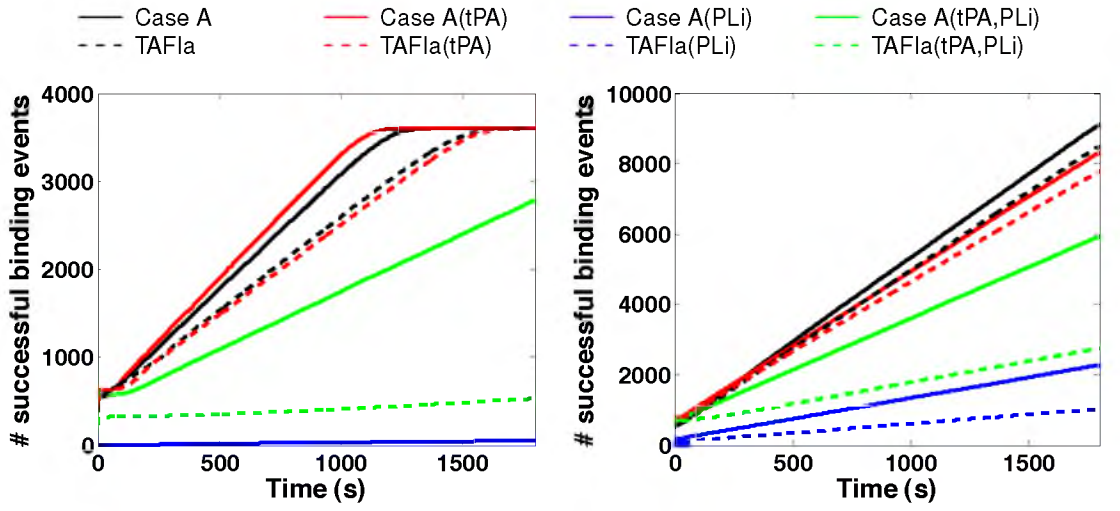

(a) Coarse clot

(b) Fine clot

Figure 5.8. Number of successful tPA binding events as a function of time for TAFIa runs with Case A parameters. Plots are averages of 10 independent simulations. Solid lines indicate runs without TAFIa, dashed lines indicate runs with TAFIa. (a) Coarse clot with 3605 total fibers (and 3605 possible successful binding events). (b) Fine clot with 14145 total fibers.

5.3 Discussion

We investigated the effects of inhibitors on single fiber and whole clot lysis. First, the tPA inhibitor PAI-1 was included in the macroscale model by prescribing a tPA removal probability on fibers in regions of clot containing PAI-1 (Section 5.1). Then the indirect fibrinolytic inhibitor TAFIa was included in the microscale model by adding new state variables and reactions (Section 5.2 and Appendix I). The plasmin inhibitor α_2-AP was modeled indirectly on the microscale by allowing plasmin to unbind, and then immediately removing the unbound plasmin from the simulation. We studied the effects of PAI-1, TAFIa, and α_2-AP independently, as well as the combined effect of TAFIa and α_2-AP.

In all versions of our model, we assume the clot is a homogeneous 3-dimensional square lattice. However, there are many ways inhomogeneity can arise in a clot: varying fiber size in different regions of the clot; arrangement of fibers in the clot; the presence (and distribution) of cells like platelets; chemistry such as varying concentrations of PAI-1. We focus on the latter two causes of clot heterogeneity. The physical presence of platelets is modeled by defining regions of the clot to be undegradable. The chemical presence of platelets is included via PAI-1, which is modeled indirectly by prescribing a tPA removal probability on fibers in regions of the clot containing platelets.

Results of the macroscale model with platelets and PAI-1 suggest that PAI-1 concentrations in the clot must be larger than the measured 5 nM concentration in order to retard lysis. If the PAI-1 concentration is only 5 nM, lysis rates are not reduced, even if 20% of the clot is composed of platelets (Figure 5.2). However, if platelets can create local concentrations of PAI-1 on the order of 1 μM, lysis can be greatly affected; as the fraction of domain composed of platelets increases, lysis is greatly reduced when $p_{\text{removal}} = 0.0875$ (Figure 5.3).

When the larger tPA removal probability is used, the distribution of platelets in the clot has a significant effect on lysis. If the platelet regions are spaced closely together in the center of the clot, lysis is much faster and more complete than if they are spaced evenly throughout the clot, suggesting that the surface area of the platelet regions is important (Figure 5.5). tPA is more likely to be inhibited by PAI-1 if the surface area of platelet regions exposed to the rest of the clot is large; tPA is only inhibited in the platelet regions, so if the surface area of these regions is large, tPA will be more likely to enter a platelet region. Thus, it is not just the amount of platelets in a clot that will determine the ease with which the clot can be degraded, but also their distribution within the clot.

The results described above were obtained under the assumption that PAI-1 only inhibits unbound tPA. Also, we assumed that PAI-1 is short-lived and cannot diffuse through the whole clot, and therefore is only present in the local vicinity around platelets. However, if we imagine that PAI-1 has diffused away from the platelets and we define a low probability of tPA removal on all edges in the clot (not just edges in the platelet regions), then we can provide support for the hypothesis that PAI-1 regulates lysis. We find that if PAI-1 can inhibit all tPA, whether or not it is bound, lysis is severely hindered (Figure 5.4). However, if PAI-1 only inhibits free tPA, lysis is able to proceed unimpeded (Figure 5.4). This suggests that in the presence of low levels of fibrin, PAI-1 can effectively inhibit tPA and prevent systemic lysis. When a blood clot develops, tPA binds to fibrin and is protected from PAI-1. Lysis begins because the tPA is no longer inhibited.

When we include TAFIa in the microscale model, fewer plasmin molecules are produced than when we do not account for TAFIa. There are two consequences of fewer plasmin molecules: tPA stays bound longer because it is forced to unbind by plasmin less frequently (Table 5.2), and single fiber lysis times increase (Figure 5.7). TAFIa slightly increases single fiber lysis times in the absence of α_2-AP, and drastically increases them in the presence of α_2-AP (Figure 5.7). In our model without α_2-AP, TAFIa only slows down lysis by 3-8% in thin fibers and 8-30% in thick fibers (depending on whether tPA can rebind or not). With α_2-AP, however, TAFIa slows down lysis by 35-240% (thin), or 800% to stopping lysis almost completely (thick).

In all situations tested, adding TAFIa to the microscale model decreases the macroscale lysis front velocity (Table 5.3). Lysis front velocities are slower in the presence of TAFIa for three reasons: fewer plasmin molecules are produced, so single fiber lysis times are longer; tPA is slower to diffuse to new fibers because tPA leaving times are longer; and, when plasmin can unbind, the probability that a bound tPA molecule initiates lysis is smaller. When both α_2-AP and TAFIa are present, our model predicts that virtually no lysis of thick fibers or coarse clots will occur. However, experiments show that TAFIa cannot completely stop lysis, and the effect of TAFIa on clot lysis saturates with a half-maximal effect at 1 nM TAFIa [?]. In the future, we plan to use our multiscale model with TAFIa to investigate the saturating behavior of TAFIa on clot lysis.

Experimental results suggest that TAFIa has no effect on lysis in the absence of α_2-AP [?], inconsistent with our findings. Yet, our results may provide a possible explanation for the experimental results. From the model, we find that TAFIa and α_2-AP both individually

slow down single fiber and full clot lysis. α_2-AP is the more effective inhibitor (compare solid blue curves to dashed black curves in Figures 5.7 and 5.8), but the biggest increase in single fiber lysis times (and biggest decrease in front velocities) occurs when both α_2-AP *and* TAFIa are present (blue dashed curves in Figures 5.7 and 5.8). Perhaps the effect of TAFIa is more apparent in conjunction with α_2-AP because there are fewer plasmin molecules. In the absence α_2-AP, there is more plasmin in the system and the continued plasmin-mediated degradation of fibrin is able to mask the effects of TAFIa. In the presence of α_2-AP, there are fewer plasmin molecules and the plasmin-mediated degradation of fibrin is slower, so the effect of TAFIa is more visible.

Also, it is possible that there is very little positive feedback during lysis, contrary to general belief. If exposure of new binding sites facilitates the creation of more plasmin, then removing those binding sites with TAFIa should reduce the amount of plasmin produced and consequently slow lysis, even in the absence of α_2-AP. However, this is not seen experimentally, and the model predicts only a small retardation of lysis in the absence of α_2-AP. When we do not allow tPA to rebind to the cross section, the model has minimal positive feedback; it does not matter how many new binding sites are exposed, additional plasmin molecules cannot be created if tPA cannot rebind to the new sites. The only positive feedback in the model occurs on the protofibril to which tPA is bound. As the 5 cryptic doublets at that binding location are exposed by plasmin, PLG can bind to the new sites and tPA can activate the PLG to plasmin. Perhaps it is the TAFIa-mediated inhibition of this minimal positive feedback that increases lysis times in the model.

We can study additional positive feedback by allowing tPA to rebind. The exposure of binding sites as lysis progresses provides more places for PLG to bind, so when tPA rebinds, it is more likely to be on a protofibril that contains PLG. The tPA is therefore more likely to create a plasmin molecule, which begins degrading and exposing binding sites. In this way, lysis is sped up by the positive feedback achieved by tPA rebinding. We see that TAFIa has more of an effect on lysis when tPA can rebind because it prevents the positive feedback in that situation; TAFIa slows the coarse clot lysis front velocity by 19% without tPA rebinding, and by 28% with tPA rebinding, when plasmin does not unbind. So the lack of inhibition of lysis seen in TAFIa experiments without α_2-AP could suggest that there is not as much positive feedback in the lytic process as previously assumed. Therefore, our model results in comparison to experiments are inconclusive with respect to tPA rebinding. Without tPA rebinding, α_2-AP slows lysis to unrealistic levels (Figure 5.8(a),

solid blue curve) or stops lysis completely in the presence of TAFIa (lack of dashed blue curve in Figure 5.8(a)). Adding tPA rebinding to these simulations recovers more reasonable lysis rates (Figure 5.8(a), solid and dashed green curves), suggesting that tPA does rebind physiologically. However, the experimental observation of no effect of TAFIa alone on lysis rates suggests there is little tPA rebinding. Future work will more carefully address and explore the presumed positive feedback within the fibrinolytic system.

CHAPTER 6

CONCLUSION

Fibrinolytic rates must be maintained in a tightly regulated range to prevent severe health complications such as heart attack, stroke, and excessive bleeding. Clinical research is aimed at developing both fibrinolytic and anitfibrinolytic drugs to treat patients with abnormally functioning fibrinolytic systems. The goal of our mathematical research is to elucidate biochemical mechanisms of the fibrinolytic system to better understand how lysis occurs. Our mathematical models can be used to propose useful biological experiments and suggest targets for drug development.

We developed a 1-dimensional reaction-diffusion model of fibrinolysis that extended preceding models by considering more detailed reaction chemistry and the spatial heterogeneity of fibrin (Chapter 2). More so than previous models, our model predicts spatial protein concentrations at the lysis front that are consistent with experimental data. However, we conclude that even with our model improvements, 1-D continuum models are unable to accurately describe the observed differences in lysis behavior between fine and coarse clots.

The 1-D model results, along with the observation that a 5 nM tPA concentration (typical concentration used in experiments) is only about 3 tPA molecules/μm^3, motivated the creation of a 3-D stochastic model of fibrinolysis (Chapters 3-5). Our model is the first 3-dimensional fibrinolysis model, and the first mathematical model to simultaneously consider lysis at the single fiber and whole clot scales. It is also the first to acknowledge the low protein concentrations by treating tPA and plasmin stochastically. Our model is multiscale and involves stochastic and deterministic spatiotemporal dynamics. The microscale model represents a fiber cross section and contains detailed biochemical reactions. It provides information about single fiber lysis times, the number of plasmin molecules that can be activated by a single tPA molecule, and the length of time tPA stays bound to a given fiber cross section. Data from the microscale model is used in a macroscale model of the full fibrin clot, which gives lysis front velocities and spatial tPA distributions.

Results from the multiscale model suggest that the number of tPA molecules exposed

to the front of the clot determines whether coarse clots lyse faster or slower than fine clots. For our clot geometry and parameter values, if there are fewer than 287 tPA molecules/μm^2 at the clot front, coarse clots lyse faster than fine clots because they contain fewer fibers. As the number of tPA molecules increases, the advantage of having fewer fibers is erased because tPA can start lysis on all fibers at the front of both types of clots (Chapters 3 and 4).

We use the multiscale model to predict ranges of parameter values that have yet to be measured experimentally, and to suggest targets for future fibrinolytic drugs. A simple model of plasmin unbinding allows us to estimate the relative values of plasmin unbinding and crawling rates (Appendix G). We propose that the crawling rate must be much larger than the unbinding rate in order for plasmin to crawl effectively; if the rates are similar, plasmin will unbind and be inhibited by α_2-AP before it has a chance to crawl. We can also hypothesize values of PLG and tPA binding and unbinding rates. Based on our model results, we estimate that the binding rate of PLG is in the range $k_{\text{on}}^{\text{PLG}} \in (1 \times 10^{-3},\ 1 \times 10^{-1})$ μM^{-1}s^{-1}, and that the binding rate of tPA is in the range $k_{\text{on}}^{\text{tPA}} \in (1 \times 10^{-2}, 1)$ μM^{-1}s^{-1} (Chapter 4). PLG and tPA dissociation constants have been measured, so given the binding rates estimated above, the unbinding rates are computed as necessary to achieve the measured dissociation constants.

If a tPA variant with a different dissociation constant can be engineered, our model suggests values for this new dissociation constant that will most effectively increase clot lysis rates. Increasing the dissociation constant from its physiological value increases the clot lysis rate because tPA binds less strongly to the clot front and consequently starts lysis on more fibers throughout the clot. However, there appears to be an optimal value of the tPA dissociation constant with respect to the resulting lysis rate (Chapter 4).

We are able to study the effect of inhibitors on fibrinolysis using our multiscale model. We find that α_2-AP greatly inhibits single fiber and full clot lysis (Chapter 4). TAFIa slightly retards lysis on its own, but is much more effective in the presence of α_2-AP (Chapter 5). The presence of α_2-AP likely makes the effect of TAFIa more apparent (compared to the effect of TAFIa alone) because it removes plasmin molecules from the simulation. When plasmin is more abundant, TAFIa-mediated cleavage of binding sites is overwhelmed by plasmin-mediated degradation, and the inhibitory effect of TAFIa is weak. At measured physiological concentrations, the tPA inhibitor PAI-1 also seems to have a weak inhibitory effect on lysis. The PAI-1 concentration in blood clots must be higher

than the 5 nM concentration measured in platelet rich plasma in order to retard lysis (Chapter 5). If higher PAI-1 concentrations are present, then lysis rates decrease and often prevent complete degradation of the clot. In simulations with a 1 μM PAI-1 concentration, the number and distribution of platelets in the clot affects the progression of lysis.

The multiscale model raises questions about some generally accepted beliefs about fibrinolysis. It is believed that PLG is able to diffuse through the pores in a single fibrin fiber, however our calculation of protofibril spacing in a fiber (coupled with experimental estimates of PLG diameters), suggests that PLG is too large to diffuse between protofibrils (Appendix A). Also, model results suggest that positive feedback does not have a large effect on clot lysis (Chapter 4). It is generally accepted that the plasmin-mediated exposure of new binding sites during lysis increases PLG binding, and hence increases plasmin production and fibrin degradation. However, model results in the presence and absence of positive feedback do not differ greatly. We believe that the low tPA concentration is responsible for the lack of expected positive feedback. It does not matter how many additional PLG binding sites get exposed during lysis – if there is no available tPA to bind to those sites, additional plasmin cannot be created.

Analysis of our stochastic multiscale model suggests several interesting biological experiments with significance to clinical practice and future mathematical modeling work. First, we propose an experiment to test the hypothesis that the number of tPA molecules relative to the surface area of clot exposed to the molecules determines whether coarse clots lyse faster or slower than fine clots. We imagine many coarse clots formed under identical conditions. A different volume and concentration of tPA (i.e., a different number of tPA molecules) will be added to the edge of each clot and lysis front velocities will be calculated. Then the same tPA concentrations and volumes will be added to the edges of fine clots (all formed under identical conditions) and lysis front velocities will be recorded. We hypothesize that with fewer tPA molecules, coarse clots will lyse faster than fine clots, but as the number of tPA molecules increases, fine clot lysis rates will be faster than coarse clot lysis rates. This could help explain why some experiments show faster lysis rates in coarse clots [?, ?], while others display little difference in lysis rate or faster rates in fine clots [?, ?, ?].

A second experiment driven by results of our model involves engineering tPA variants with larger-than-physiological dissociation constants and testing their effectiveness in clot lysis. The model predicts that tPA with a dissociation constant one order of magnitude

bigger than physiological (call this tPA-1) increases lysis rates more than tPA with a dissociation constant two orders of magnitude bigger than physiological (call this tPA-2). An experiment in which normal tPA, tPA-1, and tPA-2 are used to lyse fibrin clots formed under identical conditions should start to elucidate desirable characteristics of fibrinolytic drugs. Based on our model, we propose that one such characteristic is weaker binding to fibrin; if tPA binds less strongly to fibrin, it can diffuse through the clot more easily and initiate lysis on more fibers.

Now that technology has progressed to the point that accurate single fiber experiments are possible, we can use our model to suggest single fiber lysis experiments that may be worth investigating. Finding a relationship between fiber diameter and the time it takes for the fiber to degrade could give us an idea about what "degradation" of a fiber actually means. In the model, we assume that degradation occurs when a given percentage of binding sites have been lysed. This results in single fiber lysis times scaling quadratically with diameter: a thick fiber with twice the diameter of a thin fiber will take four times longer to degrade. If single fiber lysis experiments showed a similar relationship between diameter and lysis time, we might hypothesize that *percentage* of degraded fibrin determines lysis. However, if a thick fiber with diameter twice the thin fiber takes more than four times longer to degrade, we might hypothesize that the raw *number* of degraded fibrin monomers determines lysis.

Finally, we do not know if such experiments are currently possible, but in the future it would be interesting to study single molecules. For example, how long does a tPA molecule stay bound to a single fiber? Does the length of time it stays bound differ depending on the size of the fiber? When the tPA molecule unbinds, does it rebind elsewhere on the fiber? The model predicts that if tPA is usually forced to unbind from fibrin by plasmin-mediated degradation, then tPA will stay bound to thick fibers longer than to thin fibers. Thick fibers have more space for plasmin to crawl, and therefore the plasmin encounters the tPA less frequently. If, however, tPA usually unbinds on its own, the model predicts no difference in the length of time tPA stays bound to different fibers. Experiments that measure the length of time tPA stays bound to a fiber could be used in conjunction with the model to predict whether tPA is forced to unbind by plasmin or unbinds on its own. Also, the model predicts that very few plasmin molecules (1-2, on average) are responsible for the degradation of a single fiber, and that single fiber lysis time is often determined by the amount of time it takes tPA to create a plasmin molecule. In the future, it would be interesting if a single

fiber experiment could determine when, and how much, plasmin is created.

The model framework we created lends itself to future research. We plan on more thoroughly investigating the role (and existence) of positive feedback in fibrinolysis. Part of this work will involve revisiting the tPA rebinding probability calculation (Appendix E). We have only briefly studied the effect of TAFIa on lysis. Future work will address the experimental observation that lysis rate saturates as a function of TAFIa [?, ?]. The activation of TAFIa from TAFI is also a consideration for future work. Thrombin, plasmin, and the thrombin-thrombomodulin complex all convert TAFI to TAFIa, but they all do so with wildly different rates [?, ?, ?]. Understanding the relative importance of each activator in physiological conditions will provide information about how the TAFIa in a blood clot is created. This information can then be used to develop therapeutics that increase fibrinolysis rates by preventing TAFIa production.

It will also be important to study lysis of more heterogeneous fibrin clots. So far our clots have been 3-dimensional square lattices, with all fibers in a given clot having the same diameter. However, the mesh of fibers near platelets is often tightly packed, with thicker fibers and a coarser mesh of fibrin in regions of clot away from platelets. Allowing for this type of variation in fiber diameter and pore size within our model clot will be necessary to study more physiological clots. It could also be interesting (and clinically relevant) to study lysis of a thrombus, which often has very thick fibers packed closely together. The macroscale model clot geometry will need to be adjusted to accommodate heterogeneous clots, but neither the microscale model algorithm nor the macroscale model algorithm will require adjustments.

Finally, as more fibrinolysis experiments are conducted (perhaps inspired by our modeling), we acquire new information that can be incorporated into our models. In this way, mathematical modeling and biological experimentation complement and motivate each other; advances in modeling suggest avenues of research for experimentalists, and new experiments provide information that makes models more realistic.

APPENDIX A

PROTOFIBRIL SPACING IN A FIBRIN FIBER

The following calculation can be done for any size fiber, but for concreteness, consider a 97.5-nm diameter fibrin fiber. For ease of computation, assume the fiber cross section is a square of equal area to the circular cross section (Figure A.1):

$$\text{Area} = \pi(48.75 \text{ nm})^2 = 7466.19 \text{ nm}^2 \approx (86.4 \text{ nm}) \times (86.4 \text{ nm}).$$

Since a fibrin fiber is approximately 20% protein, 20% of the cross sectional area (or

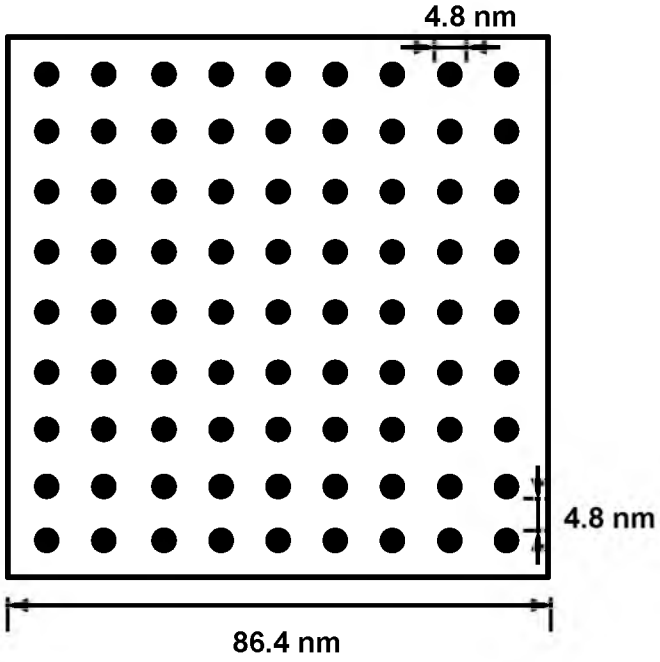

Figure A.1. Diagram of protofibril spacing in a 97.5-nm diameter fiber cross section. The circular fiber cross section is approximated by a square of equal area. Black circles are protofibril cross sections, each with diameter 4.8 nm. The distance from the edge of one protofibril to the edge of a neighboring protofibril is also 4.8 nm.

1493.238 nm^2) should be protein. The diameter of a protofibril is approximately 4.8 nm. We assume that a protofibril is a solid cylinder of protein, so the amount of fibrin in the cross section of a single protofibril is $\pi(2.4 \text{ nm})^2 = 18.09 \text{ nm}^2$. This means there should be

$$\frac{1493.238 \text{ nm}^2}{18.09 \text{ nm}^2} \approx 82$$

protofibrils in the 97.5-nm diameter fibrin fiber. We can leave out one protofibril (to get a square number), without drastically changing the protein concentration (with 81 protofibrils, the percentage of fibrin in the fiber is 19.63%). Equally spacing the 81 protofibrils in 9 rows of 9 in the square cross section results in an edge-to-edge distance between protofibrils of 4.8 nm (Figure A.1).

APPENDIX B

1-D MODEL EQUATIONS

$$\frac{\partial a}{\partial t} = \frac{\partial}{\partial x}\left(D_{\mathrm{tPA}}\frac{\partial a}{\partial x}\right) - k_{\mathrm{on}}^{\mathrm{a},0,0}a(s^{0,0}+2n^{0,0}) + k_{\mathrm{off}}^{\mathrm{a},1,0}(s^{1,0}+n^{1,0}) - k_{\mathrm{on}}^{\mathrm{a},0,2}a(s^{0,2}+n^{0,2}) \tag{B.1}$$
$$+ k_{\mathrm{off}}^{\mathrm{a},1,2}(s^{1,2}+n^{1,2}) - k_{\mathrm{on}}^{\mathrm{a},0,3}a(s^{0,3}+n^{0,3}) + k_{\mathrm{off}}^{\mathrm{a},1,3}(s^{1,3}+n^{1,3}) + 2k_{\mathrm{off}}^{\mathrm{a},1,1}n^{1,1}$$
$$- k_{\mathrm{on}}^{\mathrm{a},1,0}an^{1,0} + \frac{k_{\mathrm{cat}}\sigma s^{1,3}}{K_{\mathrm{M}}+\mathit{doublets}+\frac{K_{\mathrm{M}}}{K_{\mathrm{M}}^{\mathrm{n}}}n} + \frac{k_{\mathrm{cat}}\sigma s^{1,2}}{K_{\mathrm{M}}+\mathit{doublets}+\frac{K_{\mathrm{M}}}{K_{\mathrm{M}}^{\mathrm{n}}}n}$$
$$+ \frac{k_{\mathrm{cat}}\sigma s^{1,0}}{K_{\mathrm{M}}+\mathit{doublets}+\frac{K_{\mathrm{M}}}{K_{\mathrm{M}}^{\mathrm{n}}}n} + \frac{k_{\mathrm{cat}}\sigma n^{1,2}}{K_{\mathrm{M}}+\mathit{doublets}+\frac{K_{\mathrm{M}}}{K_{\mathrm{M}}^{\mathrm{n}}}n} + \frac{k_{\mathrm{cat}}\sigma n^{1,3}}{K_{\mathrm{M}}+\mathit{doublets}+\frac{K_{\mathrm{M}}}{K_{\mathrm{M}}^{\mathrm{n}}}n}$$
$$+ \frac{k_{\mathrm{cat}}\sigma n^{1,0}}{K_{\mathrm{M}}+\mathit{doublets}+\frac{K_{\mathrm{M}}}{K_{\mathrm{M}}^{\mathrm{n}}}n} + 2\frac{k_{\mathrm{cat}}\sigma n^{1,1}}{K_{\mathrm{M}}+\mathit{doublets}+\frac{K_{\mathrm{M}}}{K_{\mathrm{M}}^{\mathrm{n}}}n}$$

$$\frac{\partial p}{\partial t} = \frac{\partial}{\partial x}\left(D_{\mathrm{PLG}}\frac{\partial p}{\partial x}\right) - k_{\mathrm{on}}^{\mathrm{p},0,0}p(s^{0,0}+2n^{0,0}) + k_{\mathrm{off}}^{\mathrm{p},0,2}(s^{0,2}+n^{0,2}) - k_{\mathrm{on}}^{\mathrm{p},1,0}p(s^{1,0}+n^{1,0}) \tag{B.2}$$
$$+ k_{\mathrm{off}}^{\mathrm{p},1,2}(s^{1,2}+n^{1,2}) + 2k_{\mathrm{off}}^{\mathrm{p},2,2}n^{2,2} - k_{\mathrm{on}}^{\mathrm{p},0,2}pn^{0,2} + k_{\mathrm{off}}^{\mathrm{p},2,3}n^{2,3} - k_{\mathrm{on}}^{\mathrm{p},0,3}pn^{0,3}$$
$$+ \frac{k_{\mathrm{cat}}\sigma s^{1,2}}{K_{\mathrm{M}}+\mathit{doublets}+\frac{K_{\mathrm{M}}}{K_{\mathrm{M}}^{\mathrm{n}}}n} + \frac{k_{\mathrm{cat}}\sigma s^{0,2}}{K_{\mathrm{M}}+\mathit{doublets}+\frac{K_{\mathrm{M}}}{K_{\mathrm{M}}^{\mathrm{n}}}n} + \frac{k_{\mathrm{cat}}\sigma n^{1,2}}{K_{\mathrm{M}}+\mathit{doublets}+\frac{K_{\mathrm{M}}}{K_{\mathrm{M}}^{\mathrm{n}}}n}$$
$$+ \frac{k_{\mathrm{cat}}\sigma n^{0,2}}{K_{\mathrm{M}}+\mathit{doublets}+\frac{K_{\mathrm{M}}}{K_{\mathrm{M}}^{\mathrm{n}}}n} + 2\frac{k_{\mathrm{cat}}\sigma n^{2,2}}{K_{\mathrm{M}}+\mathit{doublets}+\frac{K_{\mathrm{M}}}{K_{\mathrm{M}}^{\mathrm{n}}}n} + \frac{k_{\mathrm{cat}}\sigma n^{2,3}}{K_{\mathrm{M}}+\mathit{doublets}+\frac{K_{\mathrm{M}}}{K_{\mathrm{M}}^{\mathrm{n}}}n}$$

$$\frac{ds^{0,0}}{dt} = -k_{\text{on}}^{\text{a},0,0} a s^{0,0} + k_{\text{off}}^{\text{a},1,0} s^{1,0} - k_{\text{on}}^{\text{p},0,0} p s^{0,0} + k_{\text{off}}^{\text{p},0,2} s^{0,2} + k_{\text{off}}^{\text{i},0,3} s^{0,3} - \frac{k_{\text{cat}} \sigma s^{0,0}}{K_{\text{M}} + doublets + \frac{K_{\text{M}}}{\kappa_{\text{M}}^{\text{n}}} n} - k_{\text{move}}(s^{1,3} s^{0,0} + n^{1,3} s^{0,0}) \tag{B.3}$$

$$\frac{ds^{1,0}}{dt} = k_{\text{on}}^{\text{a},0,0} a s^{0,0} - k_{\text{off}}^{\text{a},1,0} s^{1,0} - k_{\text{on}}^{\text{p},1,0} p s^{1,0} + k_{\text{off}}^{\text{p},1,2} s^{1,2} + k_{\text{off}}^{\text{i},1,3} s^{1,3} - \frac{k_{\text{cat}} \sigma s^{1,0}}{K_{\text{M}} + doublets + \frac{K_{\text{M}}}{\kappa_{\text{M}}^{\text{n}}} n} + k_{\text{move}}(s^{1,3} s^{0,0} + 2 s^{1,3} n^{0,0}) \tag{B.4}$$

$$\frac{ds^{0,2}}{dt} = -k_{\text{on}}^{\text{a},0,2} a s^{0,2} + k_{\text{off}}^{\text{a},1,2} s^{1,2} + k_{\text{on}}^{\text{p},0,0} p s^{0,0} - k_{\text{off}}^{\text{p},0,2} s^{0,2} - \frac{k_{\text{cat}} \sigma s^{0,2}}{K_{\text{M}} + doublets + \frac{K_{\text{M}}}{\kappa_{\text{M}}^{\text{n}}} n} \tag{B.5}$$

$$\frac{ds^{0,3}}{dt} = -k_{\text{on}}^{\text{a},0,3} a s^{0,3} + k_{\text{off}}^{\text{a},1,3} s^{1,3} - k_{\text{off}}^{\text{i},0,3} s^{0,3} - \frac{k_{\text{cat}} \sigma s^{0,3}}{K_{\text{M}} + doublets + \frac{K_{\text{M}}}{\kappa_{\text{M}}^{\text{n}}} n} + k_{\text{move}}(s^{1,3} s^{0,0} + n^{1,3} s^{0,0}) \tag{B.6}$$

$$\frac{ds^{1,2}}{dt} = -k_{\text{cat}}^{\text{ap}} s^{1,2} + k_{\text{on}}^{\text{a},0,2} a s^{0,2} - k_{\text{off}}^{\text{a},1,2} s^{1,2} + k_{\text{on}}^{\text{p},1,0} p s^{1,0} - k_{\text{off}}^{\text{p},1,2} s^{1,2} - \frac{k_{\text{cat}} \sigma s^{1,2}}{K_{\text{M}} + doublets + \frac{K_{\text{M}}}{\kappa_{\text{M}}^{\text{n}}} n} \tag{B.7}$$

$$\frac{ds^{1,3}}{dt} = k_{\text{cat}}^{\text{ap}} s^{1,2} + k_{\text{on}}^{\text{a},0,3} a s^{0,3} - k_{\text{off}}^{\text{a},1,3} s^{1,3} - k_{\text{off}}^{\text{i},1,3} s^{1,3} - \frac{k_{\text{cat}} \sigma s^{1,3}}{K_{\text{M}} + doublets + \frac{K_{\text{M}}}{\kappa_{\text{M}}^{\text{n}}} n} - k_{\text{move}}(s^{1,3} s^{0,0} + 2 s^{1,3} n^{0,0}) \tag{B.8}$$

$$\frac{dn}{dt} = - \frac{k_{\mathrm{cat}}^{\mathrm{n}} \sigma n}{K_{\mathrm{M}}^{\mathrm{n}} + n + \frac{K_{\mathrm{M}}^{\mathrm{n}}}{K_{\mathrm{M}}} doublets} \tag{B.9}$$

$$\begin{aligned}\frac{dn^{0,0}}{dt} = & - 2k_{\mathrm{on}}^{\mathrm{a},0,0} a n^{0,0} + k_{\mathrm{off}}^{\mathrm{a},1,0} n^{1,0} - 2k_{\mathrm{on}}^{\mathrm{p},0,0} p n^{0,0} + k_{\mathrm{off}}^{\mathrm{p},0,2} n^{0,2} + k_{\mathrm{off}}^{\mathrm{i},0,3} n^{0,3} \\ & - \frac{k_{\mathrm{cat}} \sigma n^{0,0}}{K_{\mathrm{M}} + doublets + \frac{K_{\mathrm{M}}}{K_{\mathrm{M}}^{\mathrm{n}}} n} + \frac{k_{\mathrm{cat}}^{\mathrm{n}} \sigma n}{K_{\mathrm{M}}^{\mathrm{n}} + n + \frac{K_{\mathrm{M}}^{\mathrm{n}}}{K_{\mathrm{M}}} doublets} - 2k_{\mathrm{move}}(s^{1,3} n^{0,0} + n^{1,3} n^{0,0})\end{aligned} \tag{B.10}$$

$$\begin{aligned}\frac{dn^{1,0}}{dt} = & 2k_{\mathrm{on}}^{\mathrm{a},0,0} a n^{0,0} - k_{\mathrm{off}}^{\mathrm{a},1,0} n^{1,0} - k_{\mathrm{on}}^{\mathrm{p},1,0} p n^{1,0} + k_{\mathrm{off}}^{\mathrm{p},1,2} n^{1,2} + k_{\mathrm{off}}^{\mathrm{i},1,3} n^{1,3} \\ & + 2k_{\mathrm{off}}^{\mathrm{a},1,1} n^{1,1} - k_{\mathrm{on}}^{\mathrm{a},1,0} a n^{1,0} - \frac{k_{\mathrm{cat}} \sigma n^{1,0}}{K_{\mathrm{M}} + doublets + \frac{K_{\mathrm{M}}}{K_{\mathrm{M}}^{\mathrm{n}}} n} + k_{\mathrm{move}}(n^{1,3} s^{0,0} + 2n^{1,3} n^{0,0})\end{aligned} \tag{B.11}$$

$$\begin{aligned}\frac{dn^{0,2}}{dt} = & - k_{\mathrm{on}}^{\mathrm{a},0,2} a n^{0,2} + k_{\mathrm{off}}^{\mathrm{a},1,2} n^{1,2} + 2k_{\mathrm{on}}^{\mathrm{p},0,0} p n^{0,0} - k_{\mathrm{off}}^{\mathrm{p},0,2} n^{0,2} - k_{\mathrm{on}}^{\mathrm{p},0,2} p n^{0,2} \\ & + 2k_{\mathrm{off}}^{\mathrm{p},2,2} n^{2,2} + k_{\mathrm{off}}^{\mathrm{i},2,3} n^{2,3} - \frac{k_{\mathrm{cat}} \sigma n^{0,2}}{K_{\mathrm{M}} + doublets + \frac{K_{\mathrm{M}}}{K_{\mathrm{M}}^{\mathrm{n}}} n}\end{aligned} \tag{B.12}$$

$$\begin{aligned}\frac{dn^{0,3}}{dt} = & - k_{\mathrm{on}}^{\mathrm{a},0,3} a n^{0,3} + k_{\mathrm{off}}^{\mathrm{a},1,3} n^{1,3} - k_{\mathrm{on}}^{\mathrm{p},0,3} p n^{0,3} + k_{\mathrm{off}}^{\mathrm{p},2,3} n^{2,3} - k_{\mathrm{off}}^{\mathrm{i},0,3} n^{0,3} \\ & + 2k_{\mathrm{off}}^{\mathrm{i},3,3} n^{3,3} - \frac{k_{\mathrm{cat}} \sigma n^{0,3}}{K_{\mathrm{M}} + doublets + \frac{K_{\mathrm{M}}}{K_{\mathrm{M}}^{\mathrm{n}}} n} + 2k_{\mathrm{move}}(s^{1,3} n^{0,0} + n^{1,3} n^{0,0})\end{aligned} \tag{B.13}$$

$$\begin{aligned}\frac{dn^{1,2}}{dt} = & - k_{\mathrm{cat}}^{\mathrm{ap}} n^{1,2} + k_{\mathrm{on}}^{\mathrm{a},0,2} a n^{0,2} - k_{\mathrm{off}}^{\mathrm{a},1,2} n^{1,2} + k_{\mathrm{on}}^{\mathrm{p},1,0} p n^{1,0} - k_{\mathrm{off}}^{\mathrm{p},1,2} n^{1,2} \\ & - \frac{k_{\mathrm{cat}} \sigma n^{1,2}}{K_{\mathrm{M}} + doublets + \frac{K_{\mathrm{M}}}{K_{\mathrm{M}}^{\mathrm{n}}} n}\end{aligned} \tag{B.14}$$

$$\begin{aligned}\frac{dn^{1,3}}{dt} = & k_{\mathrm{cat}}^{\mathrm{ap}} n^{1,2} + k_{\mathrm{on}}^{\mathrm{a},0,3} a n^{0,3} - k_{\mathrm{off}}^{\mathrm{a},1,3} n^{1,3} - k_{\mathrm{off}}^{\mathrm{i},1,3} n^{1,3} - \frac{k_{\mathrm{cat}} \sigma n^{1,3}}{K_{\mathrm{M}} + doublets + \frac{K_{\mathrm{M}}}{K_{\mathrm{M}}^{\mathrm{n}}} n} \\ & - k_{\mathrm{move}}(n^{1,3} s^{0,0} + 2n^{1,3} n^{0,0})\end{aligned} \tag{B.15}$$

$$\frac{dn^{1,1}}{dt} = k_{\mathrm{on}}^{\mathrm{a},1,0} a n^{1,0} - 2k_{\mathrm{off}}^{\mathrm{a},1,1} n^{1,1} - \frac{k_{\mathrm{cat}} \sigma n^{1,1}}{K_{\mathrm{M}} + doublets + \frac{K_{\mathrm{M}}}{K_{\mathrm{M}}^{\mathrm{n}}} n} \tag{B.16}$$

$$\frac{dn^{2,2}}{dt} = k_{\mathrm{on}}^{\mathrm{p},0,2} p n^{0,2} - 2k_{\mathrm{off}}^{\mathrm{p},2,2} n^{2,2} - \frac{k_{\mathrm{cat}} \sigma n^{2,2}}{K_{\mathrm{M}} + doublets + \frac{K_{\mathrm{M}}}{K_{\mathrm{M}}^{\mathrm{n}}} n} \tag{B.17}$$

$$\frac{dn^{2,3}}{dt} = k_{\mathrm{on}}^{\mathrm{p},0,3} p n^{0,3} - k_{\mathrm{off}}^{\mathrm{p},2,3} n^{2,3} - k_{\mathrm{off}}^{\mathrm{i},2,3} n^{2,3} - \frac{k_{\mathrm{cat}} \sigma n^{2,3}}{K_{\mathrm{M}} + doublets + \frac{K_{\mathrm{M}}}{K_{\mathrm{M}}^{\mathrm{n}}} n} \tag{B.18}$$

$$\frac{dn^{3,3}}{dt} = - 2k_{\mathrm{off}}^{\mathrm{i},3,3} n^{3,3} - \frac{k_{\mathrm{cat}} \sigma n^{3,3}}{K_{\mathrm{M}} + doublets + \frac{K_{\mathrm{M}}}{K_{\mathrm{M}}^{\mathrm{n}}} n} \tag{B.19}$$

APPENDIX C

DETAILED DEFINITIONS FOR GILLESPIE ALGORITHM

Here we define the specific vectors that appear in the master equation,

$$\frac{\partial P}{\partial t}(\underline{x}, t|\underline{x}_0, t_0) = \sum_{j=1}^{22}[a_j(\underline{x} - \underline{v}_j)P(\underline{x} - \underline{v}_j, t|\underline{x}_0, t_0) - a_j(\underline{x})P(\underline{x}, t|\underline{x}_0, t_0)],$$

that describes the microscale model reactions. Using the notation explained in Figure 3.3, the state vector is

$$\underline{x} = \Big[N_{\mathrm{PLG}}, \quad N_{12}, \quad N_{10}, \quad N_{13}, \quad N_{03}, \quad N_{23}, \quad N_{33}, \quad \emptyset, \quad \emptyset_3, \quad N\Big], \tag{C.1}$$

where x_i is the number of molecules of type i in the system. The stoichiometric matrix describing the 22 possible reactions that can occur is

$$V = \begin{pmatrix} \underline{v}_1 \\ \underline{v}_2 \\ \underline{v}_3 \\ \underline{v}_4 \\ \underline{v}_5 \\ \underline{v}_6 \\ \underline{v}_7 \\ \underline{v}_8 \\ \underline{v}_9 \\ \underline{v}_{10} \\ \underline{v}_{11} \\ \underline{v}_{12} \\ \underline{v}_{13} \\ \underline{v}_{14} \\ \underline{v}_{15} \\ \underline{v}_{16} \\ \underline{v}_{17} \\ \underline{v}_{18} \\ \underline{v}_{19} \\ \underline{v}_{20} \\ \underline{v}_{21} \\ \underline{v}_{22} \end{pmatrix} = \begin{pmatrix} 0 & -1 & 1 & 0 & 0 & 0 & 0 & 0 & 0 & 0 \\ 0 & 1 & -1 & 0 & 0 & 0 & 0 & 0 & 0 & 0 \\ 0 & 0 & 1 & -1 & 0 & 0 & 0 & 0 & 0 & 0 \\ 0 & 0 & 0 & -1 & 1 & 0 & 0 & 0 & 0 & 0 \\ 0 & 0 & 0 & 0 & -1 & 1 & 0 & 0 & 0 & 0 \\ 0 & 0 & 0 & 0 & 1 & -1 & 0 & 0 & 0 & 0 \\ 0 & 0 & 0 & 0 & 1 & 0 & -1 & 0 & 0 & 0 \\ 1 & -1 & 0 & 0 & 0 & 0 & 0 & 0 & 0 & 0 \\ 1 & 0 & -1 & 0 & 0 & 0 & 0 & 0 & 0 & 0 \\ 1 & 0 & 0 & 0 & -1 & 0 & 0 & 0 & 0 & 0 \\ 1 & 0 & 0 & 0 & 0 & -1 & 0 & 0 & 0 & 0 \\ 0 & -1 & 0 & 1 & 0 & 0 & 0 & 0 & 0 & 0 \\ 0 & 0 & 0 & 0 & 0 & 0 & 0 & 1 & -1 & 0 \\ 0 & 0 & 0 & -1 & 0 & 0 & 0 & 1 & 0 & 0 \\ 0 & 0 & 0 & 0 & -1 & 0 & 0 & 1 & 0 & 0 \\ 0 & 0 & 0 & 0 & 0 & -1 & 0 & 1 & 0 & 0 \\ 0 & 0 & 0 & 0 & 0 & 0 & -1 & 1 & 0 & 0 \\ 1 & 0 & 0 & 0 & 0 & 0 & 0 & 0 & 0 & -1 \\ 1 & 0 & 0 & 0 & 0 & 0 & 0 & 0 & 0 & -1 \\ 1 & 0 & 0 & 0 & 0 & 0 & 0 & 0 & 0 & -1 \\ 1 & 0 & 0 & 0 & 0 & 0 & 0 & 0 & 0 & -1 \\ 1 & 0 & 0 & 0 & 0 & 0 & 0 & 0 & 0 & -1 \end{pmatrix},$$

and the propensity function is

$$\underline{a} = \Big[k_{\text{off}}^{\text{PLG}} x_2,\, k_{\text{on}}^{\text{PLG}} [\text{PLG}]^{\text{free}} x_3,\, k_{\text{off}}^{\text{PLi}} x_4,\, k_{\text{off}}^{\text{tPA}} x_4,\, k_{\text{on}}^{\text{PLG}} [\text{PLG}]^{\text{free}} x_5,\, k_{\text{off}}^{\text{PLG}} x_6,\, k_{\text{off}}^{\text{PLi}} x_7,$$
$$k_{\text{off}}^{\text{tPA}} x_2,\, k_{\text{off}}^{\text{tPA}} x_3,\, k_{\text{off}}^{\text{PLi}} x_5,\, k_{\text{off}}^{\text{PLi}} x_6,\, k_{\text{cat}}^{\text{ap}} x_2,\, k_{\text{off}}^{\text{PLi}} x_9,\, k_{\text{deg}} x_4,\, k_{\text{deg}} x_5,\, k_{\text{deg}} x_6,\, k_{\text{deg}} x_7,$$
$$k_{\text{cat}}^{n} n x_4,\, k_{\text{cat}}^{n} n x_5,\, k_{\text{cat}}^{n} n x_6,\, k_{\text{cat}}^{n} n x_7,\, k_{\text{cat}}^{n} n x_9\Big],$$

where n is the number of cryptic doublets at the binding location of interest. We use this information in the Gillespie Algorithm as follows:

0. Initialize $t = t_0$, $\underline{x} = \underline{x}_0$.

1. With the system in state $\underline{x}$ at time t, evaluate the propensity function $\underline{a}$ and the sum $a_0(\underline{x}) = \sum_{j=1}^{22} a_j(\underline{x})$.

2. Choose two independent random variables, $r_1, r_2 \in U[0,1]$. Set $\tau = \frac{1}{a_0(\underline{x})} \ln\left(\frac{1}{r_1}\right)$ (when the next reaction happens), and set i to be the smallest integer such that $\sum_{j=1}^{i} a_j(\underline{x}) > r_2 a_0(\underline{x})$ (which reaction happens next).

3. Carry out reaction i and set $t = t + \tau$, $\underline{x} = \underline{x} + \underline{v}_i$. Return to step 1.

APPENDIX D

QUASI-STEADY STATE CALCULATION FOR PLG

Here we describe the quasi-steady state assumption calculation for plasminogen (PLG) in the microscale model. Assume we have a system consisting solely of PLG and doublets (pairs of binding sites to which PLG can bind). Let p = free PLG concentration, N_{00}^j = concentration of N_{00} doublets of type j, N_{02}^j = concentration of N_{02} doublets of type j, and N_{22}^j = concentration of N_{22} doublets of type j, where j=i for intact, j=n for nicked. Similarly, let k_{on}^j and k_{off}^j denote the rates for PLG binding to, and unbinding from, fibrin of type j. Then we have the system of equations

$$\begin{aligned}
\frac{dN_{00}^i}{dt} &= -2k_{\text{on}}^i p N_{00}^i + k_{\text{off}}^i N_{02}^i \\
\frac{dN_{02}^i}{dt} &= -k_{\text{off}}^i N_{02}^i + 2k_{\text{on}}^i p N_{00}^i - k_{\text{on}}^i p N_{02}^i + 2k_{\text{off}}^i N_{22}^i \\
\frac{dN_{22}^i}{dt} &= -2k_{\text{off}}^i N_{22}^i + k_{\text{on}}^i p N_{02}^i \\
\frac{dN_{00}^n}{dt} &= -2k_{\text{on}}^n p N_{00}^n + k_{\text{off}}^n N_{02}^n \\
\frac{dN_{02}^n}{dt} &= -k_{\text{off}}^n N_{02}^n + 2k_{\text{on}}^n p N_{00}^n - k_{\text{on}}^n p N_{02}^n + 2k_{\text{off}}^n N_{22}^n \\
\frac{dN_{22}^n}{dt} &= -2k_{\text{off}}^n N_{22}^n + k_{\text{on}}^n p N_{02}^n.
\end{aligned}$$

Making the quasi-steady state assumption we set the right hand sides of the above equations equal to zero. Let the total concentration of binding sites be F, so

$$F = \underbrace{N_{00}^i + N_{02}^i + N_{22}^i}_{F_i} + \underbrace{N_{00}^n + N_{02}^n + N_{22}^n}_{F_n}.$$

Then doing a bit of algebra gives the probability of having each type of doublet:

$$P(N_{00}^i) = \frac{0.5k_D^i F_i}{p\gamma_i(F_i+F_n)}, \qquad P(N_{00}^n) = \frac{0.5k_D^n F_n}{p\gamma_n(F_i+F_n)},$$
$$P(N_{02}^i) = \frac{F_i}{\gamma_i(F_i+F_n)}, \qquad P(N_{02}^n) = \frac{F_n}{\gamma_n(F_i+F_n)},$$
$$P(N_{22}^i) = \frac{0.5pF_i}{k_D^i\gamma_i(F_i+F_n)}, \qquad P(N_{22}^n) = \frac{0.5pF_n}{k_D^n\gamma_n(F_i+F_n)}.$$

where $\gamma_j = (1 + 0.5\frac{k_D^j}{p} + 0.5\frac{p}{k_D^j})$, $j = i$ or n. For $k_D^i = 38$ μM, $k_D^n = 2.2$ μM, $p = 2$ μM,

$$P(N_{00}^i) = 0.9025\Big(\frac{F_i}{F_i+F_n}\Big), \qquad P(N_{00}^n) = 0.2744\Big(\frac{F_n}{F_i+F_n}\Big),$$
$$P(N_{02}^i) = 0.0950\Big(\frac{F_i}{F_i+F_n}\Big), \qquad P(N_{02}^n) = 0.4989\Big(\frac{F_n}{F_i+F_n}\Big),$$
$$P(N_{22}^i) = 0.0025\Big(\frac{F_i}{F_i+F_n}\Big), \qquad P(N_{22}^n) = 0.2268\Big(\frac{F_n}{F_i+F_n}\Big).$$

In the model, we use these probabilities to determine where a plasmin molecule crawls. Once we know if the plasmin is moving onto a nicked or intact doublet, then we use the above probabilities without the $\left(\frac{F_i}{F_i+F_n}\right)$ factor to determine if the given nicked or intact doublet is N_{00}, N_{02}, or N_{22}.

APPENDIX E

tPA REBINDING PROBABILITY

Consider a molecule that can diffuse in a sphere of radius R_1 and bind to a partially absorbing inner sphere of radius $R_0 < R_1$. We think of R_0 as the size of the fiber cross section of interest, and R_1 as the distance to the next cross section along the fiber. Let $\pi(r)$ be the probability of binding anywhere within the sphere of radius R_0 having started at radius r, so

$$D\frac{1}{r^2}\frac{\partial}{\partial r}\left(r^2\frac{\partial \pi}{\partial r}\right) - k_0\pi = -k_0 \quad \text{for } r \leq R_0 \quad \text{and} \tag{E.1}$$

$$D\frac{1}{r^2}\frac{\partial}{\partial r}\left(r^2\frac{\partial \pi}{\partial r}\right) = 0 \quad \text{for } R_0 < r \leq R_1, \tag{E.2}$$

where k_0 is the binding rate. Assuming that R_1 is an absorbing boundary gives the boundary condition $\pi(R_1) = 0$.

Solving for $\pi(R_0)$ gives the rebinding probability, i.e. the probably that a molecule starting at R_0 rebinds anywhere in the sphere of radius R_0:

$$\pi(R_0) = 1 - \frac{R_1}{R_0}\left(\frac{1}{1 + (R_1 - R_0)\sqrt{\frac{k_0}{D}}\coth\left(\sqrt{\frac{k_0}{D}}R_0\right)}\right), \tag{E.3}$$

where $D = 10^7\ \frac{\text{nm}^2}{\text{s}}$ (typical diffusion constant for an enzyme), $R_1 = 22.5$ nm (the distance to the next tPA binding site along the length of a fibrin fiber), $R_0 = 0.5$ nm (the assumed "thickness" of the cross section), and $k_0 = k_{\text{on}}^{\text{tPA}}B$, where $k_{\text{on}}^{\text{tPA}}$ is the binding affinity of tPA to fibrin (in units of $\frac{1}{\mu\text{M}\cdot\text{s}}$), and B is the concentration of binding sites in the cross section (in units of μM).

When tPA unbinds from a doublet we pick a random number. tPA rebinds if the random number is less than the rebinding probability, otherwise we conclude that the tPA molecule diffused away. The probability that a molecule will bind in the region $r \leq R_0$ is higher when there is a high concentration of binding sites and/or a strong binding affinity. The rebinding

probability changes with time because B increases initially as binding sites are exposed, and then decreases as degradation proceeds. However, for our parameters, $\pi(R_0) = \mathcal{O}(10^{-6})$, and we conclude that tPA essentially never rebinds.

To derive Equations (E.1) and (E.2), consider the probability of a molecule being at position r_2, in state α_2 at time t_2 given that it started at position r_3, state α_3 at time t_3, $p(r_2, \alpha_2, t_2, r_3, \alpha_3, t_3)$. r_i is a continuous variable describing the physical location of the molecule, and α_i is a discrete variable describing the state of the molecule. $\alpha_i = 0$ indicates the molecule is unbound, and $\alpha_i = 1$ means the molecule is bound. When the molecule binds it remains bound, so

$$p(r_2, 1, t_2, r_3, 1, t_3) = 1, \tag{E.4}$$

$$p(r_2, 0, t_2, r_3, 1, t_3) = 0. \tag{E.5}$$

Let

$$\begin{aligned} P(r_2, t_2, r_3, t_3) &= p(r_2, 0, t_2, r_3, 0, t_3), \\ Q(r_2, t_2, r_3, t_3) &= p(r_2, 1, t_2, r_3, 0, t_3). \end{aligned}$$

Since the molecule can diffuse and bind, P and Q satisfy the differential equations

$$\frac{\partial P}{\partial t_2}(r_2, t_2, r_3, t_3) = L_{r_2} P(r_2, t_2, r_3, t_3) - k_0 \chi(r_2) P(r_2, t_2, r_3, t_3) \tag{E.6}$$

$$\frac{\partial Q}{\partial t_2}(r_2, t_2, r_3, t_3) = k_0 \chi(r_2) P(r_2, t_2, r_3, t_3), \tag{E.7}$$

where L_{r_2} is the diffusion operator on r_2, k_0 is the binding rate, and $\chi(r_2)$ is an indicator function such that

$$\chi(r_2) = \begin{cases} 1 & \text{if } r_2 \leq R_0 \\ 0 & \text{otherwise.} \end{cases}$$

Define $g(t_1, r_2) = \int Q(r_1, t_1, r_2, 0) dr_1$, the probability the molecule is bound at time t_1 given it started at position r_2 at time $t_2 = 0$. Then

$$\begin{aligned}\frac{\partial g}{\partial t_1} &= \int \frac{\partial}{\partial t_1} Q(r_1, t_1, r_2, 0) dr_1 \\ &= \int k_0 \chi(r_1) P(r_1, t_1, r_2, 0) dr_1 \qquad \text{(E.8)} \\ &= -\int_{t_1}^{\infty} \int \frac{\partial}{\partial t_1} k_0 \chi(r_1) P(r_1, t_1, r_2, 0) dr_1 dt_1. \qquad \text{(E.9)}\end{aligned}$$

We show below that

$$\frac{\partial}{\partial t_1} P(r_1, t_1, r_2, 0) = [L^*_{r_2} - k_0 \chi(r_2)] P(r_1, t_1, r_2, 0). \qquad \text{(E.10)}$$

Accepting this as true and using it in equation (E.9), we obtain

$$\begin{aligned}\frac{\partial g}{\partial t_1} &= -\int_{t_1}^{\infty} \int k_0 \chi(r_1) [L^*_{r_2} - k_0 \chi(r_2)] P(r_1, t_1, r_2, 0) dr_1 dt_1 \\ &= -[L^*_{r_2} - k_0 \chi(r_2)] \int_{t_1}^{\infty} \left(\int \frac{\partial}{\partial t_1} Q(r_1, t_1, r_2, 0) dr_1 \right) dt_1 \\ &= [L^*_{r_2} - k_0 \chi(r_2)] \left(\int Q(r_1, t_1, r_2, 0) dr_1 - \int Q(r_1, \infty, r_2, 0) dr_1 \right). \qquad \text{(E.11)}\end{aligned}$$

Taking the limit of $\frac{\partial g}{\partial t_1}$ as $t_1 \to 0$ gives (via Equation (E.8))

$$\begin{aligned}\lim_{t_1 \to 0} \frac{\partial g}{\partial t_1} &= \lim_{t_1 \to 0} \int k_0 \chi(r_1) P(r_1, t_1, r_2, 0) dr_1 \\ &= \int k_0 \chi(r_1) \delta(r_1 - r_2) dr_1 \\ &= k_0 \chi(r_2). \qquad \text{(E.12)}\end{aligned}$$

So Equation (E.9) becomes

$$k_0 \chi(r_2) = -[L^*_{r_2} - k_0 \chi(r_2)] \int Q(r_1, \infty, r_2, 0) dr_1. \qquad \text{(E.13)}$$

Let $\pi(r_2) = \int Q(r_1, \infty, r_2, 0) dr_1$, so

$$[L^*_{r_2} - k_0 \chi(r_2)] \pi(r_2) = -k_0 \chi(r_2). \qquad \text{(E.14)}$$

Equation (E.14) is equivalent to equations (E.1) and (E.2).

It remains to show equation (E.10). Because we have discrete and continuous variables, the Chapman-Kolmogorov equation is

$$p(r_1,\alpha_1,t_1,r_3,\alpha_3,t_3) = \sum_{\alpha_2=0,1}\int p(r_1,\alpha_1,t_1,r_2,\alpha_2,t_2)p(r_2,\alpha_2,t_2,r_3,\alpha_3,t_3)dr_2, \quad \text{(E.15)}$$

where the function on the left hand side is independent of t_2. Taking derivatives with respect to t_2 and dropping the terms that evaluate to 0 gives

$$\begin{aligned}
0 &= \int \frac{\partial}{\partial t_2} p(r_1,0,t_1,r_2,0,t_2)p(r_2,0,t_2,r_3,0,t_3)dr_2 \\
&+ \int p(r_1,0,t_1,r_2,0,t_2)\frac{\partial}{\partial t_2} p(r_2,0,t_2,r_3,0,t_3)dr_2 \\
&= \int \frac{\partial}{\partial t_2} P(r_1,t_1,r_2,t_2)P(r_2,t_2,r_3,t_3)dr_2 \\
&+ \int P(r_1,t_1,r_2,t_2)\frac{\partial}{\partial t_2} P(r_2,t_2,r_3,t_3)dr_2 \\
&= \int \frac{\partial}{\partial t_2} P(r_1,t_1,r_2,t_2)P(r_2,t_2,r_3,t_3)dr_2 \\
&+ \int P(r_1,t_1,r_2,t_2)[L_{r_2} - k_0\chi(r_2)]P(r_2,t_2,r_3,t_3)dr_2.
\end{aligned}$$

Integrating by parts yields

$$\begin{aligned}
0 &= \int \frac{\partial}{\partial t_2} P(r_1,t_1,r_2,t_2)P(r_2,t_2,r_3,t_3)dr_2 \\
&+ \int P(r_2,t_2,r_3,t_3)[L^*_{r_2} - k_0\chi(r_2)]P(r_1,t_1,r_2,t_2)dr_2, \quad \text{(E.16)}
\end{aligned}$$

where $L^*_{r_2}$ is the adjoint operator of L_{r_2}. Equation (E.16) simplifies to produce the adjoint equation

$$\frac{\partial}{\partial t_2} P(r_1,t_1,r_2,t_2) + [L^*_{r_2} - k_0\chi(r_2)]P(r_1,t_1,r_2,t_2) = 0. \quad \text{(E.17)}$$

Because this is a time homogeneous process, $P(r_1,t_1,r_2,0) = P(r_1,0,r_2,-t_2)$, and

$$\frac{\partial}{\partial t_1} P(r_1,t_1,r_2,0) = -\frac{\partial}{\partial t_2} P(r_1,0,r_2,-t_2), \quad \text{(E.18)}$$

which with equation (E.17) gives

$$\frac{\partial}{\partial t_1} P(r_1,t_1,r_2,0) = [L^*_{r_2} - k_0\chi(r_2)]P(r_1,t_1,r_2,0).$$

APPENDIX F

MODIFIED MODEL GILLESPIE DEFINITIONS

Here we define the specific vectors that appear in the master equation,

$$\frac{\partial P}{\partial t}(\underline{x}, t|\underline{x}_0, t_0) = \sum_{j=1}^{34}[a_j(\underline{x} - \underline{v}_j)P(\underline{x} - \underline{v}_j, t|\underline{x}_0, t_0) - a_j(\underline{x})P(\underline{x}, t|\underline{x}_0, t_0)],$$

that describes the modified microscale model reactions. In the modified model, tPA can convert any PLG at the same binding location to plasmin, plasmin can degrade any doublet at the same binding location, and plasmin can unbind (if $k_{\text{unbind}}^{\text{PLi}} \neq 0$). The state vector is

$$\underline{x}^T = \begin{pmatrix} N_{\text{PLG}} \\ N_{12} \\ N_{10} \\ N_{13} \\ N_{03} \\ N_{23} \\ N_{33} \\ \emptyset \\ \emptyset_3 \\ N \end{pmatrix},$$

where x_i is the number of molecules of type i in the system. Using the notation explained in Figure 3.3, N_{ij} denotes a doublet with molecules of type i and j bound, where $i, j = 0$ (nothing), 1 (tPA), 2 (PLG), 3 (plasmin). N denotes a cryptic doublet and $\emptyset$ denotes a degraded doublet. The stoichiometric matrix describing the 34 possible reactions that can occur is

$$V = \begin{pmatrix} \underline{v}_1 \\ \underline{v}_2 \\ \underline{v}_3 \\ \underline{v}_4 \\ \underline{v}_5 \\ \underline{v}_6 \\ \underline{v}_7 \\ \underline{v}_8 \\ \underline{v}_9 \\ \underline{v}_{10} \\ \underline{v}_{11} \\ \underline{v}_{12} \\ \underline{v}_{13} \\ \underline{v}_{14} \\ \underline{v}_{15} \\ \underline{v}_{16} \\ \underline{v}_{17} \\ \underline{v}_{18} \\ \underline{v}_{19} \\ \underline{v}_{20} \\ \underline{v}_{21} \\ \underline{v}_{22} \\ \underline{v}_{23} \\ \underline{v}_{24} \\ \underline{v}_{25} \\ \underline{v}_{26} \\ \underline{v}_{27} \\ \underline{v}_{28} \\ \underline{v}_{29} \\ \underline{v}_{30} \\ \underline{v}_{31} \\ \underline{v}_{32} \\ \underline{v}_{33} \\ \underline{v}_{34} \end{pmatrix} = \begin{pmatrix} 1 & 0 & -1 & 0 & 0 & 0 & 0 & 0 & 0 & 0 \\ 0 & -1 & 1 & 0 & 0 & 0 & 0 & 0 & 0 & 0 \\ 0 & 1 & -1 & 0 & 0 & 0 & 0 & 0 & 0 & 0 \\ 0 & 0 & 1 & -1 & 0 & 0 & 0 & 0 & 0 & 0 \\ 0 & 0 & 0 & -1 & 1 & 0 & 0 & 0 & 0 & 0 \\ 0 & 0 & 0 & 0 & -1 & 1 & 0 & 0 & 0 & 0 \\ 0 & 0 & 0 & 0 & 1 & -1 & 0 & 0 & 0 & 0 \\ 0 & 0 & 0 & 0 & 1 & 0 & -1 & 0 & 0 & 0 \\ 1 & -1 & 0 & 0 & 0 & 0 & 0 & 0 & 0 & 0 \\ 1 & 0 & 0 & 0 & -1 & 0 & 0 & 0 & 0 & 0 \\ 1 & 0 & 0 & 0 & 0 & -1 & 0 & 0 & 0 & 0 \\ -1 & 0 & 0 & 0 & 1 & 0 & 0 & 0 & 0 & 0 \\ 0 & 0 & 0 & 0 & 0 & 0 & 0 & 1 & -1 & 0 \\ 0 & 0 & 0 & -1 & 0 & 0 & 0 & 1 & 0 & 0 \\ 0 & 0 & 0 & 0 & -1 & 0 & 0 & 1 & 0 & 0 \\ 0 & 0 & 0 & 0 & 0 & -1 & 0 & 1 & 0 & 0 \\ 0 & 0 & 0 & 0 & 0 & 0 & -1 & 1 & 0 & 0 \\ 1 & 0 & 0 & 0 & 0 & 0 & 0 & 0 & 0 & -1 \\ 1 & 0 & 0 & 0 & 0 & 0 & 0 & 0 & 0 & -1 \\ 1 & 0 & 0 & 0 & 0 & 0 & 0 & 0 & 0 & -1 \\ 1 & 0 & 0 & 0 & 0 & 0 & 0 & 0 & 0 & -1 \\ 1 & 0 & 0 & 0 & 0 & 0 & 0 & 0 & 0 & -1 \\ 1 & 0 & 0 & 0 & 0 & -1 & 0 & 0 & 0 & 0 \\ 1 & 0 & 0 & 0 & -1 & 0 & 0 & 0 & 0 & 0 \\ 0 & 0 & 0 & 0 & 1 & 0 & -1 & 0 & 0 & 0 \\ 0 & 0 & 1 & -1 & 0 & 0 & 0 & 0 & 0 & 0 \\ 0 & 0 & 0 & 0 & 0 & 0 & 0 & 0 & 1 & -1 \\ 0 & 0 & -1 & 0 & 0 & 0 & 0 & 1 & 0 & 0 \\ 0 & -1 & 0 & 0 & 0 & 0 & 0 & 1 & 0 & 0 \\ -1 & 0 & 0 & 0 & 0 & 0 & 0 & 1 & 0 & 0 \\ -1 & 0 & 0 & 0 & 0 & 0 & 0 & 1 & 0 & 0 \\ -1 & 0 & 0 & 0 & 0 & 1 & 0 & 0 & 0 & 0 \\ 0 & -1 & 0 & 1 & 0 & 0 & 0 & 0 & 0 & 0 \\ 0 & 0 & 0 & 0 & 0 & -1 & 1 & 0 & 0 & 0 \end{pmatrix}$$

and the propensity function is

$$\underline{a} = \begin{pmatrix} a_1 \\ a_2 \\ a_3 \\ a_4 \\ a_5 \\ a_6 \\ a_7 \\ a_8 \\ a_9 \\ a_{10} \\ a_{11} \\ a_{12} \\ a_{13} \\ a_{14} \\ a_{15} \\ a_{16} \\ a_{17} \\ a_{18} \\ a_{19} \\ a_{20} \\ a_{21} \\ a_{22} \\ a_{23} \\ a_{24} \\ a_{25} \\ a_{26} \\ a_{27} \\ a_{28} \\ a_{29} \\ a_{30} \\ a_{31} \\ a_{32} \\ a_{33} \\ a_{34} \end{pmatrix} = \begin{pmatrix} k_{\text{off}}^{\text{PLG}} x_2 \\ k_{\text{on}}^{\text{PLG}} [\text{PLG}]^{\text{free}} x_3 \\ k_{\text{off}}^{\text{PLi}} x_4 \\ k_{\text{off}}^{\text{tPA}} x_4 \\ k_{\text{on}}^{\text{PLG}} [\text{PLG}]^{\text{free}} x_5 \\ k_{\text{off}}^{\text{PLG}} x_6 \\ k_{\text{off}}^{\text{PLi}} x_7 \\ k_{\text{off}}^{\text{tPA}} x_2 \\ k_{\text{off}}^{\text{tPA}} x_3 \\ k_{\text{off}}^{\text{PLi}} x_5 \\ k_{\text{off}}^{\text{PLi}} x_6 \\ k_{\text{cat}}^{\text{ap}} x_1 \chi \\ k_{\text{off}}^{\text{PLi}} x_9 \\ k_{\text{deg}} x_4 \\ k_{\text{deg}} x_5 \\ k_{\text{deg}} x_6 \\ k_{\text{deg}} x_7 \\ k_{\text{cat}}^{n} n x_4 \\ k_{\text{cat}}^{n} n x_5 \\ k_{\text{cat}}^{n} n x_6 \\ k_{\text{cat}}^{n} n x_7 \\ k_{\text{cat}}^{n} n x_9 \\ k_{\text{unbind}}^{\text{PLi}} x_6 \\ k_{\text{unbind}}^{\text{PLi}} x_5 \\ k_{\text{unbind}}^{\text{PLi}} x_7 \\ k_{\text{unbind}}^{\text{PLi}} x_4 \\ k_{\text{unbind}}^{\text{PLi}} x_9 \\ k_{\text{deg}} x_3 \\ k_{\text{deg}} x_2 \\ k_{\text{deg}} x_1 \\ k_{\text{deg}} x_1 \\ k_{\text{cat}}^{\text{ap}} x_1 \chi \\ k_{\text{cat}}^{\text{ap}} x_2 \chi \\ k_{\text{cat}}^{\text{ap}} x_6 \chi \end{pmatrix}$$

where n is the number of cryptic doublets at the binding location of interest, $\chi = 1$ if there is a tPA molecule at the current binding location, and $\chi = 0$ if there is no tPA molecule. χ appears in the reactions describing tPA-mediated conversion of PLG to plasmin, because those reactions are not possible unless tPA is present somewhere on the binding location.

APPENDIX G

PLASMIN CRAWLING AND UNBINDING RATES

Consider a plasmin molecule with 2 "feet" it can use to crawl. There are 4 possible states this molecule can be in: S_{11} (both feet are bound to fibrin), S_{10} (the first foot is bound to fibrin, the second is unbound), S_{01} (the second foot is bound to fibrin, the first is unbound), and S_{00} (both feet are unbound) (Figure G.1(a)). Plasmin is bound to fibrin in all states except S_{00}. The molecule transitions between states according to the reaction diagram in Figure G.1(b), where we have grouped the S_{10} and S_{01} states into one state (also called S_{10}). We imagine that the plasmin molecule crawls by unbinding one foot and

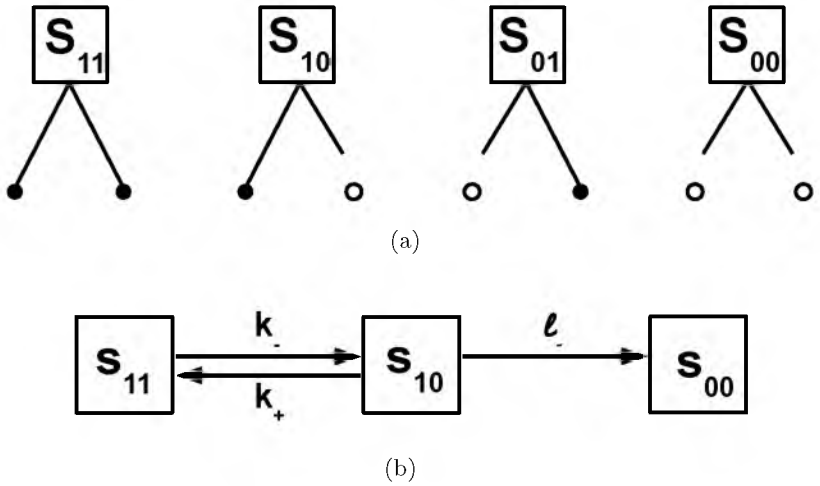

Figure G.1. Basic model for plasmin crawling. (a) The 4 possible states a plasmin molecule with 2 feet can be in. A filled circle represents fibrin with a plasmin foot bound and an open circle represents fibrin without a plasmin foot bound. (b) Reaction diagram for a plasmin molecule transitioning between states. The possibility of an unbound plasmin (S_{00}) binding is neglected since we are interested in what happens prior to the plasmin molecule unbinding.

rebinding it elsewhere, while keeping the other foot bound, so S_{10} represents the states in which plasmin will either step (bind the unbound foot) or unbind completely (unbind the bound foot). We are interested in the mean exit time (i.e., the time before plasmin totally unbinds and enters the S_{00} state), and the mean number of transitions that can be completed in that time. We leave out the possibility of S_{00} to S_{10} transitions since we want to know the number of transitions that occur before the plasmin molecule reaches the S_{00} state. The rate of transitioning from S_{11} to S_{10} is k_-, the rate of transitioning from S_{10} to S_{11} is k_+, and the rate of transitioning from S_{10} to S_{00} is l_-.

In the model depicted in Figure G.1(b), we assume that transition from S_{10} to S_{11} is an attempted crawling step. We say "attempted" because this model cannot tell us *where* the foot bound, only that it did bind. A true step would be one in which the foot bound to a different site than that from which it unbound. So the mean number of transitions (i.e., steps) between states S_{10} and S_{11} obtained with this model will be an overestimate, since not all these transitions will result in a true crawling step. There must be a large number of transitions before total unbinding (i.e., before reaching state S_{00}) in order for a plasmin molecule to crawl. We calculate the mean number of transitions as follows:

Assume the plasmin molecule is in state S_{10}. The probability the first transition is to S_{11} is $\frac{k_+}{k_+ + l_-}$, and the probability the first transition is to S_{00} is $\left(1 - \frac{k_+}{k_+ + l_-}\right) = \frac{l_-}{k_+ + l_-}$. However, several transitions between states S_{10} and S_{11} may occur before plasmin unbinds (reaches state S_{00}). Let N be the number of times plasmin transitions to S_{11} before unbinding and calculate the probability distribution for N,

$$P[N = n] = \underbrace{\left(\frac{k_+}{k_+ + l_-}\right)^n}_{\substack{\text{prob. there are n} \\ S_{10} \to S_{11} \text{ transitions}}} \underbrace{\left(1 - \frac{k_+}{k_+ + l_-}\right)}_{\substack{\text{prob. of } S_{10} \to S_{00} \\ \text{transition}}}. \tag{G.1}$$

Let $A = \frac{k_+}{k_+ + l_-}$, so

$$P[N = n] = A^n(1 - A)$$

is the probability of n transitions before unbinding. Then the expected number of transitions before unbinding is

$$\begin{aligned} E =& \sum_{n=1}^{\infty} nA^n(1-A) \\ =& A(1-A)\sum_{n=1}^{\infty} nA^{n-1} \\ =& A(1-A)\frac{d}{dA}\left(\frac{1}{1-A}\right) \\ =& \frac{A}{1-A} \\ =& \frac{k_+}{l_-}. \end{aligned}$$

The intrinsic plasmin unbinding rate from fibrin is l_-. We see that this intrinsic unbinding rate (or the rate of one foot unbinding when one is already unbound) must be small in comparison to k_+ (the rate of one foot binding when the other is bound) in order for plasmin to make many crawling steps. If the rates are similar, then $k_+ \approx l_-$ and the molecule only takes 1 step, on average. The rate l_- is comparable to the plasmin unbinding rate that we use in the microscale model ($k^{\text{PLi}}_{\text{unbind}}$), and k_+ can be thought of as a crawling rate ($k^{\text{PLi}}_{\text{crawl}}$). Therefore, if we take $k^{\text{PLi}}_{\text{unbind}} = 0.05$ s^{-1} and $k^{\text{PLi}}_{\text{crawl}} = 57.6$ s^{-1}, we satisfy the condition $l_- << k_+$ and are guaranteed that plasmin will actually crawl. (A final note: We see that k_- (the rate of one foot unbinding when both are bound) does not affect how many steps occur, but k_- will affect how long it takes a step to occur. That is, k_- affects travel time, not distance traveled.)

APPENDIX H

QUASI-STEADY STATE CALCULATION FOR PLG AND TAFIa

Assume we have a system consisting solely of plasminogen, TAFIa, and doublets. Let p = free plasminogen concentration, T = free TAFIa concentration, N_{00}^j = concentration of N_{00} doublets of type j, N_{02}^j = concentration of N_{02} doublets of type j, and N_{22}^j = concentration of N_{22} doublets of type j, where j=i for intact, j=n for nicked. Similarly, let k_{on}^j and k_{off}^j denote the rates of plasminogen binding to, and unbinding from, fibrin of type j. Since TAFIa can only bind to nicked doublets, we also have N_{04}, N_{24}, and N_{44}. TAFIa binding and unbinding rates are denoted k_{on}^T and k_{off}^T, respectively, with dissociation constant $k_{\text{D}}^T = k_{\text{off}}^T/k_{\text{on}}^T$. TAFIa and PLG compete for binding sites on nicked fibrin (Figure H.1), which gives the system of equations

$$
\begin{aligned}
\frac{dN_{00}^i}{dt} &= -2k_{\text{on}}^i p N_{00}^i + k_{\text{off}}^i N_{02}^i \\
\frac{dN_{02}^i}{dt} &= -k_{\text{off}}^i N_{02}^i + 2k_{\text{on}}^i p N_{00}^i - k_{\text{on}}^i p N_{02}^i + 2k_{\text{off}}^i N_{22}^i \\
\frac{dN_{22}^i}{dt} &= -2k_{\text{off}}^i N_{22}^i + k_{\text{on}}^i p N_{02}^i \\
\frac{dN_{00}^n}{dt} &= -2k_{\text{on}}^n p N_{00}^n + k_{\text{off}}^n N_{02}^n + k_{\text{off}}^T N_{04} - 2k_{\text{on}}^T T N_{00}^n \\
\frac{dN_{02}^n}{dt} &= -k_{\text{off}}^n N_{02}^n + 2k_{\text{on}}^n p N_{00}^n - k_{\text{on}}^n p N_{02}^n + 2k_{\text{off}}^n N_{22}^n - k_{\text{on}}^T T N_{02}^n + k_{\text{off}}^T N_{24} \\
\frac{dN_{22}^n}{dt} &= -2k_{\text{off}}^n N_{22}^n + k_{\text{on}}^n p N_{02}^n \\
\frac{dN_{04}}{dt} &= 2k_{\text{on}}^T T N_{00}^n - k_{\text{off}}^T N_{04} - k_{\text{on}}^T T N_{04} + 2k_{\text{off}}^T N_{44} - k_{\text{on}}^n p N_{04} + k_{\text{off}}^n N_{24} \\
\frac{dN_{24}}{dt} &= k_{\text{on}}^T T N_{02}^n - k_{\text{off}}^n N_{24} - k_{\text{off}}^T N_{24} + k_{\text{on}}^n p N_{04} \\
\frac{dN_{44}}{dt} &= -2k_{\text{off}}^T N_{44} + k_{\text{on}}^T T N_{04}.
\end{aligned}
$$

Making the quasi-steady state assumption we set the right hand sides of the above equations equal to zero. Let F_i and F_n be the total concentration of intact and nicked

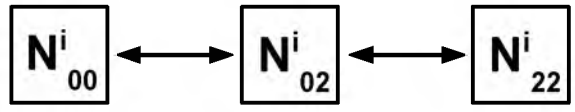

(a) intact doublets

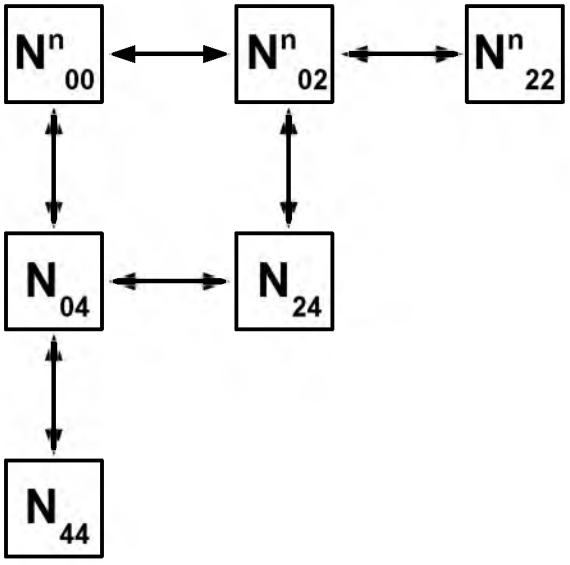

(b) nicked doublets

Figure H.1. Reaction diagrams for the PLG and TAFIa quasi-steady state approximation. a) Reaction diagram for intact doublets. TAFIa cannot bind to intact doublets, so the reactions only include PLG. b) Reaction diagram for nicked doublets. TAFIa and PLG compete for binding sites.

doublets, respectively, so

$$F_i = N^i_{00} + N^i_{02} + N^i_{22} \tag{H.1}$$

$$F_n = N^n_{00} + N^n_{02} + N^n_{22} + N_{04} + N_{24} + N_{44}. \tag{H.2}$$

Solving the system of equations in Maple gives the probability of having each type of doublet:

$$P(N^i_{00}) = 0.9025F_i, \qquad P(N^n_{00}) = 0.224804F_n, \qquad P(N_{04}) = 0.089922F_n$$
$$P(N^i_{02}) = 0.0950F_i, \qquad P(N^n_{02}) = 0.408740F_n, \qquad P(N_{24}) = 0.081748F_n$$
$$P(N^i_{22}) = 0.0025F_i, \qquad P(N^n_{22}) = 0.185794F_n, \qquad P(N_{44}) = 0.008992F_n,$$

where we have used $k_{\mathrm{D}}^{i} = 38$ μM, $k_{\mathrm{D}}^{n} = 2.2$ μM, $k_{\mathrm{D}}^{\mathrm{T}} = 0.1$ μM, $p = 2$ μM, and $T = 20$ nM. (Note: the symbolic solution to the system of equations involves many messy terms, but the on and off rates only appear together in ratios, so we only need to know the k_{D} values.)

APPENDIX I

MODIFIED MODEL GILLESPIE DEFINITIONS WITH TAFIa

Here we define the specific vectors that appear in the master equation,

$$\frac{\partial P}{\partial t}(\underline{x}, t|\underline{x}_0, t_0) = \sum_{j=1}^{54}[a_j(\underline{x} - \underline{v}_j)P(\underline{x} - \underline{v}_j, t|\underline{x}_0, t_0) - a_j(\underline{x})P(\underline{x}, t|\underline{x}_0, t_0)],$$

that describes the modified microscale model reactions. In the modified model, tPA can convert any PLG at the same binding location to plasmin, plasmin can degrade any doublet at the same binding location, plasmin can unbind (if $k_{\text{unbind}}^{\text{PLi}} \neq 0$), and TAFIa is present. The state vector is

$$\underline{x}^T = \begin{pmatrix} N_{\text{PLG}} \\ N_{12} \\ N_{10} \\ N_{13} \\ N_{03} \\ N_{23} \\ N_{33} \\ \emptyset \\ \emptyset_3 \\ N \\ N_{14} \\ N_{34} \\ C \\ C_3 \end{pmatrix},$$

where x_i is the number of molecules of type i in the system. Using the notation explained in Figure 3.3, N_{ij} denotes a doublet with molecules of type i and j bound, where $i, j =$ 0 (nothing), 1 (tPA), 2 (PLG), 3 (plasmin), 4 (TAFIa). N denotes a cryptic doublet, C denotes a cleaved doublet, and $\emptyset$ denotes a degraded doublet. The stoichiometric matrix

describing the 54 possible reactions that can occur is

$$V = \begin{pmatrix} \underline{v}_1 \\ \underline{v}_2 \\ \underline{v}_3 \\ \underline{v}_4 \\ \underline{v}_5 \\ \underline{v}_6 \\ \underline{v}_7 \\ \underline{v}_8 \\ \underline{v}_9 \\ \underline{v}_{10} \\ \underline{v}_{11} \\ \underline{v}_{12} \\ \underline{v}_{13} \\ \underline{v}_{14} \\ \underline{v}_{15} \\ \underline{v}_{16} \\ \underline{v}_{17} \\ \underline{v}_{18} \\ \underline{v}_{19} \\ \underline{v}_{20} \\ \underline{v}_{21} \\ \underline{v}_{22} \\ \underline{v}_{23} \\ \underline{v}_{24} \\ \underline{v}_{25} \\ \underline{v}_{26} \\ \underline{v}_{27} \\ \underline{v}_{28} \\ \underline{v}_{29} \\ \underline{v}_{30} \\ \underline{v}_{31} \\ \underline{v}_{32} \\ \underline{v}_{33} \\ \underline{v}_{34} \\ \underline{v}_{35} \\ \underline{v}_{36} \\ \underline{v}_{37} \\ \underline{v}_{38} \\ \underline{v}_{39} \\ \underline{v}_{40} \\ \underline{v}_{41} \\ \underline{v}_{42} \\ \underline{v}_{43} \\ \underline{v}_{44} \\ \underline{v}_{45} \end{pmatrix} = \begin{pmatrix} 1 & 0 & -1 & 0 & 0 & 0 & 0 & 0 & 0 & 0 & 0 & 0 & 0 & 0 \\ 0 & -1 & 1 & 0 & 0 & 0 & 0 & 0 & 0 & 0 & 0 & 0 & 0 & 0 \\ 0 & 1 & -1 & 0 & 0 & 0 & 0 & 0 & 0 & 0 & 0 & 0 & 0 & 0 \\ 0 & 0 & 1 & -1 & 0 & 0 & 0 & 0 & 0 & 0 & 0 & 0 & 0 & 0 \\ 0 & 0 & 0 & -1 & 1 & 0 & 0 & 0 & 0 & 0 & 0 & 0 & 0 & 0 \\ 0 & 0 & 0 & 0 & -1 & 1 & 0 & 0 & 0 & 0 & 0 & 0 & 0 & 0 \\ 0 & 0 & 0 & 0 & 1 & -1 & 0 & 0 & 0 & 0 & 0 & 0 & 0 & 0 \\ 0 & 0 & 0 & 0 & 1 & 0 & -1 & 0 & 0 & 0 & 0 & 0 & 0 & 0 \\ 1 & -1 & 0 & 0 & 0 & 0 & 0 & 0 & 0 & 0 & 0 & 0 & 0 & 0 \\ 1 & 0 & 0 & 0 & -1 & 0 & 0 & 0 & 0 & 0 & 0 & 0 & 0 & 0 \\ 1 & 0 & 0 & 0 & 0 & -1 & 0 & 0 & 0 & 0 & 0 & 0 & 0 & 0 \\ -1 & 0 & 0 & 0 & 1 & 0 & 0 & 0 & 0 & 0 & 0 & 0 & 0 & 0 \\ 0 & 0 & 0 & 0 & 0 & 0 & 0 & 1 & -1 & 0 & 0 & 0 & 0 & 0 \\ 0 & 0 & 0 & -1 & 0 & 0 & 0 & 1 & 0 & 0 & 0 & 0 & 0 & 0 \\ 0 & 0 & 0 & 0 & -1 & 0 & 0 & 1 & 0 & 0 & 0 & 0 & 0 & 0 \\ 0 & 0 & 0 & 0 & 0 & -1 & 0 & 1 & 0 & 0 & 0 & 0 & 0 & 0 \\ 0 & 0 & 0 & 0 & 0 & 0 & -1 & 1 & 0 & 0 & 0 & 0 & 0 & 0 \\ 1 & 0 & 0 & 0 & 0 & 0 & 0 & 0 & 0 & -1 & 0 & 0 & 0 & 0 \\ 1 & 0 & 0 & 0 & 0 & 0 & 0 & 0 & 0 & -1 & 0 & 0 & 0 & 0 \\ 1 & 0 & 0 & 0 & 0 & 0 & 0 & 0 & 0 & -1 & 0 & 0 & 0 & 0 \\ 1 & 0 & 0 & 0 & 0 & 0 & 0 & 0 & 0 & -1 & 0 & 0 & 0 & 0 \\ 1 & 0 & 0 & 0 & 0 & 0 & 0 & 0 & 0 & -1 & 0 & 0 & 0 & 0 \\ 1 & 0 & 0 & 0 & 0 & 0 & 0 & 0 & 0 & 0 & -1 & 0 & 0 & 0 \\ 1 & 0 & 0 & 0 & 0 & 0 & 0 & 0 & 0 & 0 & 0 & -1 & 0 & 0 \\ 0 & 0 & 1 & 0 & 0 & 0 & 0 & 0 & 0 & 0 & -1 & 0 & 0 & 0 \\ 0 & 0 & -1 & 0 & 0 & 0 & 0 & 0 & 0 & 0 & 1 & 0 & 0 & 0 \\ 0 & 0 & 0 & 0 & 1 & 0 & 0 & 0 & 0 & 0 & 0 & -1 & 0 & 0 \\ 0 & 0 & 0 & 0 & -1 & 0 & 0 & 0 & 0 & 0 & 0 & 1 & 0 & 0 \\ -1 & 0 & 0 & 0 & 0 & 0 & 0 & 0 & 0 & 0 & 0 & 0 & 1 & 0 \\ 0 & 0 & 0 & 0 & 0 & 0 & 0 & 0 & 0 & 0 & 0 & -1 & 1 & 0 \\ 0 & 0 & 0 & 0 & 0 & 0 & 0 & 0 & 0 & 0 & -1 & 0 & 1 & 0 \\ 0 & 0 & 0 & 0 & 0 & 0 & 0 & 0 & 0 & 0 & 0 & 0 & 1 & -1 \\ 1 & 0 & 0 & 0 & 0 & -1 & 0 & 0 & 0 & 0 & 0 & 0 & 0 & 0 \\ 1 & 0 & 0 & 0 & -1 & 0 & 0 & 0 & 0 & 0 & 0 & 0 & 0 & 0 \\ 0 & 0 & 0 & 0 & 1 & 0 & -1 & 0 & 0 & 0 & 0 & 0 & 0 & 0 \\ 0 & 0 & 1 & -1 & 0 & 0 & 0 & 0 & 0 & 0 & 0 & 0 & 0 & 0 \\ 0 & 0 & 0 & 0 & 0 & 0 & 0 & 0 & 1 & -1 & 0 & 0 & 0 & 0 \\ 1 & 0 & 0 & 0 & 0 & 0 & 0 & 0 & 0 & 0 & 0 & -1 & 0 & 0 \\ 0 & 0 & 0 & 0 & 0 & 0 & 0 & 0 & 0 & 0 & 0 & 0 & 1 & -1 \\ 0 & 0 & 0 & 0 & 0 & 0 & 0 & 0 & 1 & 0 & 0 & -1 & 0 & 0 \\ 0 & 0 & 0 & 0 & 0 & 0 & 0 & 0 & 1 & 0 & 0 & 0 & 0 & -1 \\ 1 & 0 & 0 & 0 & 0 & 0 & 0 & 0 & 0 & -1 & 0 & 0 & 0 & 0 \\ 1 & 0 & 0 & 0 & 0 & 0 & 0 & 0 & 0 & -1 & 0 & 0 & 0 & 0 \\ 0 & 0 & 0 & 0 & 0 & 0 & 0 & 1 & 0 & 0 & -1 & 0 & 0 & 0 \\ 0 & 0 & 0 & 0 & 0 & 0 & 0 & 1 & 0 & 0 & 0 & 0 & -1 & 0 \end{pmatrix}$$

$$\begin{pmatrix} \underline{v}_{46} \\ \underline{v}_{47} \\ \underline{v}_{48} \\ \underline{v}_{49} \\ \underline{v}_{50} \\ \underline{v}_{51} \\ \underline{v}_{52} \\ \underline{v}_{53} \\ \underline{v}_{54} \end{pmatrix} = \begin{pmatrix} 0 & 0 & -1 & 0 & 0 & 0 & 0 & 1 & 0 & 0 & 0 & 0 & 0 & 0 \\ 0 & -1 & 0 & 0 & 0 & 0 & 0 & 1 & 0 & 0 & 0 & 0 & 0 & 0 \\ -1 & 0 & 0 & 0 & 0 & 0 & 0 & 1 & 0 & 0 & 0 & 0 & 0 & 0 \\ -1 & 0 & 0 & 0 & 0 & 0 & 0 & 1 & 0 & 0 & 0 & 0 & 0 & 0 \\ -1 & 0 & 0 & 0 & 0 & 0 & 0 & 0 & 0 & 0 & 0 & 0 & 1 & 0 \\ -1 & 0 & 0 & 0 & 0 & 1 & 0 & 0 & 0 & 0 & 0 & 0 & 0 & 0 \\ -1 & 0 & 0 & 0 & 0 & 0 & 0 & 0 & 0 & 0 & 0 & 1 & 0 & 0 \\ 0 & -1 & 0 & 1 & 0 & 0 & 0 & 0 & 0 & 0 & 0 & 0 & 0 & 0 \\ 0 & 0 & 0 & 0 & 0 & -1 & 1 & 0 & 0 & 0 & 0 & 0 & 0 & 0 \end{pmatrix},$$

and the propensity function is the 54-component vector

$$\underline{a} = \begin{pmatrix} a_1 \\ a_2 \\ a_3 \\ a_4 \\ a_5 \\ a_6 \\ a_7 \\ a_8 \\ a_9 \\ a_{10} \\ a_{11} \\ a_{12} \\ a_{13} \\ a_{14} \\ a_{15} \\ a_{16} \\ a_{17} \\ a_{18} \\ a_{19} \\ a_{20} \\ a_{21} \\ a_{22} \\ a_{23} \\ a_{24} \\ a_{25} \\ a_{26} \\ a_{27} \end{pmatrix} = \begin{pmatrix} k_{\text{off}}^{\text{PLG}} x_2 \\ k_{\text{on}}^{\text{PLG}} [\text{PLG}]^{\text{free}} x_3 \\ k_{\text{off}}^{\text{PLi}} x_4 \\ k_{\text{off}}^{\text{tPA}} x_4 \\ k_{\text{on}}^{\text{PLG}} [\text{PLG}]^{\text{free}} x_5 \\ k_{\text{off}}^{\text{PLG}} x_6 \\ k_{\text{off}}^{\text{PLi}} x_7 \\ k_{\text{off}}^{\text{tPA}} x_2 \\ k_{\text{off}}^{\text{tPA}} x_3 \\ k_{\text{off}}^{\text{PLi}} x_5 \\ k_{\text{off}}^{\text{PLi}} x_6 \\ k_{\text{cat}}^{\text{ap}} x_1 \chi \\ k_{\text{off}}^{\text{PLi}} x_9 \\ k_{\text{deg}} x_4 \\ k_{\text{deg}} x_5 \\ k_{\text{deg}} x_6 \\ k_{\text{deg}} x_7 \\ k_{\text{cat}}^{n} n x_4 \\ k_{\text{cat}}^{n} n x_5 \\ k_{\text{cat}}^{n} n x_6 \\ k_{\text{cat}}^{n} n x_7 \\ k_{\text{cat}}^{n} n x_9 \\ k_{\text{off}}^{\text{tPA}} x_{11} \\ k_{\text{off}}^{\text{PLi}} x_{12} \\ k_{\text{off}}^{\text{TAFI}} x_{11} \\ k_{\text{on}}^{\text{TAFI}} [\text{TAFIa}]^{\text{free}} x_3 \\ k_{\text{off}}^{\text{TAFI}} x_{12} \end{pmatrix}$$

$$\begin{pmatrix} a_{28} \\ a_{29} \\ a_{30} \\ a_{31} \\ a_{32} \\ a_{33} \\ a_{34} \\ a_{35} \\ a_{36} \\ a_{37} \\ a_{38} \\ a_{39} \\ a_{40} \\ a_{41} \\ a_{42} \\ a_{43} \\ a_{44} \\ a_{45} \\ a_{46} \\ a_{47} \\ a_{48} \\ a_{49} \\ a_{50} \\ a_{51} \\ a_{52} \\ a_{53} \\ a_{54} \end{pmatrix} = \begin{pmatrix} k_{\text{on}}^{\text{TAFI}}[\text{TAFIa}]^{\text{free}}x_5 \\ k_{\text{cleave}}x_1 \\ k_{\text{cleave}}x_{12} \\ k_{\text{cleave}}x_{11} \\ k_{\text{off}}^{\text{PLi}}x_{14} \\ k_{\text{unbind}}^{\text{PLi}}x_6 \\ k_{\text{unbind}}^{\text{PLi}}x_5 \\ k_{\text{unbind}}^{\text{PLi}}x_7 \\ k_{\text{unbind}}^{\text{PLi}}x_4 \\ k_{\text{unbind}}^{\text{PLi}}x_9 \\ k_{\text{unbind}}^{\text{PLi}}x_{12} \\ k_{\text{unbind}}^{\text{PLi}}x_{14} \\ k_{\text{deg}}x_{12} \\ k_{\text{deg}}x_{14} \\ k_{\text{cat}}^{n}nx_{12} \\ k_{\text{cat}}^{n}nx_{14} \\ k_{\text{deg}}x_{11} \\ k_{\text{deg}}x_{13} \\ k_{\text{deg}}x_3 \\ k_{\text{deg}}x_2 \\ k_{\text{deg}}x_1 \\ k_{\text{deg}}x_1 \\ k_{\text{cleave}}x_1 \\ k_{\text{cat}}^{\text{ap}}x_1\chi \\ k_{\text{cat}}^{\text{ap}}x_1\chi \\ k_{\text{cat}}^{\text{ap}}x_2\chi \\ k_{\text{cat}}^{\text{ap}}x_6\chi \end{pmatrix},$$

where n is the number of cryptic doublets at the binding location of interest, $\chi = 1$ if there is a tPA molecule at the current binding location, and $\chi = 0$ if there is no tPA molecule. χ appears in the reactions describing tPA-mediated conversion of PLG to plasmin, because those reactions are not possible unless tPA is present somewhere on the binding location.